A MESOSCALE INVESTIGATION OF THE SEA BREEZE IN THE STELLENBOSCH WINEGROWING DISTRICT

By:
CHRISNA BARBARA DU PREEZ
96041855

MASTER OF SCIENCE (METEOROLOGY)
2006

DEPARTMENT OF GEOGRAPHY, GEOINFORMATICS AND METEOROLOGY

UNIVERSITY OF PRETORIA

DISSERTATION SUMMARY

A Mesoscale Investigation of the Sea Breeze in the Stellenbosch Winegrowing District

Chrisna Barbara du Preez

Supervisor:	Ms. Liesl Dyson
Faculty:	Faculty of Natural and Agricultural Sciences
Department:	Geography, Geoinformatics and Meteorology
University:	University of Pretoria
Degree:	Master of Science (Meteorology)

This study investigates how well the Regional Atmospheric Modelling System (RAMS) simulates the sea breeze from False Bay (False Bay sea breeze) at a small resolution of 200m. It describes the influence of the sea breeze in the Stellenbosch wine growing district focusing on temperature, relative humidity and wind speed and direction through three case studies, using three different synoptic conditions. The RAMS simulations are verified against measurements done by automatic weather stations in the study area for all three case studies. The first synoptic condition investigated is when light onshore flow occurred over the south-western Cape. The RAMS model simulated the vertical and horizontal structure of the sea breeze from False Bay very well. However RAMS predicted the onset of the sea breeze 3 hours earlier than the AWS data predicted. The flow was off-shore in the second case study. The RAMS simulations as well as the observed data from the automatic weather stations, showed the two sea breezes influencing the study area, one from Table Bay, west of Stellenbosch, and one from False Bay. In this case study the model simulated the flatter head and stronger False Bay sea breeze. The third case study investigated the influence of strong onshore synoptic conditions, in which the model and observed values showed that no sea breeze developed from False Bay. From the three case studies it was found that the sea breeze is influenced by the synoptic flow and that the sea breeze causes cooling of between 3°C and 16°C and relative humidity (RH) increase of between 16 – 57% depending on the synoptic flow. RAMS was able to simulate the sea breeze theoretically correct and has the potential to be used to identify climatological areas in the wine growing areas of the Western Cape.

ACKNOWLEDGEMENTS

The author would like to express her utmost appreciation to the following people for their valued contribution that made this work possible.

- Ms. Liesl Dyson for supervising this study and her endless patience.
- Dr. Valérie Bonnardot for help with the simulations and the original project
- Prof. Sylvie Cautenet, Prof Guy Cautenet from the University of Blaise Pascal in Clermont-Ferrand, France for writing the programs and settings for the RAMS simulations and the explanations of the technical aspects of the model.
- Karlien Breedt of the ARC-Infruitec-Nietvoorbij library and Rejaene Van Dyk of the ARC-ISCW library for the searches for articles and references.
- The ARC-ISCW for time and hardware to complete this study, especially Chris Kaempffer for his support and patience.
- Winetech for funding of the Atmospheric Modelling project, of which this study was part.
- Morgaine Sumner-Wichmann for the grammar checks and general support.
- To my friends and family for all their help and encouragement when the going got tough.

TABLE OF CONTENTS

DISSERTATION SUMMARY ..... **ii**

ACKNOWLEDGEMENTS ..... **iii**

TABLE OF CONTENTS ..... **iv**

LIST OF FIGURES ..... **vii**

LIST OF TABLES ..... **xiii**

LIST OF ACRONYMS ..... **xiv**

Chapter 1 Introduction **1**

1.1 The Problem 1

1.2 The climate and topography of the Western Cape 1

1.2.1 Synoptic scale weather systems *2*

1.2.2 Rainfall over the Western Cape *3*

1.2.3 Temperatures over the Western Cape *4*

1.2.4 Wind over the Western Cape *4*

1.2.5 Sunshine and relative humidity over the Western Cape *4*

1.2.6 The climate of the 200m grid study area *5*

1.2. Viticulture in the Western Cape 5

1.3. Aims of this study 6

Chapter 2 The Sea Breeze **9**

2.1. Introduction 9

2.2. Development of the sea breeze 9

2.2.1. Definition of the sea breeze *9*

2.2.2. Sea breeze development theories *11*

2.2.3. Stages of sea breeze development *13*

2.3. Characteristics of the sea breeze 15

2.3.1. The depth of the sea breeze *15*

2.3.2. The horizontal extent of the sea breeze *16*

2.3.3. Influences on the sea breeze character 16

2.4. Influences of the sea breeze 23

2.4.1. Temperature and relative humidity *23*

2.4.2. Wind *24*

2.4.3. Cloud formation *24*

2.4.4. Pollution *25*

2.5. Summary 26

Chapter 3 The Regional Atmospheric Modelling System (RAMS) 27

3.1. Introduction 27

3.2. The RAMS model 27

3.2.1. Nesting *27*

3.2.2. Plug-compatible modules *27*

3.2.3. Isentropic analysis *28*

3.2.4. Data analysis *29*

3.2.5. Four-dimensional data assimilation (4DDA) *29*

3.2.6. Large Eddy Simulation (LES) *30*

3.3. This study 30

3.4. Summary 32

Chapter 4 Case studies 37

4.1 Introduction 37

4.2 Observational data 39

4.3 Case study 1: 3 February, 2000 – Onshore synoptic conditions 41

4.3.1 Verification of simulations with observational data *42*

4.3.2 Rams simulations *44*

4.3.3 Conclusions *54*

4.4. Case study 2: 18 February, 2000 55

4.4.1 Verification of simulations with observed data *55*

4.4.2 RAMS simulations *58*

4.4.3 Conclusions *70*

4.5. Case study 3: 19 February, 2000 71

4.5.1 Verification of simulations with observed data *72*

4.5.2 RAMS simulations *74*

4.5.3 Conclusions *82*

Chapter 5 Summary and Conclusions 84

5.1 Summary 84

5.2 Conclusions 86

5.2.1 The sea breeze in the Stellenbosch wine growing district as observed by the Automatic Weather Stations. *86*

5.2.2. The sea breeze in the Stellenbosch wine growing district as simulated by RAMS *87*

5.3 Recommendations 88

REFERENCES 89

LIST OF FIGURES

FIGURE 1.1: The geographical position of the nine provinces of South Africa. The Western Cape Province is indicated in yellow. 2

FIGURE 1.2: The ocean currents around South Africa. (Adapted from: Linacre, 2002). 2

FIGURE 1.3: The geographical location of the 5km (a), 1km (b) and 200m (c) grids of the RAMS simulation. © University of Stellenbosch, ARC Infruitec-Nietvoorbij and Department of Agriculture, Western Cape..... 7

FIGURE 2.1: A vertical cross section of the sea breeze front (SBF) penetration inland with Kelvin-Helmholtz billows developing at the boundary between the sea air and the land air. (Adapted from: Simpson, 1994)..... 10

FIGURE 2.2: Lobes and clefts in the leading edge of the sea breeze front formed by the convective instability caused by the overrunning of warm air by denser sea air (Adapted from: Simpson, 1994) 11

FIGURE 2.3: Schematic diagram illustrating the development of the pressure gradients and the sea breeze circulations, in the absence of large scale flow, according to (a) the upwards theory, (b) the sideways theory and (c) the mixed theory. The left handed plots show the initial situations, the middle plots show the initiation of the circulations while the right-hand plost show the final situations with fully developed sea breeze circulations. (Adapted from: Tijm and Van Delden, 1999)..... 13

FIGURE 2.4: An example of the effect of coastline curvature on the penetration of the sea breeze. Concave coastline causes enhanced divergence and convex coastline causes enhanced convergence. 19

FIGURE 2.5: Double sea breezes forming over a bay. The first being the bay breeze (grey arrows) and the ocean breeze (black arrows). The line arrows illustrate the convergent and divergent flow around the bay. 20

FIGURE 3.1: The vegetation (a) and soil types (b) used in the rams model runs. Vertical cross sections were performed at the locations indicated by dotted lines. 32

FIGURE 4.1: The topography of the study area with the positions of the cross sections (dotted lines) and places of interest. Heights larger than 300m are shown in red and heights lower than sea level in blue. 37

FIGURE 4.2: The topography of cross sections X1 (a), X2 (b) and X3 (c) with height indicated in meters above sea level on the y-axis and the x-axis, indicating distance from the southern edge of the study area (km). 38

FIGURE 4.3 The geographical position of five automatic weather stations (as numbers 1 to 5) in the study area. The contours indicate the topography of the area. 40

FIGURE 4.4: Synoptic map of southern Africa for 3 February, 2000 at 14:00 SAST (Adapted from: South African Weather Bureau, 2000). 41

FIGURE 4.5: A comparison between observed temperature (gray) and simulated temperature (black) in °C at the position of five automatic weather stations for 3 February, 2000. 42

FIGURE 4.6: A comparison between observed RH (gray) and simulated RH (black) in % at the position of five automatic weather stations for 3 February, 2000. 43

FIGURE 4.7: Simulated surface temperature (°C) at 11:00 SAST on 3 February, 2000. The numbers 1 – 5 indicate the geographical positions of the AWSs used in the verifications. 45

FIGURE 4.8: Simulated temperature (°C) at 11:00 SAST on 3 February, 2000, in the south-north cross section X2 45

FIGURE 4.9: Simulated temperature (°C) at 11:00 SAST on 3 February, 2000, in the south-north cross section X3 46

FIGURE 4.10: Simulated relative humidity (%) at 11:00 SAST on 3 February, 2000, in the south-north cross section X3. 46

FIGURE 4.11: Simulated surface relative humidity (%) at 11:00 SAST on 3 February, 2000. The numbers 1 – 5 indicate the geographical positions of the AWSs used in the verifications. 47

FIGURE 4.12: Simulated wind speed (ms^{-1}) and direction (black arrows) at 11:00 SAST on 3 February, 2000, in the south-north cross section X1 47

FIGURE 4.13: Simulated temperature (°C) at 14:00 SAST on 3 February, 2000, in the south-north cross section X2 48

FIGURE 4.14: Simulated surface relative humidity (%) at 14:00 SAST on 3 February, 2000. The numbers 1 – 5 indicate the geographical positions of the AWSs used in the verifications. 49

FIGURE 4.15: Simulated relative humidity (%) at 14:00 SAST on 3 February, 2000 in the south-north cross sections X1 (a) and X2 (b). 49

FIGURE 4.16: Simulated temperatures (°C) at 17:00 on 3 February, 2000 in south-north cross sections X2 (a) and X3 (b). 50

FIGURE 4.17: Simulated relative humidity (%) at 17:00 on 3 February, 2000 in south-north cross section X2. 50

FIGURE 4.18: Simulated surface wind speed (ms^{-1}) and direction (black arrows) at 17:00 SAST on 3 February, 2000. The numbers 1 – 5 indicate the geographical positions of the AWSs used in the verifications. 51

FIGURE 4.19: Simulated wind speed (ms^{-1}) and direction (black arrows) at 17:00 SAST on 3 February 2000 in the south-north cross section X1. 52

FIGURE 4.20: Simulated temperature (°C) at 23:00 SAST on 3 February, 2000 for south-north cross sections X2 (a) and X3 (b). 52

FIGURE 4.21: Simulated surface wind speed (ms^{-1}) and direction (black arrows) at 23:00 SAST on 3 February, 2000. The numbers 1 – 5 indicate the geographical positions of the AWSs used in the verifications. 53

FIGURE 4.22: Simulated wind speed (ms^{-1}) and direction (black arrows) at 23:00 SAST on 3 February, 2000 for south-north cross section X2. 54

FIGURE 4.23: A comparison between observed temperature (gray) and simulated temperature (black) in °C at the positions of the five automatic weather stations for 18 February, 2000. 56

FIGURE 4.24: Comparison between observed RH (gray) and simulated RH (black) in % at the positions of the five automatic weather stations for 18 February, 2000. 57

FIGURE 4.25: Synoptic map of southern Africa for 18 February, 2000 at 14:00 SAST (Adapted from: South African Weather Bureau, 2000) 59

FIGURE 4.26: Simulated surface temperature (°C) at 23:00 SAST on 17 February, 2000. 60

FIGURE 4.27: Simulated temperature (°C) at 23:00 SAST on 17 February, 2000 in the south-north cross section X1. 60

FIGURE 4.28: Simulated surface temperature (°C) at 02:00 SAST on 18 February, 2000. 61

FIGURE 4.29: Simulated temperatures (°C) at 02:00 SAST on 18 February, 2000 in south-north cross sections X1 (a) and X2 (b). 61

FIGURE 4.30: Simulated surface relative humidity (%) at 08:00 SAST on 18 February, 2000. The numbers 1 – 5 indicate the geographical positions of the AWSs used in the verifications. 62

FIGURE 4.31: Simulated surface wind speed (ms^{-1}) and direction (black arrows) at 08:00 SAST on 18 February, 2000. The numbers 1 – 5 indicate the geographical positions of the AWSs used in the verifications. 63

FIGURE 4.32: Simulated surface temperature (°C) at 11:00 SAST on 18 February, 2000. The numbers 1 – 5 indicate the geographical positions of the AWSs used in the verifications. 64

FIGURE 4.33: Simulated temperature (°C) at 11:00 SAST on 18 February, 2000 in the south-north cross sections X1 (a) and X2 (b). 64

FIGURE 4.34: Simulated surface wind speed (ms^{-1}) and direction (black arrows) at 11:00 SAST on 18 February, 2000. The numbers 1 – 5 indicate the geographical positions of the AWSs used in the verifications. 65

FIGURE 4.35: Simulated wind speed (ms^{-1}) and direction (black arrows) at 11:00 SAST on 18 February, 2000 in the south-north cross sections X2 (a) and X3 (b). 66

FIGURE 4.36: Simulated surface temperature (°C) at 14:00 SAST on 18 February, 2000. The numbers 1 – 5 indicate the geographical positions of the AWSs used in the verifications. 67

FIGURE 4.37: Simulated temperature (°C) at 14:00 SAST on 18 February, 2000 in the south-north cross section X1. 67

FIGURE 4.38: Simulated surface wind speed (ms^{-1}) and direction (black arrows) at 14:00 SAST on 18 February, 2000. The numbers 1 – 5 indicate the geographical positions of the AWSs used in the verifications. 68

FIGURE 4.39: Simulated wind speed (ms^{-1}) and direction (black arrows) at 14:00 SAST on 18 February, 2000 in south-north cross sections X2 (a) and X3 (b). 68

FIGURE 4.40: Simulated relative humidity (%) at 20:00 SAST on 18 February, 2000 in the south-north cross section X1. 69

FIGURE 4.41: Simulated relative humidity (%) at 23:00 SAST on 18 February, 2000 in south-north cross section X2. 70

FIGURE 4.42: Comparison between observed temperature (gray) and simulated temperature (black) in °C at the positions of the five automatic weather stations for 19 February, 2000..... 72

FIGURE 4.43: Comparison between observed relative humidity (gray) and simulated relative humidity (black) in % at the positions of the five automatic weather stations for 19 February, 2000. 73

FIGURE 4.44: Synoptic map of southern Africa for 19 February, 2000 at 14:00 (Adapted from: South African Weather Bureau, 2000) 74

FIGURE 4.45: Simulated wind speed (ms^{-1}) and direction (black arrows) at 05:00 SAST on 19 February, 2000 in the south-north cross sections X1 (b) and X2 (a). 75

FIGURE 4.46: Simulated surface wind speed (ms^{-1}) and direction (black arrows) at 05:00 SAST on 19 February, 2000. The numbers 1 – 5 indicate the geographical positions of the AWSs used in the verifications. 76

FIGURE 4.47: Simulated relative humidity (%) at 05:00 SAST on 19 February, 2000 in the south-north cross section X1. 76

FIGURE 4.48: Simulated temperature (°C) at 11:00 SAST on 19 February, 2000 in south-north cross section X2. 77

FIGURE 4.49: Simulated surface temperature (°C) at 11:00 SAST on 19 February, 2000. The numbers 1 – 5 indicate the geographical positions of the AWSs used in the verifications..... 78

FIGURE 4.50: Simulated surface relative humidity (%) at 11:00 SAST on 19 February, 2000. The numbers 1 – 5 indicate the geographical positions of the AWSs used in the verifications. 78

FIGURE 4.51: Simulated relative humidity (%) at 11:00 SAST on 19 February, 2000 in south-north cross section X2. 79

FIGURE 4.52: Simulated surface wind speed (ms^{-1}) and direction (black arrows) at 11:00 SAST on 19 February, 2000. The numbers 1 – 5 indicate the geographical positions of the AWSs used in the verifications. 79

FIGURE 4.53: Simulated wind speed (ms^{-1}) and direction (black arrows) at 11:00 SAST on 19 February, 2000 in south-north cross section X2. 80

FIGURE 4.54: Simulated temperature (°C) at 14:00 SAST on 19 February, 2000 in south-north cross section X1. 80

FIGURE 4.55: Simulated surface wind speed (ms^{-1}) and direction (black arrows) at 17:00 SAST on 19 February, 2000. The numbers 1 – 5 indicate the geographical positions of the AWSs used in the verifications. 81

FIGURE 4.56: Simulated wind speed (ms^{-1}) and direction (black arrows) at 17:00 SAST on 19 February, 2000 in south-north cross sections X1 (a) and X2 (b). 81

FIGURE 4.57: Simulated temperature (°C) at 20:00 SAST on 19 February, 2000 in south-north cross sections X1 (a) and X2 (b). 82

LIST OF TABLES

TABLE 3.1: Cross sections of the 200m grid simulations 30

TABLE 3.2: Detailed description of the settings for the RAMS simulations for this study (adapted from Walko and Tremback, 2000). 33

TABLE 4.1: Terms used to describe temperature, relative humidity and wind speed. 39

TABLE 4.2: Information on automatic weather stations used for verification of simulation data for the 200m grid. 40

LIST OF ACRONYMS

4DDA	Four-Dimensional Data Assimilation
AGL	Above Ground Level
ARC-ISCW	Agricultural Research Council – Institute for Soil, Climate and Water
ASL	Above Sea Level
AWS	Automatic Weather Station
ECMWF	European Centre for Medium-range Weather Forecasts
LES	Large Eddy Simulation
NMC	National Meteorological Center
RAMS	Regional Atmospheric Modelling System
RAMS/ISAN	RAMS Isentropic Analysis package
RH	Relative Humidity
SAST	South African Standard Time
SAWS	South African Weather Service
SBF	Sea Breeze Front
SST	Sea Surface Temperature

Chapter 1 Introduction

1.1 The Problem

The complex topography and coastline of the Western Cape Province of South Africa, plays an important role in the climate of the area. Climate is an important factor in the agriculture industry in the province, most specifically the viticulture industry which is one of the biggest agricultural contributors in the area (Wesgro, 2002).

In order to investigate the influence of the complex topography and coastline on the climate in the area, it is necessary to observe the atmosphere at a small scale. However, it is impractical to attempt to develop an automatic weather station network with a small enough resolution to observe these influences clearly. Thus it follows, that the use of a mesoscale atmospheric model, like the Regional Atmospheric Modelling System (RAMS) will enable researchers to investigate the atmosphere at a resolution of as small as 200m. This study is the first attempt at simulating the atmosphere at such a small horizontal resolution (200m) in the Western Cape and also the first attempt to simulate the influence of the sea breezes that develop in the area, at a resolution as small as 200m.

1.2 The climate and topography of the Western Cape

South Africa, situated at the southern tip of Africa, is comprised of various climatic regions. Climatologically, South Africa can be divided into summer rainfall regions, winter rainfall regions and year-round rainfall regions (Schulze, 1965). The rainfall in winter increases south and south-westward, resulting in the purely winter rainfall zone being confined to the extreme south-western corner of South Africa. The remaining 85% of the country receives more than half of it's rainfall in summer (Schulze, 1965). The focus area of this study is situated in the south-western part of the Western Cape Province (Western Cape from here on).

The Western Cape (Fig. 1.1) consists of a complex system of coastal plains and mountainous areas, including the Cape Peninsula, which consists of folded mountains most of which rise above 600m (Schulze, 1996). This region is flanked by the Atlantic Ocean which carries the cold Benguela current to the west and the warmer Agulhas current to the south (Fig. 1.2) These two currents cause significant sea surface temperature differences between Table Bay to the west and False Bay to the south (Bonnardot *et al.*, 2002).

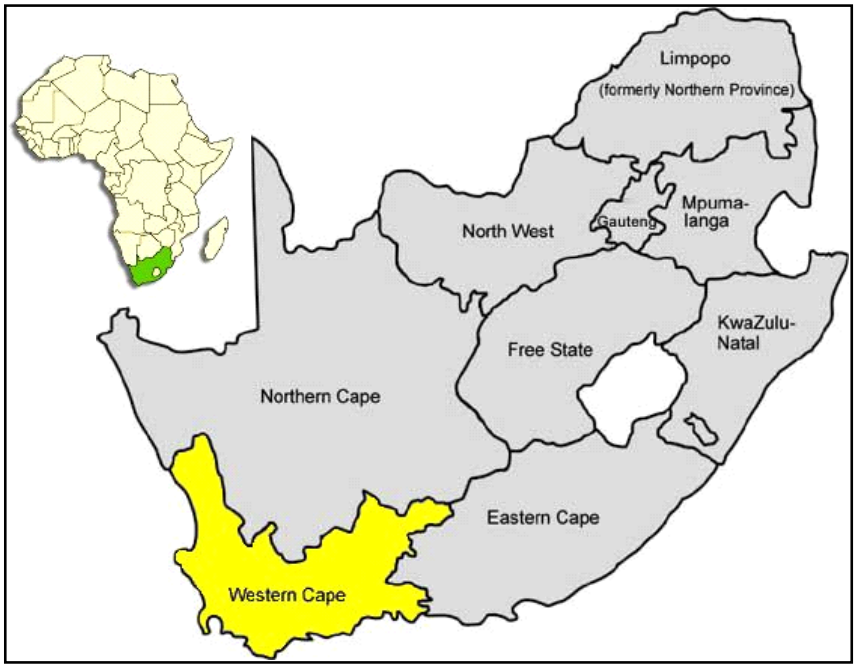

FIGURE 1.1: The geographical position of the nine provinces of South Africa. The Western Cape Province is indicated in yellow.

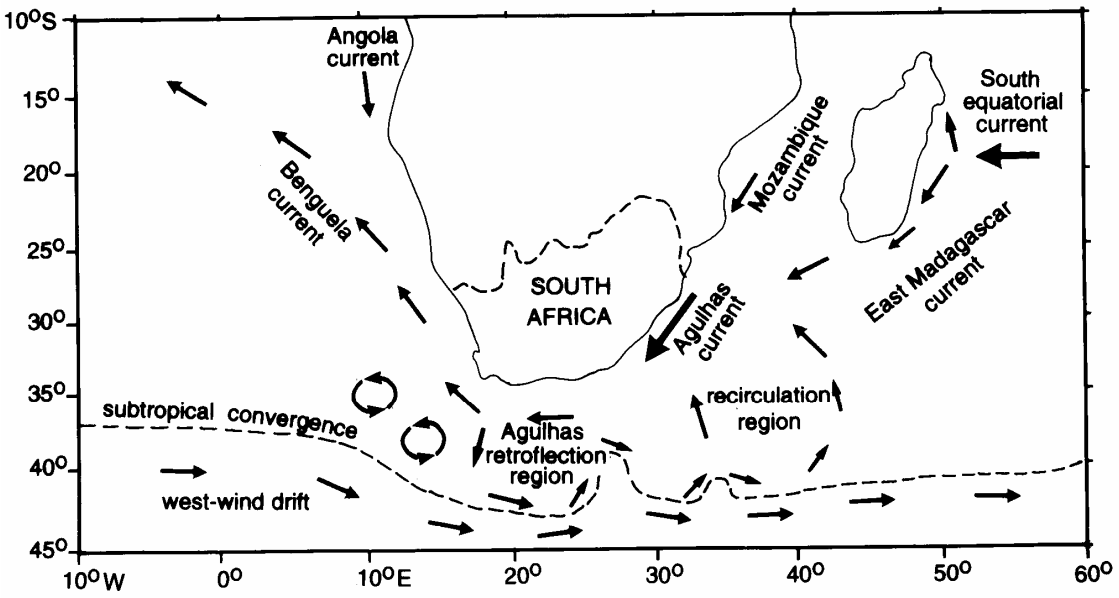

FIGURE 1.2: The ocean currents around South Africa. (Adapted from: Linacre, 2002).

1.2.1 Synoptic scale weather systems

There are 9 different synoptic circulation patterns which influence the summer weather in the whole of South Africa and the Western Cape in particular (Taljaard, 1994). These synoptic systems are:

- High over the west and south-west coasts and the western plateau

- High over the southern coastal belt and adjacent sea
- High over the Kwa-Zulu Natal and Eastern Cape
- Wedge of high pressure advancing eastward along the south-east coast
- Inverted V-through over the south coast and southern Cape
- Inverted V-trough over the south-east coast
- Trough over Namibia or the West Coast
- Marked low or V-trough extending southward across Botswana
- High pressure dominating over all parts of the land

The case studies in this study took place on days in February, thus the summer circulation patterns and weather are applicable. The summer months in the Western Cape are generally characterized by sunny and dry conditions. Systems that influence the weather over this area during summer include surface high pressure systems, the west coast trough and coastal lows. Surface high pressure systems that ridge regularly along the coastal areas cause clouds to develop along the coastal belt. However, precipitation is usually limited with this ridging process and, as it progresses eastward, the cloud cover ceases. When the surface high pressure system is situated east of the country, a tight east-west pressure gradient can develop over the country, causing an easterly wind over the south-western Cape. On these days, temperatures can become extremely high. The west-coast trough is usually associated with the development of convective clouds develop in the eastern interior of the Western Cape. When the interior regions receive rainfall, it is usually in association with a west-coast trough, although such rainfall is limited in the summer months (Taljaard, 1994).

Ridging of a high pressure system south of the country causes easterly flow over the interior of South Africa in the lower layers of the atmosphere. This results in descending air along the west coast and the formation of the west coast coastal low (De Wet, 1984). A coastal low is a low pressure system which develops along the coast, is generally shallow and does not extend into the atmosphere deeper than 1500m above sea level (ASL) (Estie, 1984). Southward moving coastal lows occur frequently during the summer months on the West Coast of South Africa (Walker, 1984) when the continental heat low is well developed over the western parts of southern Africa. Fog can occur in the wake of the coastal low, if the pressure gradients are relatively slack. Berg winds can occur ahead of the coastal low (Estie, 1984). Both the fog and berg winds can occur in the regions south of Stellenbosch where the study area is located.

1.2.2 Rainfall over the Western Cape

The annual average rainfall in the Western Cape region is 600mm. However, the mountain ranges in the area receive heavy orographic rains with some places receiving over 2500mm per year (Schulze,

1996). The rainy season is from May to September (winter). The majority of the rain is brought by westerly depressions in which the rain-bearing winds, often strong and gusty, are north-westerly at first, shifting to south-westerly. Orographic rain also occurs in the valleys and mountains of the Western Cape. Very occasionally, (approximately five times per year) thunderstorms occur. (Schulze, 1965, Schulze, 1996).

1.2.3 Temperatures over the Western Cape

The temperature varies considerably spatially and in association with the different synoptic weather systems influencing the Western Cape. The biggest influence on air temperatures in the Western Cape is the proximity of the cool ocean which results in cooler temperatures at the coast during onshore flow. Off-shore flow causes much warmer temperatures over the coastal belt, due to the dry origin of the air and the adiabatic heating as the air is forced to descend from over the escarpment. (Taljaard, 1994, and Schulze, 1996). The average daily maximum temperature over the Western Cape is approximately 28°C in mid-summer and 17°C in mid-winter, but extreme maxima can reach 43°C in summer and 30°C in winter. Average daily minimum temperature is about 15°C in January and 6°C in July. Extreme minima can occur with temperatures as low as 4°C in summer and -5°C in winter, depending on altitude and synoptic system (Schulze, 1965). At Cape Town, the mean temperature is 21°C in summer and 13°C in winter (Schulze, 1996).

1.2.4 Wind over the Western Cape

The prevailing wind directions are northerly and southerly in winter and southerly to south-easterly in summer (Schulze, 1996). In summer, the southerly and south-easterly winds can reach average hourly wind speeds of 21ms^{-1} and the winds may gust up to 29ms^{-1} (South African Weather Bureau, 1975). Northerly to south-westerly winds can cause unstable conditions with prefrontal rain and post frontal showers. These unstable conditions occur predominantly in winter (Schulze, 1996). In summer, while the south-easterly winds are associated with fair or fine weather, they are often associated with orographic rain over the South Western Cape Mountains. Berg winds are hot, dry, offshore winds that may last for several days or blow only for a few hours. In this study the bergwind would be a northerly wind across the study area. As the air moves over the escarpment, it descends and heats adiabatically, causing very high temperatures in the Western Cape.

1.2.5 Sunshine and relative humidity over the Western Cape

Sunshine duration varies from about 60% of the possible duration of sunshine in July to over 70% in January (Schulze, 1965). At the coast, the mean humidity in the mornings is on average 85-90%

in summer. In the interior, it averages about 60%. The average noon time relative humidity (RH) in February is 52% (South African Weather Bureau, 1986).

1.2.6 The climate of the 200m grid study area

In the smaller study area used for this specific study the average temperature for February (the period used for the case studies) is 22°C with the average maximum temperature 28.7°C and the average minimum temperature being, 16.6°C (ARC-ISCW, 2000). The average RH for February is 71.5%, with the average maximum RH 88.7% and the average minimum RH 50.42% (ARC-ISCW, 2000). The average daily wind speed over the area is 2.4ms^{-1} over the area (ARC-ISCW, 2000) as measured at weather stations of the ARC-ISCW weather station network in the study area at 2m above ground level (AGL).

1.2. Viticulture in the Western Cape

The Western Cape's Mediterranean climate, along with the cooling influence from the Benguela current, makes the south-western Cape ideal for the cultivation of wine (Hughes and Maze, 2006). Agriculture in the Western Cape contributes 23% of the total gross income from the agricultural sector in South Africa (Wesgro, 2002). It accounts for 5.9% of the Western Cape's Gross Regional Product, while viticulture is the fourth largest contributor, comprising 12% of the total agricultural output. (Wesgro, 2002). Wine is one of the most important exports from the Western Cape, therefore, it is important for the wine produced in the Western Cape to be of good quality in order to be competitive in the ever expanding international wine market. The South African wine industry considers the identification of terroir units very important. The knowledge of the terroir of a farm, and the use of that knowledge in the planning of viticultural blocks and farming practices, leads to better quality and, hence, more competitive, wines on the international wine market. Terroir is a complex term to describe the interaction between soil, climate, topography and plant genotype which results in a unique product (wine) (Falcetti, 1994). Climate, more specifically the meso-climate, is an important aspect of the terroir concept.

The temperature difference between the cold ocean and the warm land in the Western Cape provides the ideal conditions needed for sea breezes to develop in the area. The cooler temperatures and higher RH associated with the sea breeze have important implications for the viticulture industry. Amongst other things, temperature influences the coloration of grapes (Kliewer and Torres, 1972). The cooling effect of the sea breeze could also contribute to better, deeper colour in red wines. The temperature threshold for optimum colour is 20°C to 25°C in the daytime and between 10°C and 15°C at night (Bonnardot, 2004). Temperatures that are outside the optimum range cause stress. Stress leads to

poor colour in the grapes. In white wines, cooler temperatures tend to cause fresher, more acidic wines and contribute to a finer bouquet and aroma. Warmer temperatures cause the aroma in white wines to forfeit its freshness and the wines will have a higher alcohol content, often lacking balance (Becker, 1977). Temperature and relative humidity play an important role in the photosynthesis of the grape vines. The thresholds for optimum temperature and relative humidity for grape vine photosynthesis is between 25°C and 30°C. Below or above that threshold the vines experience stress and the physiology of the vines are affected (Bonnardot, 2004). The ideal RH for photosynthesis is between 60 and 70% (Bonnardot, 2004). Higher relative humidity causes a decrease in diffusive resistance in grape vines under water stress and also in otherwise stressed vines (Düring, 1976). High winds speeds causes tattering and burning and, in extreme cases, total loss of leaves, shoots and berries. This loss results in reduced vine capacity in photosynthate production and, if it happens prior to flowering, wind damage has a direct effect on the ability of the vine to set fruit (Hamilton 1989). Vine stomatal resistance has also been found to increase in windy conditions (Campbell-Clause 1988). Through the stomatal resistance, wind affects transpiration, evapotranspiration (Campbell-Clause, 1988) and photosynthesis (Freeman *et al*. 1982) in vines. Subsequently, these factors, influenced by the sea breeze, in turn influences grapevine functioning and the resulting wine character and quality.

Every facet of plant growth and development is subjected to the influence of temperature, relative humidity and wind (Coombe, 1987). During harvest time, (February) it is especially important to know how the sea breeze contributes to create the ideal temperature, RH, and wind conditions, as climate conditions at harvest time are an important influence on the character of the resulting wine (Carey *et al*., 2003). It is also important to understand how different synoptic conditions contribute to the development of the sea breeze, in order for the producers to make the necessary harvest decisions, ensuring a good quality wine.

1.3. Aims of this study

This study has two aims:

- to identify how well the Regional Atmospheric Modelling System (RAMS) simulates the sea breeze at a 200m resolution in the Western Cape wine growing districts
- to investigate the influence of the sea breeze in the Stellenbosch winegrowing district on temperature, relative humidity (RH) and wind speed and direction for different synoptic conditions. This was done by investigating information gathered through the use of RAMS and the automatic weather stations (AWSs) in the area.

These are the first steps in a larger project aimed at identifying the various terroir units in the South African wine growing areas with the goal of improving the quality of South African wine.

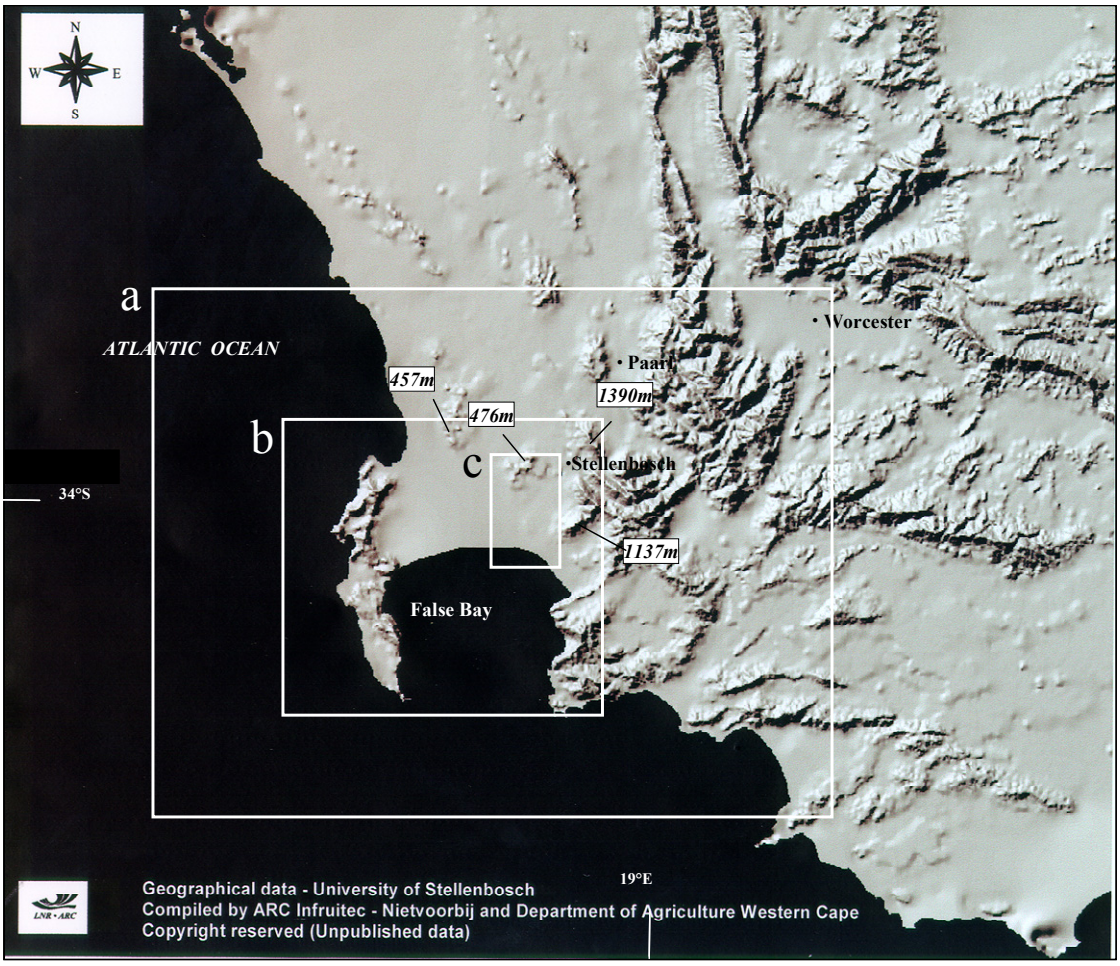

FIGURE 1.3: The geographical location of the 5km (a), 1km (b) and 200m (c) grids of the RAMS simulation. © University of Stellenbosch, ARC Infruitec-Nietvoorbij and Department of Agriculture, Western Cape.

To achieve these aims, three case studies were conducted. Simulations were done by RAMS for three different synoptic conditions. The outputs from RAMS were then verified against five automatic weather stations in the study area. The first case study considered the influence of the sea breeze for the weak onshore synoptic conditions on the 3rd of February, 2000. The second case study investigated the influence of the sea breeze for the off-shore flow on the 18th February, 2000. The third case study investigated the influence of the sea breeze for the strong onshore synoptic flow on the 19th February, 2000.

The RAMS simulations were done with nested grids of 25km, 5km, 1km and 200m. This study focuses only on the 200m grid. The positions of the smaller 3 grids are shown in figure 1.3 and are indicated with an a (5km), b (1km) and c (200m) respectively.

The grid used in this study is the 200m grid situated south and west of Stellenbosch. This grid includes Bottelaryberg Mountain with a height of 476m ASL and ends just west of Helderberg Mountain which has a height of 1137m ASL. The 1km grid includes the mountainous Cape Peninsula, Table Bay and False Bay, and Helderberg and Simonsberg Mountains, north-east of Stellenbosch (1390m). The 5km grid covers most of the extreme Western Cape and reaches as far inland as Worcester.

The definition of the sea breeze, the factors influencing the development of the sea breeze and the influences of the sea breeze on meteorological variables are discussed in Chapter 2. In Chapter 3, the RAMS model and its settings are detailed. In Chapter 4, the three case studies are discussed. The RAMS data are verified against the AWS data and the characteristics of the sea breeze under the different synoptic conditions as simulated by RAMS are discussed. The results are summarized in Chapter 5.

Chapter 2 The Sea Breeze

2.1. Introduction

This chapter takes a closer look at the sea breeze by detailing the process of sea breeze development, providing the definition of the sea breeze, and describing the different theories that exist on the development of the sea breeze. The upward, sideways, mixed and the hydrostatic adjustment theories are explained. The different stages of the sea breeze development are looked at and the characteristics of the sea breeze are illustrated. These characteristics include: the depth and horizontal extent of the system: factors influencing the sea breeze character are detailed, they include: the influence of synoptic conditions, topography, coastline curvature, surface roughness, Coriolis Force, sea surface temperatures and clouds and soil moisture. Lastly, the influence of the sea breeze on the ambient environment is discussed by looking at the changes in temperature, relative humidity, wind, cloud formation and pollution dispersion caused by the sea breeze.

2.2. Development of the sea breeze

2.2.1. Definition of the sea breeze

The sea breeze is defined as a diurnal circulation which is driven by the difference in temperature between the air masses over land and water. The ocean, or any other large body of water, is in constant motion and has a high thermal conductivity, causing heating or cooling at the surface to be transported through the depths of the ocean, thus giving small variations in temperature to the ocean surface and the air above it. Land, on the other hand, has low thermal conductivity and therefore exhibits a considerable variation in temperature on a daily basis. This difference in temperature leads to a pressure gradient between land and sea, that results in a low-level onshore flow, the sea breeze, during the day and a weaker off-shore flow, the land breeze, during the night (Clarke, 1955). This system of movement is called the sea breeze system and consists of the inflowing sea breeze, the rising of the air over land, the return flow in the higher parts of the atmosphere and the sinking of air over the ocean. The development of the sea breeze will be discussed in more detail in the next section.

The leading edge of the sea breeze (Fig. 2.1) is called the sea breeze front (SBF). The inland penetration of the SBF can be observed by abrupt changes in air temperature, wind direction and humidity as cool, moist sea air gets carried inland (Chiba, 1993). Simpson (1994) suggested that the sea breeze front could be represented as a gravity (density) current. The density difference is due to the temperature differences between the sea breeze and the land air, with 3°C representing a density change of roughly

1% as established from extensive field measurements in the USA, UK, Australia, as well as laboratory experiments. As denser maritime air meets the warmer land air, a sharp leading edge is formed with a height of about twice that of the density current flowing inland. Kelvin-Helmholtz billows may form due to the interaction of the two air masses of different density moving relative to one another.

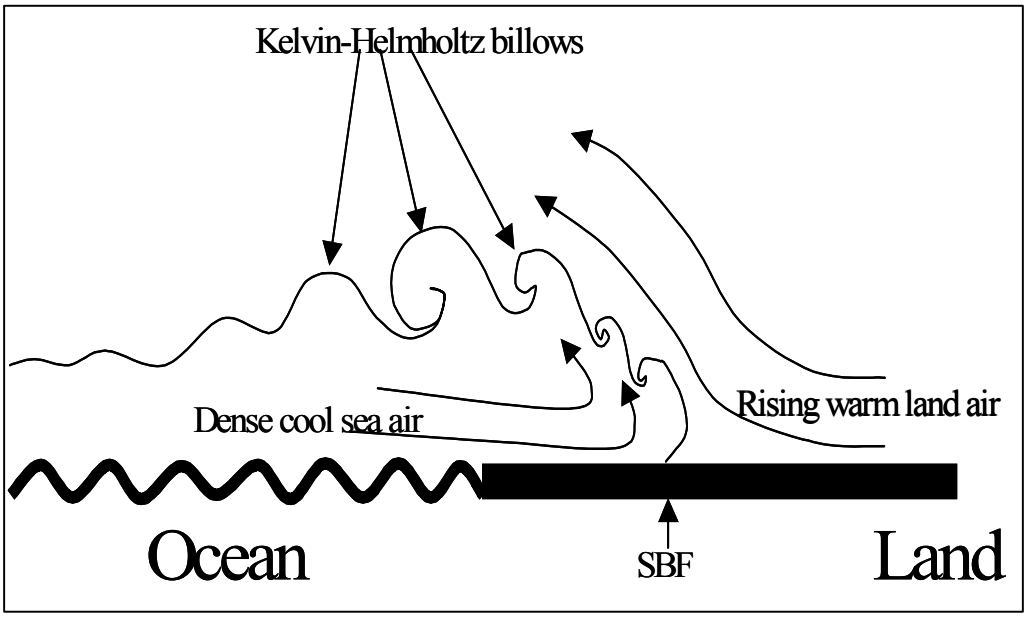

FIGURE 2.1: A vertical cross section of the sea breeze front (SBF) penetration inland with Kelvin-Helmholtz billows developing at the boundary between the sea air and the land air. (Adapted from: Simpson, 1994)

The leading edge of the SBF consists of a continually changing pattern of lobes and clefts about one kilometre across, (Fig. 2.2). These are formed by convective instability, caused by the overrunning of warm land air at ground level by denser sea air (Britter and Simpson, 1978). The lobes and clefts disappear at night when radiative cooling occurs in the near surface layers of the sea breeze (Abbs and Physick 1992).

For the sea breeze to start to blow, the temperature difference between land and sea has to be large enough to overcome any large-scale circulation (Simpson, 1994). Black and Tarny (1963) suggested, for example, that a large area of black asphalt near the coast would induce a stronger sea breeze circulation, which in turn would lead to cloud formation and rain. Another example, discussed by Lindesay and Tyson (1990), was the sea breezes that develop in the central Namib Desert (Namibia). The desert is bounded to the west by the consistently cold ocean and to the east by the escarpment which becomes strongly heated by day and similarly cooled by night. This, together with the pronounced diurnal heating and cooling of the desert itself, causes strong thermal gradients, which in turn are responsible for strong and long lived sea breezes (Lindesay and Tyson, 1990). In this area, the thermo-topographic

airflows frequently have a regional significance equalling or exceeding that of the general circulation. (Lindesay and Tyson, 1990).

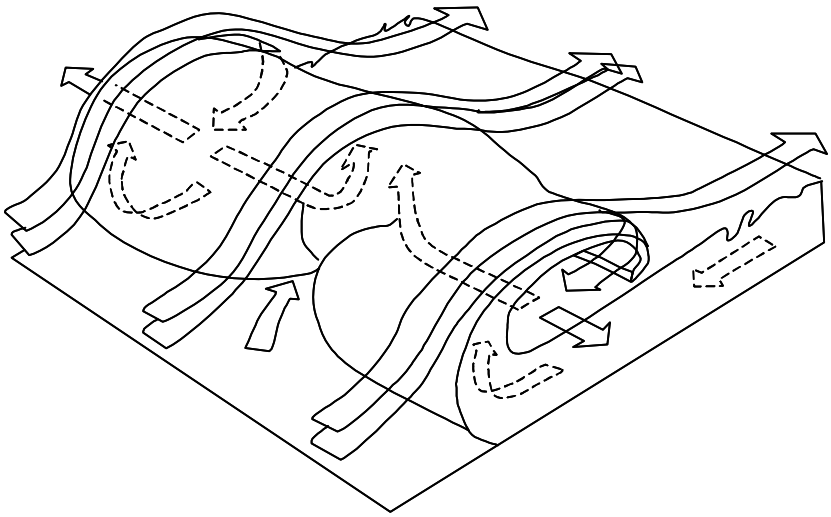

FIGURE 2.2: Lobes and clefts in the leading edge of the sea breeze front formed by the convective instability caused by the overrunning of warm air by denser sea air (Adapted from: Simpson, 1994)

Atkinson (1981) suggested that a local pressure gradient of 1hPa per 50 km was required for a sea breeze to develop. Oliphant *et al*., (2001) found that pressure differences of less than 0.5 hPa were sufficient to develop quite intense local airflow over a tropical island located north of Australia.

2.2.2. Sea breeze development theories

There are different theories as to how the pressure difference between land and sea air develops. These are the upward, sideways, mixed and hydrostatic adjustment theories.

a) The upward theory

The most common theory used in describing the development of a sea breeze is that which Tijm and Van Delden (1999) called the 'upward' theory. This theory was also described by Koschmieder (1933), Defant (1951), Willet and Sanders (1959), Atkinson (1981), Pielke (1984), Preston-Whyte and Tyson (1988), Abbs and Physick (1992) and Oliphant *et al.,* (2001) in their respective studies of the sea breeze. They concurred that on clear days with little synoptic influence, the lower layers of air over land is heated more rapidly than those over sea. The air over land is therefore warmer than the air over sea and thus, assuming hydrostatic equilibrium, the vertical pressure gradient is therefore larger over sea than over land. Further assuming the pressure at the surface remains the same at first, the pressure above the surface is then higher, at a specific height, over land than over sea. A horizontal pressure gradient develops, which causes a flow of air from land to sea. This convergence over sea and divergence over land in the

higher levels then causes the pressure at the surface to fall over land and to rise over sea. This pressure difference at the surface initiates the sea breeze, (Fig. 2.3(a)).

b) The sideways theory

The second theory on the development of the sea breeze is called the 'sideways' theory (Tijm and Van Delden, 1999). A level of no pressure change is assumed to exist at a certain height above the convective boundary layer. The sideways expansion of each column of air over land produces a change in pressure which is transmitted horizontally at the speed of sound. The resulting pressure difference at the low levels is responsible for the onset of the sea breeze (Fig. 2.3(b)). The pressure at the surface falls less rapidly at the coast than farther inland due to advection of cold sea air (Simpson 1994).

c) The mixed theory

The third theory combines the first two theories. The warm air over land expands vertically and horizontally, causing the sea breeze and return current to be initiated at the same time (Fig. 2.3(c)). From observations made by Gotske *et al.,* (1957), using stations geographically close to one another, but with large difference in altitude, it appeared that during late morning and afternoon, the pressure fell near the earth's surface while it rose at higher altitudes. The level of no pressure change was located at about 800m above the surface in this particular experiment.

d) The hydrostatic adjustment theory

All three of the above mentioned explanations neglect the process of hydrostatic adjustment, which according to Tijm and Van Delden (1999) and Bannon (1995) is accompanied by sound wave propagation. They stated that sound waves are generated over land when the air expands due to diabatic heating. Vertically travelling sound waves induce a pressure increase through the entire atmosphere above the heated layer within a few minutes. Horizontally travelling sound waves induce a surface-pressure decrease over land and a surface pressure increase over the sea. With the resulting pressure gradient, the sea breeze is initiated.

None of the above theories have been disproved and the debate still continues between scientists as to which of the theories best describes the development of the sea breeze. However there is no doubt that the sea breeze does develop and that the development moves through different stages as is discussed in the next section.

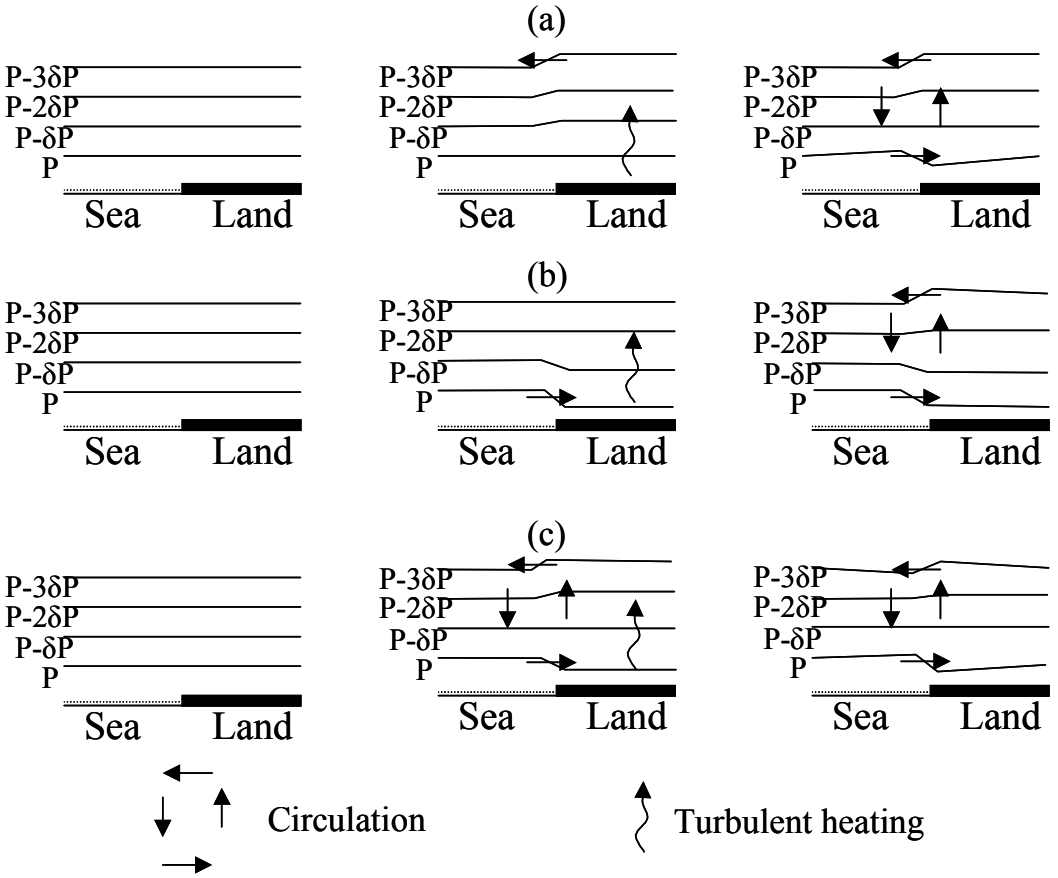

FIGURE 2.3: Schematic diagram illustrating the development of the pressure gradients and the sea breeze circulations, in the absence of large scale flow, according to (a) the upwards theory, (b) the sideways theory and (c) the mixed theory. The left handed plots show the initial situations, the middle plots show the initiation of the circulations while the right-hand plost show the final situations with fully developed sea breeze circulations. (Adapted from: Tijm and Van Delden, 1999)

2.2.3. Stages of sea breeze development

The word surge is used to describe a sudden increase in wind speed at anemometer level with no necessary connotation to temperature change (Clarke, 1983). For the case of an onshore geostrophic wind, Clarke (1984), in his studies in Northern Australia, identified five stages in the development of a sea breeze surge, namely, the immature stage, the early mature stage, the late mature stage, the early degenerate stage and the late degenerate stage.

a) The immature stage

The 'immature stage' is found where the inland penetration of the sea breeze increases with time, the circulation is unsteady and assumes the shape of a raised head. (Fig. 2.1) In the head, the dense marine air is swept up and backward and is maintained by convective overturning (Clarke 1984; Buckley and Kurzeja 1997). Off-shore airflow creates a shear zone that lifts the denser air, creating billows or horizontal vortices along the interface at the head and top of the front. These Kelvin-Helmholtz (KH)

billows are unstable and eventually break down, leaving a turbulent wake that plays a crucial role in the mixing process (Simpson, 1994).

b) The early mature stage

This stage occurs in the late afternoon. By this time the head is about twice the height of the flow behind it, but it does not have a pronounced nose and the SBF is very steep vertically (Sha *et al*., 1991). The sea breeze surge is still not a steady-state gravity current, but acceleration of the surge has started (Clarke, 1984). The speed of the sea breeze front is controlled by the density difference across it at any time, which in turn is determined by the amount of heat supplied (Simpson *et al.,* 1977). There are three stages in the speed of penetration of the sea breeze. These three stages can be explained by taking into account that the temperature of the sea breeze increases as it moves inland. Consequently, the temperature contrast across the front decreases and the sea breeze decelerates after the initial acceleration which occurred during the immature stage. Kelvin-Helmholtz instability increases the top drag and this increased friction also causes deceleration of the sea breeze. (Sha *et al.,* 1991). Veering or backing of the wind, because of Coriolis force influence, could also cause a decrease in speed, as observed by Tijm *et al.* (1999a) in their studies of the sea breezes in the Netherlands. Sea breezes on the Namibian coast showed clear evidence of adjusting to the Coriolis force (Lindesay and Tyson 1990). The speed of the sea breeze front varied between 5-7ms^{-1} at first to 1-2ms^{-1} later in the day in a study done by Fosberg and Schroeder (1966) in California. Other studies found similar speeds of the sea breeze in different parts of the world, *e.g.* Greece, (Prezerakos, 1986; Asimakopoulos *et al*., 1999), England (Simpson, 1994) and also in model simulations (Estoque, 1961; Sha *et al.,* 1991). In late afternoon the solar heating decreases, but the temperature of land air still increases gradually. At the same time, the temperature of the sea air becomes cooler, as the sea air arriving at the front has had less heat added to it since crossing the coast. As a result, the temperature difference across the front increases and the sea breeze begins to accelerate again. In the nocturnal stage of the sea breeze, horizontal advection of cool sea air is instrumental in maintaining the frontal density gradient. This advection of cool sea air ceases once the air, which crossed the coast near sunset, reaches the front (Abbs and Physick, 1992). During the early evening, the leading edge of the surge begins to flatten as the moist cool air supply gets cut off.

c) The late mature stage

The front remains sharp as the centre of the horizontal vortex shifts to the leading edge of the circulation in this stage.

d) The early degenerate stage

After sunset, the sea breeze surge flattens and spreads inland as an unsteady gravity current. This results in a reduction in height of the sea breeze head, because of reduced vertical mixing. As the sea breeze moves inland, prefrontal perturbations and/or gravity waves in the stable layer may be generated due to the existing temperature inversion. A sea breeze cut-off vortex (undular bore) often forms at this time and it penetrates even further inland (Clarke 1984, Bukley and Kurzeja 1997). An example of this is the "morning glory" that occurs in the southern and central parts of Australia.

e) The late degenerate stage

Physick and Smith (1985) showed that once the vortex has formed, the main heating process that occurs is the subsidence warming in the descending arm of the circulation, which leads to the decay of the density gradient and the vortex itself. The circulation is no longer closed and may be considered as an unsteady long wave followed by the degenerating gravity current (Buckley and Kurzeja 1997). The Coriolis force turns the flow and limits the inland penetration, while surface cooling decouples the layers (Buckley and Kurzeja 1997).

2.3. Characteristics of the sea breeze

2.3.1. The depth of the sea breeze

The depth of the sea air, usually defined by the level of zero onshore wind component, is often less than half the vertical extent of the sea breeze system (Abbs and Physick, 1992). At any given location, the depth of the sea breeze varies with the time of day, due to the migration of the system inland and to thickening of the layer of sea air as the day progresses. Atkinson (1981) theorized that the ability of a local circulation to penetrate vertically into the troposphere is a function of its intensity, of atmospheric stability and of the synoptic wind. The tropics offer the greatest potential for vertical development, because of the strong heat supply, the radiative instability of the troposphere and the weakness of synoptic flows (Oliphant *et al*., 2001). Variations of the height of flow can also be caused by sea air over-riding land air (Koschmieder, 1936). In Florida, the depth of the sea breeze varies between 20m and 1km (Cangialosi, 2003). In Indonesia the sea breeze depth varied between 0.4km to 1.4km, depending on the time of day (Hadi *et al*., 2002). Along the New South Wales coast, Australia, Batt (2005) reported sea breeze depths varying between 100m to 800m.

2.3.2. The horizontal extent of the sea breeze

The sea breeze system extends over land and sea and grows in both directions as the day progresses (Physick, 1980). In a modelling study of the southern England sea breeze, Physick (1980) found that after stable conditions set in about an hour before sunset, the sea breeze circulation detached itself from the coastline and moved inland, decreasing in size during the night until it virtually disappeared by 23:00 local time over 100km inland.

The distance of inland penetration of the sea breeze varies considerably over different parts of the world. Factors such as temperature differences between land air and sea air, along with other factors such as the Coriolis force influences and the distance the sea breeze penetrates inland (Simpson, 1994). The inland penetration of sea breezes varies between 30km, in Boston, USA (Davis *et al.,* 1980), and 300 km in southern and central Australia (Clarke *et al.,* 1981). The distance it penetrates inland depends primarily on the heating over land, but ambient wind is also an important factor (Clarke 1983). Markedly different sea breezes can occur in the same region within a few days, depending on the synoptic conditions and variation in the temperature difference between sea and land air (Physick, 1980). The synoptic wind affects not only the formation of the sea breeze, but also its subsequent movement inland (Simpson *et al*., 1977).

2.3.3. Influences on the sea breeze character

The factors that influence the character of sea/land breeze systems include: the synoptic wind (*e.g.* Arritt, 1993); the Coriolis force (*e.g.* Zhong and Takle, 1993); topography (*e.g.* Abbs and Physick, 1992); coastline curvature (*e.g.* Clarke 1984); surface roughness (*e.g.* Bechtold *et al*., 1991); sea surface temperatures, (*e.g.* Franchito *et al*., 1998); soil moisture (*e.g.* Physick, 1980) and clouds (*e.g.* Segal *et al.,* 1986). The relative importance of these factors depends on the latitude, the physical environment, air mass characteristics and synoptic scale pressure gradients (Oliphant *et al*., 2001).

a) Synoptic influences

The pronounced sensitivity of the sea breeze to the direction of the synoptic flow has been attributed by most investigators to the lack of heating and convective mixing over water (*e.g.* Estoque, 1962; Mahrer and Pielke 1977b) and to the enhancement of the horizontal temperature (and consequently pressure) gradient due to the convergence between the sea breeze and the opposing large-scale flow (Atkinson, 1981). The synoptic influence on the sea breeze can be classified into four different categories: onshore synoptic flow; calm to moderate opposing flow (with inland penetration of the sea

breeze); strong opposing synoptic flow (sea breeze develops with no inland penetration) and very strong opposing synoptic flow (no sea breeze, flow off-shore everywhere). (Arritt, 1993)

i) Onshore synoptic flow

Clarke (1983, 1984) modelled deeply penetrating sea breezes and found that when the sea breeze was aided by an onshore component of the large-scale flow, it ascended mountain ranges and was still detected, in some form, hundreds of kilometres inland. Modest assisting ambient wind causes sea breeze surges to form well inland even relatively late in the day and move more rapidly than when no assisting wind is present (Clarke, 1983). With gradient flow reinforcing the sea breeze, the circulation begins earlier in the day and penetrates perhaps 40-50km inland. The maximum vertical extent, observed in a series of studies in the New York area, under light gradient conditions was 910m with maximum speeds of 7.65–10ms^{-1} found below 303m above ground level (Frizzola and Fisher, 1963). Temperature and dew point changes were gradual in this study, although local wind changes could have been abrupt, depending on the terrain features. Arritt (1993) found, however, that when strong large-scale flow is in the same direction as the sea breeze, the convergence frontogenesis is suppressed. The resulting sea breeze is merely a weak thermal perturbation of the large-scale flow (Arritt, 1993).

ii) Calm to moderate opposing synoptic flow

Ambient wind has long been known to have a significant effect on the evolution of the sea breeze. Estoque (1962) found that ambient wind directed off-shore, intensifies the sea breeze perturbation by concentrating the horizontal temperature gradient. In a study on the effect of synoptic flow on the frontogenesis of the sea breeze, Arritt (1993) found that positive feedback is realized between the convergence frontogenesis and the strength of the front. The convergence zone is located in a region of near-neutral stability so that large vertical and horizontal wind velocities can develop. Maximum breeze intensity occurred with a 5ms^{-1} off-shore wind (Bechtold *et al.,* 1991). This maximum is obtained when the propagation speed of the sea breeze front is cancelled out by the large-scale flow, leading to a SBF stationary with respect to the coastline (Bechtold *et al.,* 1991). The SBF that develops under opposing gradient flow, forms later in the day, penetrates inland abruptly and retreats much earlier (Koschmieder and Hornickel, 1942; Frizzola and Fisher, 1963; Simpson, 1994). Bonnardot *et al.* (2005) found that the sea breeze which developed under off-shore synoptic conditions in the south-western Cape, South Africa, generated greater temperature decreases than with onshore synoptic conditions. The maximum wind speed for the sea breeze is greater for weak opposing synoptic flow than for a large-scale environment at rest (Arritt, 1993). An opposing wind lengthens the head profile and reduces the height of the foremost point, or nose (Buckley and Kurzeja, 1997). When the winds are off-shore, wedging of marine air under

the inland air results in a much shallower sea breeze, which is still characterized by the nocturnal jets ($10ms^{-1}$) which bring in marine air (Buckley and Kurzeja, 1997).

iii) Strong opposing synoptic flow

The strong opposing synoptic flow promotes convergence frontogenesis as in the previous case. The difference is that the convergence zone is typically located in a statically stable environment, so that the vertical motions are suppressed (Arritt, 1993). The horizontal velocities were also weakened, but to a lesser degree than the vertical velocities. The effect of static stability in weakening the sea breeze is generally consistent to linear theory described by Defant (1951). Strong opposing gradient wind conditions result in shallow, frontal type sea breezes (Kimble, 1946; Defant, 1951). A sea breeze could exist entirely off-shore, if the opposing large-scale flow is strong enough (Arritt, 1993). It is possible for coastal regions to be influenced by sea breeze induced convection even in the absence of onshore flow at the coastline. However, this variety of sea breeze is weaker than the sea breeze which reaches the coast. The sea breeze which remains entirely off-shore would have relatively small vertical velocities, thus reducing the ability of the sea breeze to trigger deep convection (Arritt, 1993).

iv) Very strong opposing synoptic flow

In these conditions, convergence is no longer capable of intensifying the horizontal temperature gradient. A shoreward component may still be apparent as a perturbation from the large-scale flow, but vertical velocities and horizontal temperature gradients are weak. (Arritt, 1993).

b) The influence of topography

The topography of the coastline has an important controlling effect on the sea breeze, as well as influencing the inland penetration of the sea breeze. This is due to the affect of the associated convergence/divergence, which in turn affects associated weather. It may also affect the number of sea breezes experienced (Abbs and Physick, 1992). Abbs and Physick (1992) found indications that it might also have an effect on the onset time. Modelling results (Abbs, 1986) showed that the ocean breeze responded to the effects of both heated land surface and the surrounding orography as it moved inland and that the orography was of greatest importance in cases of off-shore synoptic flow. Sea breeze and mountain circulations together produced a more intense circulation than they did when acting separately (Maher and Pielke, 1977a, Goldreich *et al*., 1986; Preston-Whyte and Tyson, 1988; Lindesay and Tyson, 1990). Observations by Buckley and Kurzeja (1997) showed greater wind speeds and higher wave amplitudes and a less well-defined front, due to the influence of topography on the sea breeze. In Kwa-

Zulu Natal (South Africa) it was difficult to separate the inland advancing sea breeze from the valley breezes which were also moving in the same direction during the day (Preston-Whyte and Tyson, 1988).

c) The influence of coastline curvature

Features on a curved coastline can affect the growth of the pressure field which creates the sea breeze (Simpson, 1994). The sea breeze usually starts to move inland at right angles to the land boundary. When the coast is straight, a more or less uniform sea breeze spreads inland. If the coast is not straight, then the flow inland is not uniform, but converges or diverges according to the curvature of the coastline (Fig. 2.4). On a curved coastline, the sea breeze converges at convex coasts and diverges at concave coasts. As most coastlines are curved in some way, this effect is very important in the development of the sea breeze and areas of convergence and divergence are frequently formed. Incoming air, which rises at the convergence line, is often associated with convective clouds and rain (Simpson, 1994; Neumann, 1951).

In regions where the coastline changes direction suddenly, such as a gulf or a bay, it is possible to produce two sea breezes (Fig. 2.5). The first of these would be the bay breeze, which is the response to the temperature difference between the waters of the bay and the surrounding coastline. The second is the ocean breeze, which originates along the 'large-scale' coastline (Abbs and Physick, 1992).

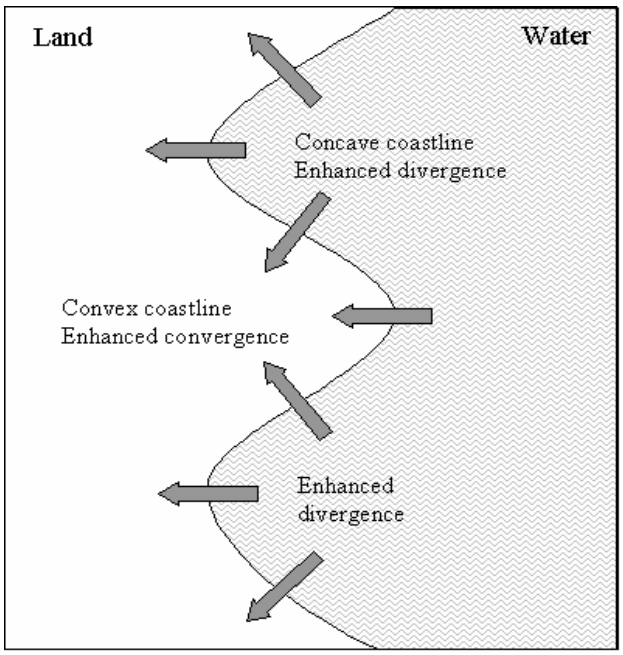

FIGURE 2.4: An example of the effect of coastline curvature on the penetration of the sea breeze. Concave coastline causes enhanced divergence and convex coastline causes enhanced convergence.

A bay possesses both concave and convex properties; a square bay, for example, would exhibit concavity in its upper reaches, while the junctions of the sides of the bay with the main body of water would constitute convex coasts. According to this simple argument, McPherson (1970) found that the sea breeze would tend to be convergent on either side of the bay and divergent directly inland from it (Fig. 2.5).

Convergence zones are especially common at headlands and peninsulas, both areas of strongly convex coastlines (Simpson, 1994). In a simple 'double coast' model (Clarke, 1984), sea breezes formed on both sides of a peninsula with two parallel coastlines and approached each other during the day. One was assisted and the other resisted by the existing gradient wind. In time, the former became more vigorous than the latter and eventually the two sea breezes collided, nearer one coast than the other. With a peninsula width of about 30 – 50 km, the vertical velocity observed because of the merger of two sea breezes was three times greater than that of the general sea breeze in the absence of a merger (Xian and Pielke, 1991). The coastline of the South-Western Cape lends itself to mergers such as these with False Bay, Table Bay and the Cape Peninsula providing ideal conditions for convergence and divergence of sea breezes to occur.

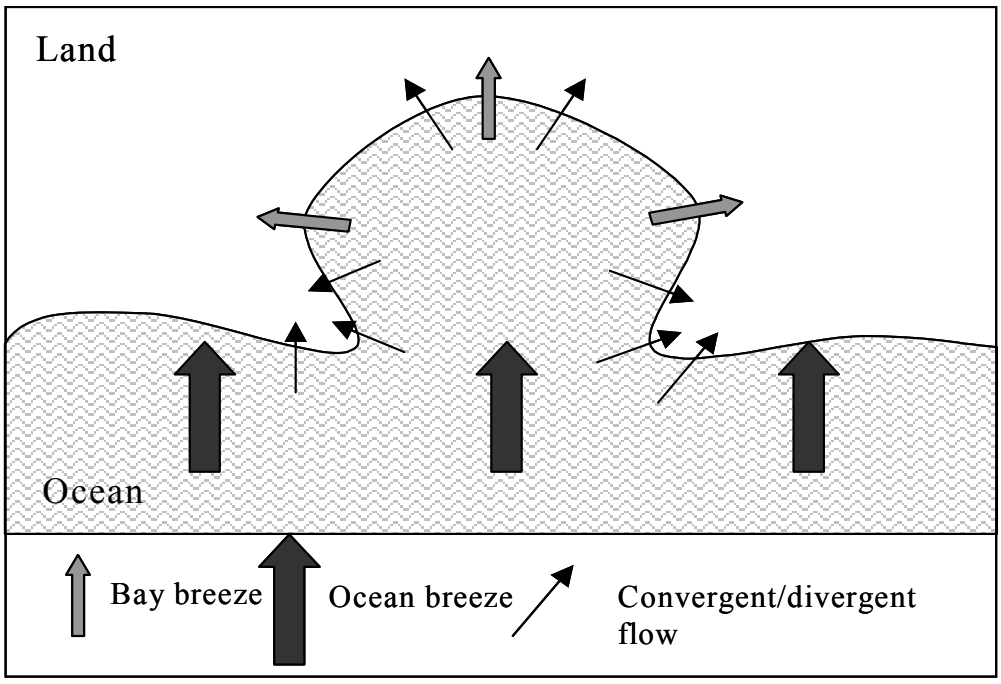

FIGURE 2.5: Double sea breezes forming over a bay. The first being the bay breeze (grey arrows) and the ocean breeze (black arrows). The line arrows illustrate the convergent and divergent flow around the bay.

d) The Coriolis influence

The Coriolis force is an apparent force that deflects any object moving over the surface of a rotating body (to the left/right in the southern/northern hemisphere) without altering its speed. The force acts at right angles to the direction of motion and declines from a maximum value at the poles to zero at the equator (Preston-Whyte and Tyson, 1988). Thus, the force is small or negligible at tropical latitudes and only influences sea breezes in latitudes higher than 5 degrees.

Neumann (1977), Burk and Staley (1978) and Kusuda and Alpert (1983) found that although the fundamental rate of change of direction of the sea breeze is given by the Coriolis parameter, this rate is not uniform in space or time because of the interactions between the meso-scale and large-scale pressure gradients with the breezes, friction and non-linear advection. The sea breeze in southern Australia has a tendency to back to the southeast during its lifetime (Abbs, 1986). In the Namib, the sea breeze backs southwest through the day under the influence of the Coriolis force (Lindesay and Tyson, 1990; Preston-Whyte and Tyson, 1988) and along the Kwa-Zulu Natal coast in South Africa, the backing to the left causes the sea breeze to be north-easterly (Preston-Whyte and Tyson, 1988).

The turning of the sea breeze limits the inland penetration (Buckley and Kurzeja, 1997) and speed of the sea breeze (Tijm *et al.,* 1999b). However, the sea breeze can penetrate far inland without being turned aside by Coriolis acceleration, if its inland component of motion is geostrophic (Clarke, 1984).

The Coriolis force, along with thermal forcing, can assist the sea breeze on a small island to obtain the same intensity as that of a larger land surface at higher latitude (Xian and Pielke, 1991). This is due to the intensity of the alongshore wind component increasing as the latitude increases. The Coriolis force is more effective in transferring momentum to the alongshore component at the expense of the onshore component as the latitude increases (Xian and Pielke, 1991).

McPherson (1970) found that Coriolis acceleration caused an asymmetry of the sea breeze with respect to a bay. The primary component of the flow was onshore, driven by the temperature gradient across the main coastline. The Coriolis acceleration acted on this flow and caused an eastward veering in this case. Along the east side of the model bay, the component of the pressure gradient force normal to the bay coast was directed eastward, or in the same sense as the Coriolis acceleration. Along the west side of the bay, however, the component of the pressure gradient force normal to the bay coast was directed westward, so that this force and the Coriolis acceleration acted in opposition. The result was a relative enhancement of the convergence west of the bay as compared to the conditions on the east side.

e) The effect of surface roughness

Surface roughness appears to have a mixing effect rather than a friction effect on the sea breeze flow (Bechtold *et al*., 1991). Comparing the east and west-coast breezes, Preston-Whyte and Tyson (1988) found that temperature gradients between the warm Agulhas current and the well-vegetated east coast of South Africa were much smaller than those along the west coast, between the vegetation bare desert and the cold Benguela current. The local winds on the east coast were thus correspondingly weaker than on the west coast. (Preston-Whyte and Tyson, 1988).

f) The influence of sea surface temperature

Because sea breeze development depends to a large extent on the temperature difference between land and sea, coastal upwelling plays a part in the initiation of sea breeze and it subsequently affects the movement and orientation of the sea breeze front. (Glen *et al.,* 2003)

A rapid decrease in sea surface temperature near the coast, characteristic of coastal upwelling, produces important alterations in the sea breeze-land breeze circulation. Coastal upwelling is defined as the rising of water from between 200 and 400m deep to the surface along coastlines where an alongshore blowing wind has the coast on its left in the Northern Hemisphere and on its right in the Southern Hemisphere (Glickman, 2000). Low-level cooling of the atmosphere over the cold water causes a shallower, sharper, faster and longer lasting sea breeze front that penetrates more than twice as far inland than it would without the upwelling (Clancy *et al.,* 1979). In general, the cold water causes an increase in the low-level sea breeze intensity (Franchito *et al*., 1998, O'Brien and Pillsbury, 1974). A model that was used by Franchito *et al.,* (1998), showed that the sea breeze was stronger at Cabo Frio, Brazil, during the months when upwelling occurred than during the months when the upwelling did not occur. They also found that upwelling was enhanced by the sea breeze primarily through the intensification of the prevailing wind caused by the sea breeze. Thus it was suggested that there was a positive feedback between the sea breeze and coastal upwelling. Clancy *et al.* (1979) found, that although this positive feedback exists between coastal upwelling and the sea breeze, it is exceedingly weak.

g) The effect of soil moisture

Soil moisture content and the type of vegetative cover determine the magnitude of the latent heat flux and thus indirectly influence the sensible heat flux. As the latter is mainly responsible for the diurnal variation of air temperature over the land, it can be seen that, in coastal regions, soil wetness is an important factor in the type of sea breeze experienced on a particular day (Physick, 1980).

In a two-dimensional model study of the influence of soil moisture on the sea breeze, Physick (1980) found that the inland penetration rate of the sea breeze varied significantly with differences in soil moisture and that the sea breeze intensity decreased as soil moisture increased. Yan and Anthes (1988) showed that sea breeze circulation associated with dry land was significantly stronger than that associated with moist land. Miao *et al.* (2003) found that a reduction of soil moisture lead to higher values of the horizontal and vertical wind components of the sea breeze as well as a more penetrative sea breeze in Spain.

h) The influence of clouds

On cloudy days, convection currents over the land (due to solar heating) are restricted. Thus, sea breeze circulation should not develop to any appreciable extent (Batt, 2005). In the Namib Desert (Namibia), middle and high-level clouds were found to have a dampening effect on the sea breeze in the summer (Lindesay and Tyson, 1990). Segal *et al.* (1986) also documented the dampening effects of clouds on sea breezes, but Sturman and Tyson (1981) found that, in New Zealand, the sea breezes develop in the presence of cloud.

2.4. Influences of the sea breeze

2.4.1. Temperature and relative humidity

The passage of the leading edge of a sea or lake breeze is indicated by a near simultaneous decrease in temperature and increase in relative humidity (Estoque *et al.,* 1976; Physick 1982).

There is an increase in surface temperature with increase in distance from the ocean and a tendency for surface cooling to occur after the passage of the sea breeze front. The rate of surface heating slows in the morning and is more rapid in the afternoon (Mahrer and Pielke, 1977b). Variation in heating rate is due to the inland advection of cooler marine air with the associated stronger surface layer winds of the sea breeze. Higher wind speeds cause increased vertical mixing of the near-surface warm air, as well as enhanced cooling by evaporation of moisture from the ground (Mahrer and Pielke, 1977b).

During an investigation of the influence of the False Bay sea breeze on wind, temperature and relative humidity in South Africa, Bonnardot *et al.* (2001) found that although the sea breeze itself reaches as far as 100km inland, the effect it has on temperature and relative humidity decreases with greater rapidity with distance from the coast.

The temperature fields of a lake breeze showed cold air behind the lake breeze front (Estoque *et al.,* 1976). The coldest air was located slightly above the surface (20m). The warmer air at the surface was presumably due to heating from the ground. The air was relatively warm near the top of the onshore flow. The top of the onshore flow was also the top of the temperature inversion (Estoque *et al*., 1976). Sensible heating could not cause these higher temperatures from the surface because the (internal) boundary layer was too shallow. The increased temperatures must, therefore, have been the result of downward advection of warm air (Tijm *et al*., 1999a). A minimum value of humidity mixing ratio was found behind the head of the front, most often about 800m behind. This indicated dry air which descended behind the front and which was subsequently mixed with the moist sea air (Simpson *et al*., 1977).

2.4.2. Wind

The arrival of the sea breeze at the surface was shown by an increase in wind speed (Asimakopoulos *et al*., 1999, Bonnardot *et al.,* 2001) and a sharp shift in wind direction (Estoque *et al.,* 1976) at the surface.

An interesting influence of the sea breeze on wind is the formation of the "morning glory" in southern and central Australia. The morning glory is an atmospheric undular bore propagation on the nocturnal or maritime inversion that forms due to the interaction of the east coast sea breeze with the nocturnal inversion. With time, this SBF develops into a closed vortex which persists for many hours following sunset (Clarke *et al*., 1981).

2.4.3. Cloud formation

The upward branch of the sea breeze development is often visible from satellite pictures in the form of cumulus clouds which develop because of the expansion, cooling and increase in relative humidity of the air parcels. If other atmospheric conditions are favourable for the formation for thunderstorms, the sea breeze may provide just enough lift to cause convective development. The area behind the SBF is clear, because of cool stable air being carried inland from the ocean. (Ackerman, 2005). In Florida, USA, it has long been recognized that the sea breezes from the east and west coasts of the peninsula strongly influence the development of deep cumulus convection (*e.g.* Pielke 1974, and Simpson *et al.,* 1980). Under synoptically undisturbed conditions, convection develops along boundary layer convergence lines associated with sea breezes. Depending on the mean wind direction, cold outflow from convection along the SBF may interact with the sea breeze convergence zone from the other coast and produce strong thunderstorms (*e.g.* Kingsmill 1995; Wilson and Megenhardt, 1997)

Neumann (1951) showed that the variation in the percentage of thunderstorms within coastal areas is connected in part with the convergent or divergent nature of the sea and land breezes involved. As sea breezes converge, the winds are deflected upward in the convergence zone and become strong updrafts (Abbs and Physick, 1992) that lead to cloud and thunderstorm formation.

2.4.4. Pollution

Changes in turbulence, critical wind velocity and boundary layer depth due to the passage of the sea breeze front, significantly impact the stable boundary layer, making it a dominant factor in trace chemical transport. (Buckley and Kurzeja, 1997).

In California, the sea breeze generally has a 'purging' effect, but the stable layering, together with the diurnal reversal of both the mountain-valley and land-sea breezes are problematic, maintaining dangerous concentrations of pollution at Los Angeles and other coastal towns (Simpson 1994). Smog is transported by a circulation resulting from interaction between the sea breeze and the thermally and topographically induced flow, known as the extended sea breeze (Kurita *et al.,* 1985; Chang *et al*., 1989; Kondo 1990; Abbs and Physick, 1992)

Simpson and Britter (1980) pointed out that no mixing took place at the interface between the sea breeze inflow and the return flow above. This implies that emissions of pollutants into the sea breeze are transported inland virtually undiluted, then rise and mix with ambient air at the front. Furthermore, a 'clean' sea breeze sweeps the polluted ambient air upward and removes it seaward at higher levels while maintaining unpolluted air at the ground.

The thermal internal boundary layer, which develops in the stable air as the sea breeze passes over land, can be responsible for enhanced surface concentrations downwind of a coastal source (Abbs and Physick, 1992). Lyons and Olsson (1973) found that not only did the same fumigation mechanism occur in Chicago, but also that the air quality problem was exacerbated by recirculation of pollutants within the lake breeze circulation. Pollutants fumigated into the inflow, rose at the front and moved back over the lake in the return flow. However, the larger pollutant particles subsided into the top region of the inflow and were brought back over land where they were fumigated to the ground once again along with the fresh emissions from the coastal sources, leading to an ever-increasing loading of the atmosphere in the shoreline region.

Ozone is formed on a time-scale of several hours through reactions involving non-methane hydrocarbons and nitrogen oxides in the presence of ultra violet radiation (Abbs and Physick, 1992). In coastal cities, the local meteorology in summertime is such that land breezes or light off-shore synoptic winds advect emissions from the morning peak traffic period out over the sea. Here the mixture is able to 'cook' for a few hours, unhindered by sources of fresh nitric oxide (NO) which are likely to reduce the ozone levels. When the sea breeze develops in the late morning, the ozone gets transported onshore and over the city and suburbs responsible for its precursors. Under these conditions, the highest ozone levels are usually found within 30 – 40 km of the coastal source (Abbs and Physick, 1992)

The deep inland penetration achieved by some sea breezes suggests that pollution from coastal regions might be transported large distances from the source (Abbs and Physick, 1992)

2.5. Summary

In this chapter the sea breeze was defined and different theories regarding its development were discussed. The five stages of development give an overall view of the movement and character of the SBF throughout its development and degeneration. The vertical and horizontal extent of the sea breeze varies from place to place and also, under different synoptic conditions, in the same location. A weak off-shore synoptic flow causes a much stronger sea breeze by concentrating the horizontal temperature gradient, than a sea breeze developing in light onshore or even calm conditions. Topography also has an important controlling effect on the sea breeze and influences the inland penetration and its associated convergence or divergence. Sea breeze and mountain circulations, together, produce a more intense circulation than they do separately. The curvature of a coastline also effects the sea breeze penetration by causing convergence or divergence for convex or concave coastlines respectively. A peninsula with a width of 30 –50km can cause vertical velocities of up to three times higher than that of the sea breezes moving from both sides of it through the merger of the two sea breezes.

Chapter 3 The Regional Atmospheric Modelling System (RAMS)

3.1. Introduction

In this chapter, the Regional Atmospheric Modelling System (RAMS) is discussed. First, the development and the general characteristics of the model are detailed and then the model specifications as used in this research are given.

3.2. The RAMS model

The RAMS is a multipurpose numerical prediction model that simulates atmospheric circulations ranging in scale from an entire hemisphere down to large eddy simulations (LES) of the planetary boundary layer. It is most frequently used to simulate atmospheric phenomena at the mesoscale (horizontal scales from 2km – 2000km). Its applications range from operational weather forecasting to air quality regulatory applications and support of basic research (Cotton *et al.,* 2003). RAMS has often been successfully used with resolutions as high as 1m for individual building simulation (Tremback and Walko, 2004), and 1cm for direct wind tunnel simulation (Trini-Castelli *et al.*, 2003; Trini-Castelli *et al.*, 2004).

The RAMS model was developed in order to merge several numerical weather simulation codes that were being used at the Colorado State University. Enhancements, such as telescoping and interactive nested grid capability (Pielke *et al.* 1992) were added to the existing capabilities of the various models used for the development of RAMS.

3.2.1. Nesting

Based on two-way grid interactive procedures, RAMS has a multiple grid-nesting scheme that allows it to solve the model equations simultaneously on any number of interacting computational meshes of differing spatial resolution which can be specified and moved by the user (Cotton *et al.,* 2003). The model has a non-hydrostatic option so that all meteorologically relevant spatial scales can be represented (Pielke *et al.,* 1992).

3.2.2. Plug-compatible modules

RAMS uses the concept of 'plug-compatible' modules in order to assist developers of parameterizations to interface into RAMS. A plug-compatible module is defined as a module where the

interface between the subroutines and the rest of RAMS is clearly defined to users of the code. The use of a FORTRAN pre-processor permits RAMS to be configured easily at the time of initialisation into one of a wide variety of different models simply by choosing the numerical or physical options required by the user (Pielke *et al.,* 1992).

3.2.3. Isentropic analysis

In order to perform data analysis tasks for the initial and boundary conditions for larger-scale runs (25km and 5km resolution), the RAMS model includes the ISentropic ANalysis package (RAMS/ISAN). In a stable stratified atmosphere where potential temperature is a monotonically increasing function of height, these levels of potential temperature may be used as a vertical coordinate, namely, the isentropic coordinate (Holton, 1992). According to Pielke *et al.* (1992) using the isentropic coordinates has several advantages over other coordinate systems when applied to large-scale (e.g. 25km resolution) data analysis.

The advantages of isentropic coordinates are:

- An objective analysis performed on an isentropic surface of synoptic scale flow better approximates the inter-station variability of the atmospheric fields, because synoptic scale flow is, at first approximation, adiabatic.
- Isentropes tend to be "packed" in frontal areas and therefore, provide enhanced resolution along frontal discontinuities.
- Short wavelength features in the vicinity of fronts can be more accurately analyzed with much less smoothing than other coordinate systems, because isentropes are sloped in the vicinity of fronts.

Disadvantages of isentropic coordinates are:

- The vertical resolution decreases as the atmospheric stability decreases (e.g. in the planetary boundary layer).
- Isentropes frequently intersect the ground.

RAMS/ISAN has the ability to combine several data sets in the data analysis and its modular structure simplifies insertion of non-standard data sets. The code also supports National Meteorological Centre (NMC) and European Centre for Medium-range Weather Forecasts (ECMWF) data files with a horizontal resolution of 2.5°. NMC rawinsonde and surface observation data sets can also be ingested into RAMS. This includes special soundings, bogus soundings or any additional surface observations that are available (Pielke *et al.,* 1992).

3.2.4. Data analysis

The horizontal wind components, pressure and relative humidity from the gridded global analysis, along with any available rawinsonde data are interpolated vertically to isentropic levels at a user-specified resolution (Pielke *et al.,*1992). The Barnes (1973) objective analysis scheme, using weighted time-series observations is then applied to these variables on the isentropic surfaces with user specified parameters in the scheme, controlling the amount of smoothing. Once the variables have been objectively analyzed to the analysis grid, the Montgomery stream function (the stream function for the geostrophic wind on an isentropic surface (Huschke, 1959)) is then obtained in a hydrostatic integration from an objectively analyzed stream function "boundary condition" at an isentropic level near the tropopause. Any horizontal interpolations use the overlapping polynomical technique described by Bleck and Haagenson (1968).

Surface variables are analyzed in a similar manner. Wind components, potential temperature and relative humidity are objectively analyzed, while pressure and the Montgomery stream function are obtained hydrostatically from the first isentrope above the ground.

Once the isentropic dataset is complete, the atmospheric variables and topography are transferred to the model grid, using overlapping polynomical interpolation (Bleck and Haagenson, 1968). First, the wind components are interpolated on the isentropic surface to the model grid point. The height of the isentropic surface can then be calculated and the wind, potential temperature and relative humidity are interpolated linearly in height to the model's σ_z coordinate levels. Sigma (σ) coordinates indicate the relationship of the air pressure at a certain level to the surface pressure. Sigma z (σ_z) indicates the geometric height of that pressure level above sea level (Phillips, 1957),

$$\sigma_z = \frac{P_z}{P_s} \qquad (1)$$

where P_z is the pressure at a certain height z and P_s is the pressure at the surface. A final hydrostatic integration is done to find the pressure on the model grid (Pielke *et al.,* 1992)

3.2.5. Four-dimensional data assimilation (4DDA)

The RAMS model also has the ability to do four-dimensional data assimilation (4DDA) (Pielke *et al.,* 1992). This involves the effective integration of time dependent observational data into a predictive

model, either done in the initial stages of nudging or in a variational scheme like the adjoint method. This method is not used in this project.

3.2.6. Large Eddy Simulation (LES)

Large Eddy simulation (LES) is a descriptor of high-resolution numerical simulations to which the RAMS model is ideally suited. The smallest resolution used in this study is 200m which makes a detailed discussion of LES unnecessary in this publication.

3.3. This study

The RAMS version 4.3 (Pielke *et al.,* 1992) was used in the non-hydrostatic mode for this study. The simulations were done with four nested grids with resolutions of 25km (grid 1), 5km (grid 2), 1km (grid 3) and 200m (grid 4) respectively. Figure 1.3 shows the 5km, 1km and 200m grids in relation to the Cape Peninsula and the nearby towns. The 200m grid was chosen to cover the winelands south and west of Stellenbosch in order to investigate the influence of the False Bay sea breeze. Three vertical cross sections in the 200m were identified. Their details are given in Table 3.1. Cross section X1 is 4km, X2 is 9km, and X3 14km from the western edge of grid 4. The results of the 200m grid simulations are discussed in the next chapter.

TABLE 3.1: Cross sections of the 200m grid simulations

Cross section	**Longitude**	**Distance from western edge of 200m Grid**
X1	18°43’41” E	4km
X2	18°46’56” E	9km
X3	18°50’12” E	14km

The detailed options activated in RAMS and their uses are given in Table 3.2. The terrain height data imported were real relief provided by the ARC-ISCW. The topographic data were interpolated with a reflected envelope topography scheme which aims to preserve the barrier heights and valley depths. This leads to steep topography in RAMS while still filtering the shortest wavelengths. Topography, however, is smoothed by filtering out details that the model cannot use. Surface roughness length is computed for the computing of surface vertical fluxes of momentum, sensible heat and latent heat. The

LEAF2 sub-model (Table 3.2) of RAMS was used and includes parameterization of the bottom layers of the atmosphere to parameterize accurately the rest of the atmospheric layers.

Sea surface temperature fields were extracted from the ECMWF datasets. Additional sea surface temperature (SST) observations of the South African Weather Service (SAWS) around the Cape Peninsula were incorporated into the ECMWF SST values to give a better distribution of the SSTs in the study area. These SSTs were considered to be constant for each model run. However, the best SST fields were incorporated for the different runs by incorporating the observed SAWS SSTs.

The lateral boundary condition (Table 3.2) is set to the value of each variable, using the value in the field immediately adjacent to the boundary in the interior for the inflow boundaries, while the outflow boundaries are calculated by a spatial differential equation. The characteristic propagation speed of internal gravity waves used in the Klemp-Wilhelmson lateral boundary condition is set to 20 ms^{-1}. Short wave radiative transfer in the model is calculated by the Chen and Cotton parameterization, which takes cloud into account, but does not differentiate between cloud water, rain or ice. This radiative parameterization is exercised to compute updated values for the radiative contribution to tendencies of both atmospheric and land surface temperatures every 900 seconds.

This study is a simulation of a real event and longitudinal variation of the solar hour angle is accounted for in the computation of shortwave solar radiation. Convective parameterization takes place, but the level of microphysics is set to not take deep convection into account. The time interval for computing the contributions to atmospheric tendencies in temperature and moisture by convective parameterization was set to 900 seconds. The initial moisture content of the soil is classified according to the soil type (Sand = dry, Loam = wet). The soil types for the 200m grid were imported as an initial surface file (Fig. 3.1b) from the Agricultural Research Council - Institute for Soil, Climate and Water (ARC-ISCW). Other surface files were topography (Fig. 4.1) and vegetation cover (Fig. 3.1a), also provided by ARC-ISCW.

The meteorological values used for the 1km, 5km and 25km grid simulations were extracted from the ECMWF data. The diffusion coefficients were parameterized according to the Mellor and Yamada (1974) method, where horizontal diffusion is computed as the product of horizontal deformation rate and a length scale squared based on the original Smagorinsky formulation. Vertical diffusion is parameterized by employing a prognostic turbulent kinetic energy. The level of moisture complexity in the atmosphere was activated for condensation of water vapour to cloud water to wherever supersaturation is observed. No other forms of liquid or ice water are considered.

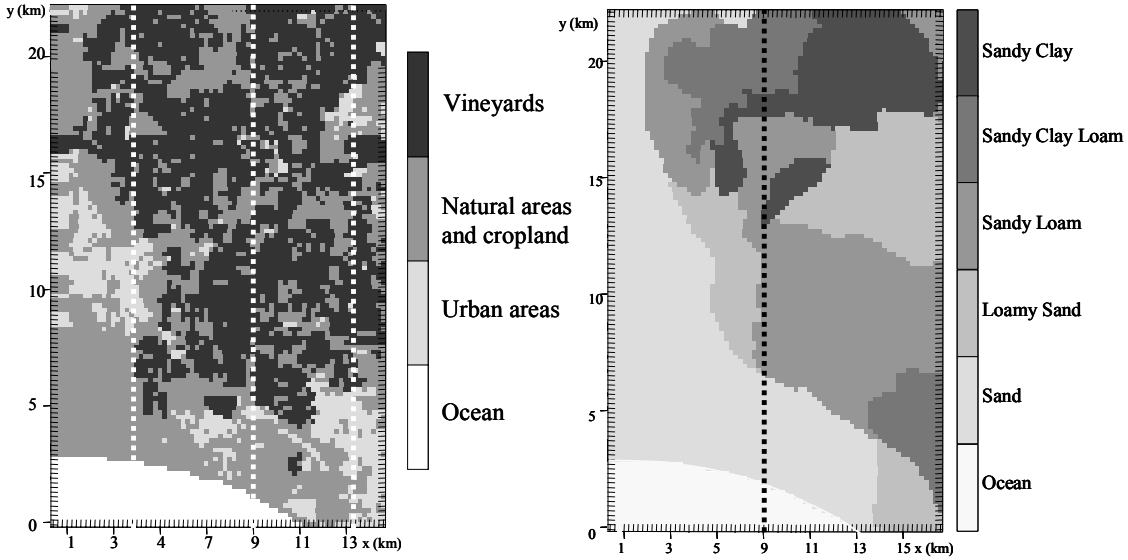

FIGURE 3.1: The vegetation (a) and soil types (b) used in the rams model runs. Vertical cross sections were performed at the locations indicated by dotted lines.

Both positive buoyancy effect of water vapour and the liquid water loading of cloud water are included in the vertical equation of motion. Radiative effects of both water vapour and cloud water are activated, if the radiation parameterization is activated.

A network of five automatic weather stations (AWSs) in the 1km and 200m grids were used to verify the simulated data with observed data on the ground where possible. The verification of the 200m grid simulations are discussed in more detail in the next chapter.

3.4. Summary

The RAMS model was discussed with the specific settings used for this study. The study area and cross sections were pointed out and the imported surface files of topography, soil type and land cover were shown.

TABLE 3.2: Detailed description of the settings for the RAMS simulations for this study (adapted from Walko and Tremback, 2000).

Name	Description	Setting options	Setting for this study
ITOPTFLG	Specifies how terrain height data is to be obtained or computed for each model grid.	0 – Topography interpolated from parent grid (nested grid only) 1 – Topography from RAMS standard topography grid 2 – Topography calculated by a RAMS subroutine 3 – Real relief data imported into RAMS from outside source	3 – Real relief provided by ARC-ISCW
ISSTFLG	Specifies how the sea surface temperature variable is to be acquired or computed for the grid.	0 – SST interpolated from parent grid 1 – SST from RAMS standard SST grid 2 – SST calculated by a RAMS subroutine 3 – Real SST data imported into RAMS from outside source	3 – REAL SST provided by ECMWF and SAWS
IUPDSST	Whether observed SSTs are to be held constant in time during a model run.	0 – Constant 1 – Linearly interpolated in time between observing times immediately before and after the current model runtime	0 – Constant, but the best SST fields were incorporated for the different runs.
ITOPSFLG	The type of processing of topographic data to final values defined on RAMS grid	1 – Conventional mean and a silhouette average are computed, and the value assigned to a certain grid cell is a weighted average, with the weights controlled by a RAMS subroutine. 2- An envelope topography scheme is used to obtain grid values from the parent grid in an attempt to preserve barrier heights. 3 – A reflected envelope topography scheme is used, which aims to preserve both barrier heights and valley depths. This method leads to the steepest topography in RAMS, while still filtering the shortest wavelengths.	3 – Interpolation with the topography filter.
TOPTWVL	Grid dependent variable specifying the wavelength, in grid-cell size units, of the smallest horizontal modes of terrain height data which are to be present on a given model grid.	0 – Off 1 – On	1- Smoothes topography by filtering out details not used by the model.
IZOFLG	Controls how surface roughness length is computed for computing surface vertical fluxes of momentum, sensible heat and latent heat.	0 – standard roughness height evaluation of surface, computed by the LEAF-2 sub-model of RAMS. It includes parameterization of bottom	0 – LEAF-2 parameterizations

		layers of the atmosphere to parameterize accurately the rest of the atmospheric layers. 1 – roughness height computed from roughness of sub-grid scale topography,	
LSFLG	Lateral boundary conditions.	0 – Sets lateral boundary value of each variable to the value in the field immediately adjacent to the boundary in the interior. This is a zero-boundary condition. 1- Similar to 0, using a zero-gradient condition at inflow boundaries, but setting values at outflow boundaries, such that the second spatial derivative in the direction normal to the boundary, is zero. 2 – Identical to 1 for the outflow boundary condition, but holds variables constant in time at the inflow boundaries. 3 - Leaves values at all boundaries, inflow and outflow, unchanged in simulations.	2 – Gradient at bottom of atmosphere 0 and at the top, calculated by differential equation.
CPHAS	Specifies the characteristic propagation speed of internal gravity waves used in the Klemp-Wilhelmson lateral boundary condition		Set to 20m/s
ISWRTYP	The options for evaluating shortwave radiative transfer in the model.	0 – No radiation 1 – Chen and Cotton parameterization 2 – Mahrer and Pielke parameterization 3 – Two-stream parameterization developed by Harrington	1 – Chen and Cotton parameterization takes cloud into account, but doesn't differentiate between cloud water, rain or ice.
RADFRQ	Specifies how often, during a model run, the radiative parameterization is to be exercised to compute updated values for the radiative contribution to tendencies of both atmospheric and land surface temperatures.	600 – 1200 seconds	900 seconds.
LONRAD	Specifies whether the longitudinal variation of solar hour angle is to be accounted for in the computation of shortwave solar radiation, or whether these angles are assumed to be constant over the model domain.	0 – Assumes hour angle is longitudinally constant 1 – Accounts for longitudinal variation	1 – Longitudinal variation, because this study is a simulation of a real event.
NNQPARM	A grid-dependent flag used to control whether the convective parameterization is to be	0 – Leaves parameterization inactive 1 – Activates parameterization	1 – Parameterization of clouds. Level of

	activated or not.		microphysics set at 2 (no deep convection).
CONFRQ	Time interval in seconds, during a simulation, at which contributions to atmospheric tendencies in temperature and moisture by convective parameterization are to be computed.		900 seconds.
SLMSTR	Used to initialize the moisture content of the soil.	Allowable values for this parameter range from 0.0, representing totally dry soil to 1.0, representing totally saturated soil	Soil moisture is classified according to soil type. Sand = dry; Loam = wet. Values are from ECMWF data and is not kept constant.
IDIFFK	Controls the type of parameterization to be used for computing both horizontal and vertical diffusion coefficients.	1 – Mellor and Yamada (1974) method. 2 – 1 dimensional analogue of the Smagorinsky scheme. 3 – Hill and Lilly stability-dependent modifications. 4 – Deardorff scheme.	1 – Mellor and Yamada method. Horizontal diffusion computed as the product of horizontal deformation rate and a length scale squared, based on the original Smagorinsky formulation. Vertical diffusion is parameterized by employing a prognostic turbulent kinetic energy.
LEVEL	Specifies the level of moisture complexity to be activated in the model for explicit cloud modelling.	1 – Activates advection, diffusion and surface flux of water, where all water substance in the atmosphere is assumed to occur as vapour, even if supersaturation occurs. Also activates the buoyancy effect of water vapour in the vertical equation of motion, as well as the radiative effects of water vapour, if radiation is activated elsewhere. 2 – Activates condensation of water vapour to cloud water, wherever supersaturation is observed. No other forms of liquid or ice water are considered. Both positive buoyancy effect of water vapour and the liquid water loading of cloud water are included in the vertical equation of	2 – Condensation of water vapour only.

		motion. Radiative effects of both water vapour and cloud water are activated, if the radiation parameterization is activated. 3 – Activates the bulk microphysics parameterization, which includes cloud water, rain, pristine ice, snow, aggregates, graupel and hail. This parameterization includes the precipitation process.	

Chapter 4 Case studies

4.1 Introduction

In this chapter, three case studies are discussed. Each of these studies was designed to investigate the influence of different synoptic conditions on the development and characteristics of the False Bay sea breeze. The accuracy of the RAMS model in simulating the sea breeze over the South Western Cape is also detailed. The simulations were done with four nested grids which had resolutions of 25km, 5km, 1km and 200m respectively (Fig. 1.3) over the Western Cape Province of South Africa.

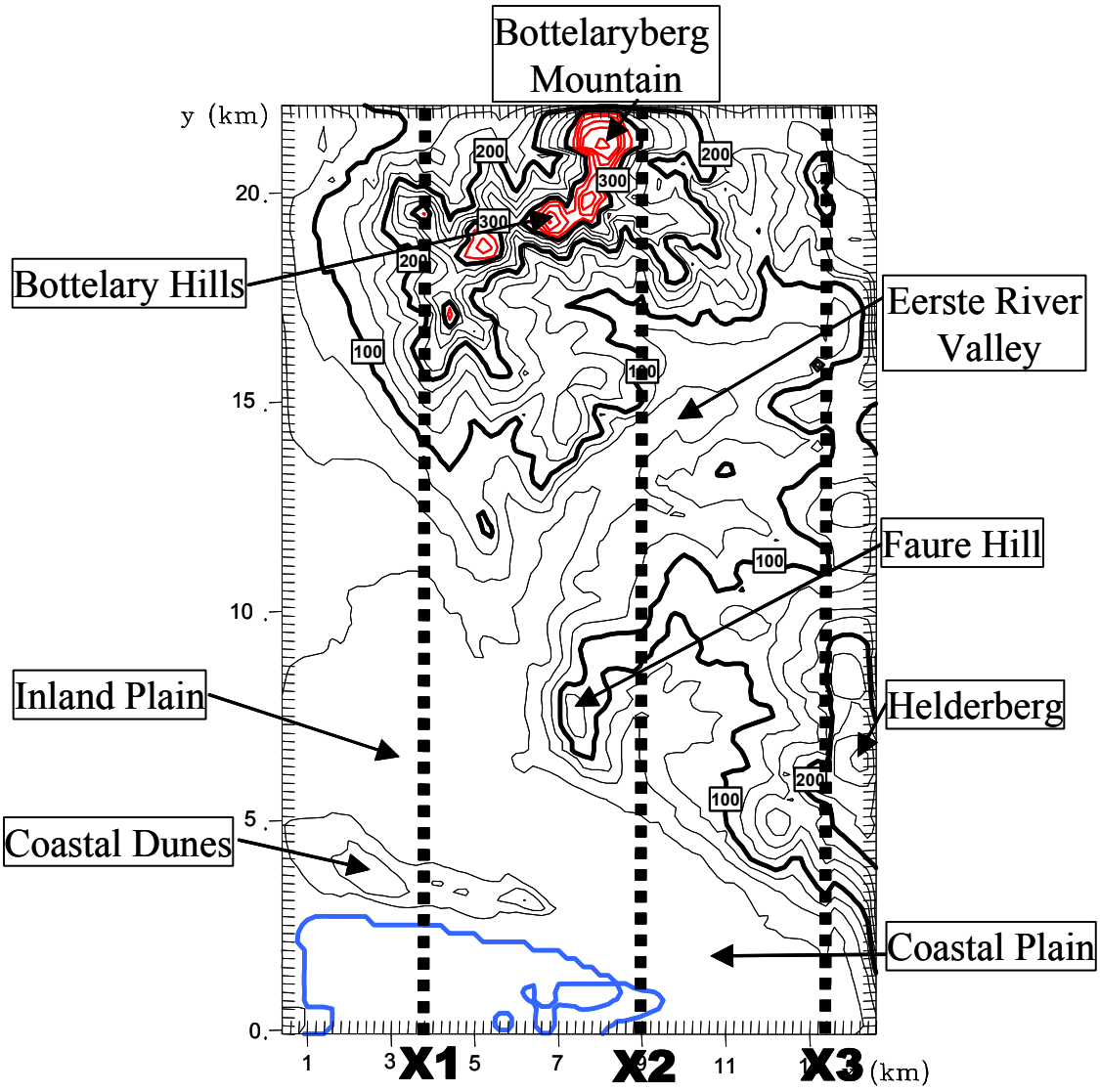

FIGURE 4.1: The topography of the study area with the positions of the cross sections (dotted lines) and places of interest. Heights larger than 300m are shown in red and heights lower than sea level in blue.

The 200m grid covers the wine lands south and west of Stellenbosch. Figure 4.1 gives the topography of the 200m grid. The contour interval is 25m and elevations higher than 300m are shown in

red. The contours lower than sea level are blue. From the topography map the Coastal Dunes, Inland Plain, Bottelary Hills, Bottelaryberg Mountain, Eerste River Valley, Faure Hill, Helderberg and the Coastal Plain can be clearly seen. The location of the 200m grid was chosen in order to investigate the influence of the False Bay sea breeze over the Stellenbosch wine lands also to have different topography in order to facilitate the study of the influence of topography on the sea breeze development and characteristics. Only the results of the 200m grid are discussed. Bonnardot *et al.,* (2001), Bonnardot *et al.,* (2002) and Bonnardot *et al.* (2005) discussed the 1km grid results for 3 and 4 February, 2000, as well as for 18 and 19 February, 2000.

Temperature, relative humidity (RH) and wind speed and direction, as simulated by RAMS, are displayed in maps which depict these variables at an elevation of 30m above the ground. Data are also available at three vertical cross sections. The locations of the vertical cross sections are depicted in figure 4.1 by X1 and X2 and X3 and the values of the meteorological variables at the three cross sections are depicted up to 1km above the ground. The modelled topography at the three cross sections is shown in Fig. 4.2 (a-c).

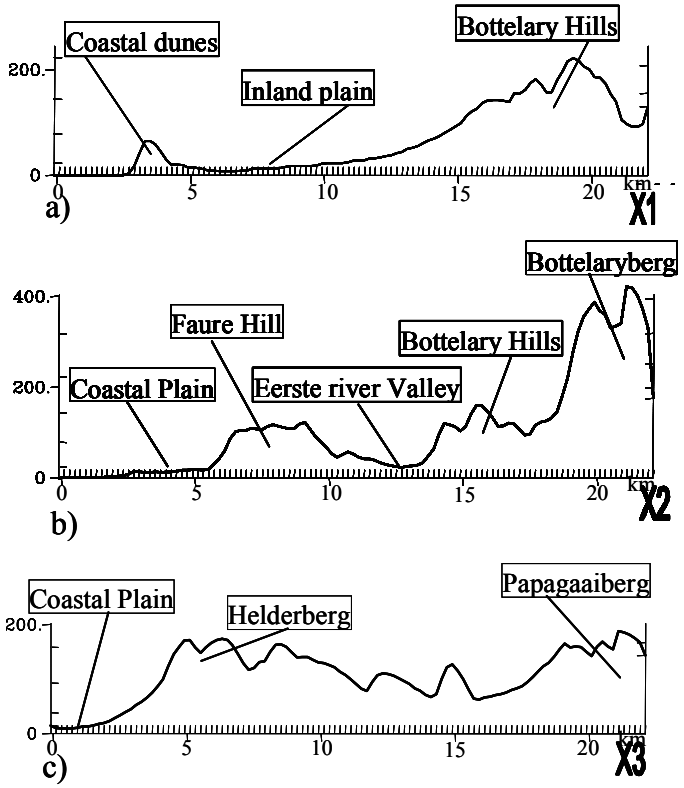

FIGURE 4.2: The topography of cross sections X1 (a), X2 (b) and X3 (c) with height indicated in meters above sea level on the y-axis and the x-axis, indicating distance from the southern edge of the study area (km).

Cross section X1 is at 18º43'41"E, 4km from the western edge of the 200m grid (Table 4.1). This cross section shows the coastal dunes, the inland plain and Bottelary Hills (Fig. 4.2 a). The second

cross section (X2) is at 18º46'56" E, 9 km from the western edge of the 200m grid (Table 3.1), covering the coastal plain, Faure Hill, the Eerste River Valley, Bottelary hills and Bottelaryberg (Fig. 4.2 b). The third cross section, X3, runs along 18º50'12" E, 14km from the western edge of the grid (Table 3.1). This cross section does not include any ocean areas, but does include the coastal plain, Helderberg and Papegaaiberg (Fig. 4.2 c).

RAMS model outputs (temperature, RH and wind speed and direction) are investigated at three-hourly intervals for each case study, starting at: 05:00 SAST for case study 1 (3 February, 2000); 23:00 SAST the previous night for case study 2 (18 February, 2000); and 02:00 SAST for case study 3 (19 February, 2000). The 3rd February, 2000, a weak onshore synoptic flow prevailed. On the 18th February, 2000, the flow was considered to be off-shore and on the 19th February, 2000, it was strong onshore. These days were chosen to investigate the influence of different synoptic conditions on the sea breeze. Larger scale flow was shown to influence the development of the sea breeze (Estoque, 1962; Mahrer and Pielke 1977a; Atkinson, 1981; Arritt, 1993).

The terms used to describe the meteorological variables are shown in Table 4.1. Temperature varies from cold (<19°C) to very hot (>35°C). Relative humidity varies between very low (<40%) to very high (>80%). Wind speed varies between light (0-4.5ms^{-1}) to very strong (>16ms^{-1}).

TABLE 4.1: Terms used to describe temperature, relative humidity and wind speed.

Temperature		Relative Humidity		Wind Speed	
	(°C)		(%)		(ms^{-1})
Cold	<19	Very Low	<40	Light	0-4.5
Cool	19-25	Low	40-60	Moderate	4.5-7
Warm	25-29	High	60-80	Fresh	7-10
Hot	29-35	Very High	>80	Strong	10-16
Very Hot	> 35			Very strong	>16

4.2 Observational data

There are eight automatic weather stations (AWSs) in the study area. These AWSs form part of the larger network of weather stations of the ARC-ISCW. Of the eight weather stations, three were disqualified for use in this study due to their location inside vineyards which may influence the accuracy of meteorological measurements.

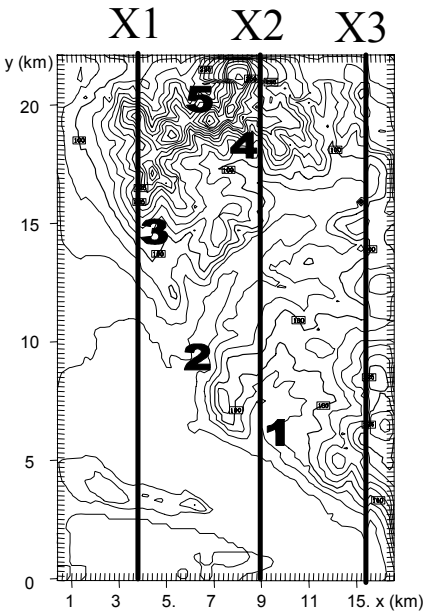

FIGURE 4.3 The geographical position of five automatic weather stations (as numbers 1 to 5) in the study area. The contours indicate the topography of the area.

The geographical positions of the five AWSs are depicted in figure 4.3 as numbers 1 to 5. The details of the stations are shown in Table 4.2.

TABLE 4.2: Information on automatic weather stations used for verification of simulation data for the 200m grid.

Station number	Station name	Shortest distance from coast	Altitude above sea level	Latitude	Longitude	Slope	Obstructions
1	Rustenhof	5km	58m	34.044°S	18.011°E	West	Big tree next to station
2	Meerlust	7km	32m	34.012°S	18.753°E	Southwest	White wall next to station and row of trees 30m West of station.
3	Jacobsdal	12km	130m	33.966°S	18.728°E	Southwest	None
4	Bonfoi	17km	160m	33.915°S	18.780°E	South	None
5	Goedehoop	18km	240m	33.915°S	18.759°E	North-Northwest	A rock to the North and bushes to the Northeast.

Of the five stations two, Stations 2 and 3, are on southwest facing slopes. Stations 1 and 4 are west and south facing, respectively, while Station 5 is on a north-northwest facing slope. Station 2 is the lowest above sea level (32m) with Station 1, 3, 4 and 5 having increasing altitudes respectively. The

obstructions next to the stations are: a big tree next to station 1; a white wall and a row of trees west of Station 2 which might influence temperature and wind observations at the station; and a rock and bushes north and northeast of Station 5, respectively.

4.3 Case study 1: 3 February, 2000 – Onshore synoptic conditions

The 3rd of February, 2000, was chosen as a case study in order to investigate the characteristics of the sea breeze over the Stellenbosch wine lands during weak synoptic onshore flow. Figure 4.6 shows the sea-level pressure field at 14:00 SAST (South African Weather Bureau, 2000). The surface trough dominated the synoptic flow over the central interior. This resulted in a generally easterly to south-easterly flow over the Cape Peninsula as shown by the 14:00 winds at Cape Town International Airport and Cape Agulhas, respectively. The air temperature at Cape Town was 29°C. The sea surface temperatures for this day was 10°C at Hout Bay on the western side of the Peninsula (Ocean Research Africa, 2002)

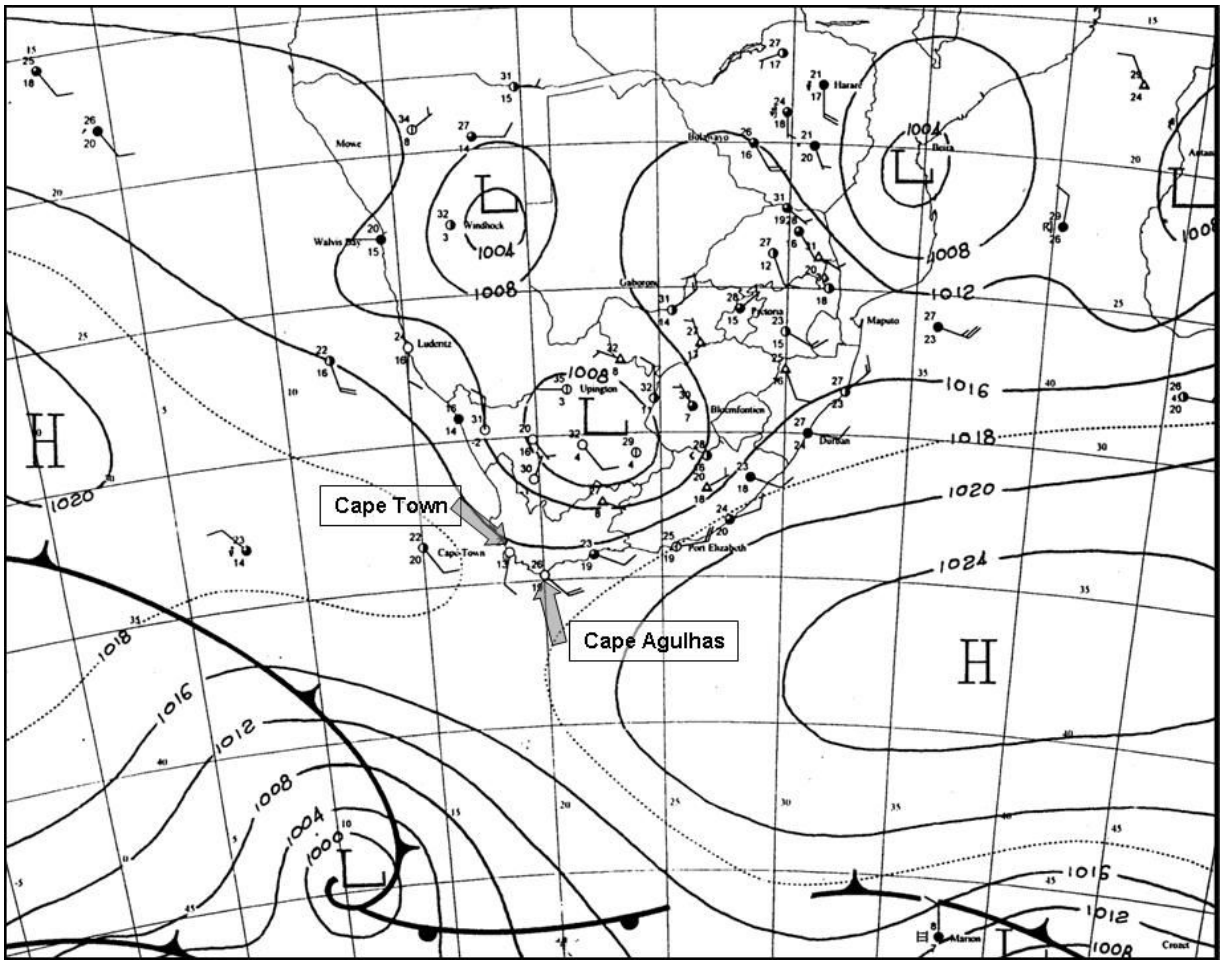

FIGURE 4.4: Synoptic map of southern Africa for 3 February, 2000 at 14:00 SAST (Adapted from: South African Weather Bureau, 2000).

4.3.1 Verification of simulations with observational data

The five stations discussed above were used to verify the RAMS simulated temperature and relative humidity. The wind data are not verified because the wind was simulated by RAMS at a height of 30m above surface level, (the first σ level in the RAMS model) and the AWS wind was measured at 2m above the ground. The contour interval for the simulated temperature maps is 1°C (Fig 4.7) and the relative humidity, 5% (Fig. 4.11). For verification purposes, the simulated temperature and RH values were interpolated to the position of the AWS, where necessary.

a) Temperature

The simulated RAMS temperature and the observed temperature at the location of the five AWSs in the study area on 3 February, 2000, are shown in figure 4.5. The observed and simulated temperatures are generally within 5°C of one another. However, the RAMS model predicts a sharp decrease in temperature at all stations between 14:00 and 17:00 (black line on Fig. 4.4).

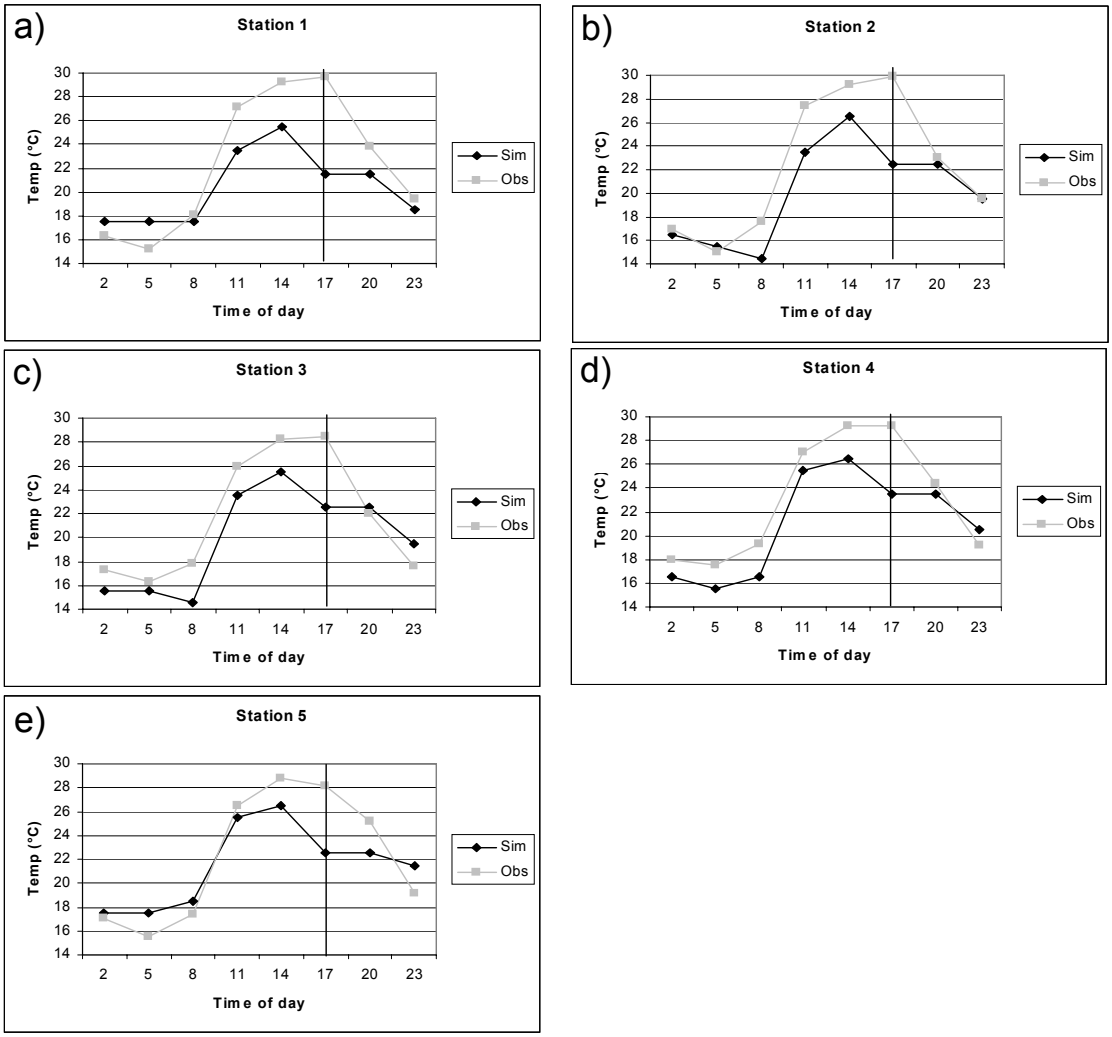

FIGURE 4.5: A comparison between observed temperature (gray) and simulated temperature (black) in °C at the position of five automatic weather stations for 3 February, 2000.

The same drop in temperature was not observed in the AWS data at this time (gray line in Fig. 4.4), but was observed approximately 3 hours later. This variation in time causes a large difference between observed and simulated temperatures at 17:00. The model predicted the invasion of the sea breeze at between 14:00 and 17:00, while it was observed in the AWS data between 17:00 and 20:00. The sharp decrease in observed temperature between 17:00 and 20:00 can be contributed to the sea breeze as sunset occurred at 20:00. Generally, RAMS slightly under-estimated the temperatures, but followed the same diurnal trends as the observed temperatures.

b) Relative humidity

The RAMS simulated RH and the observed RH at the location of the five AWSs in the study area on 3 February, 2000, are shown in Fig. 4.6.

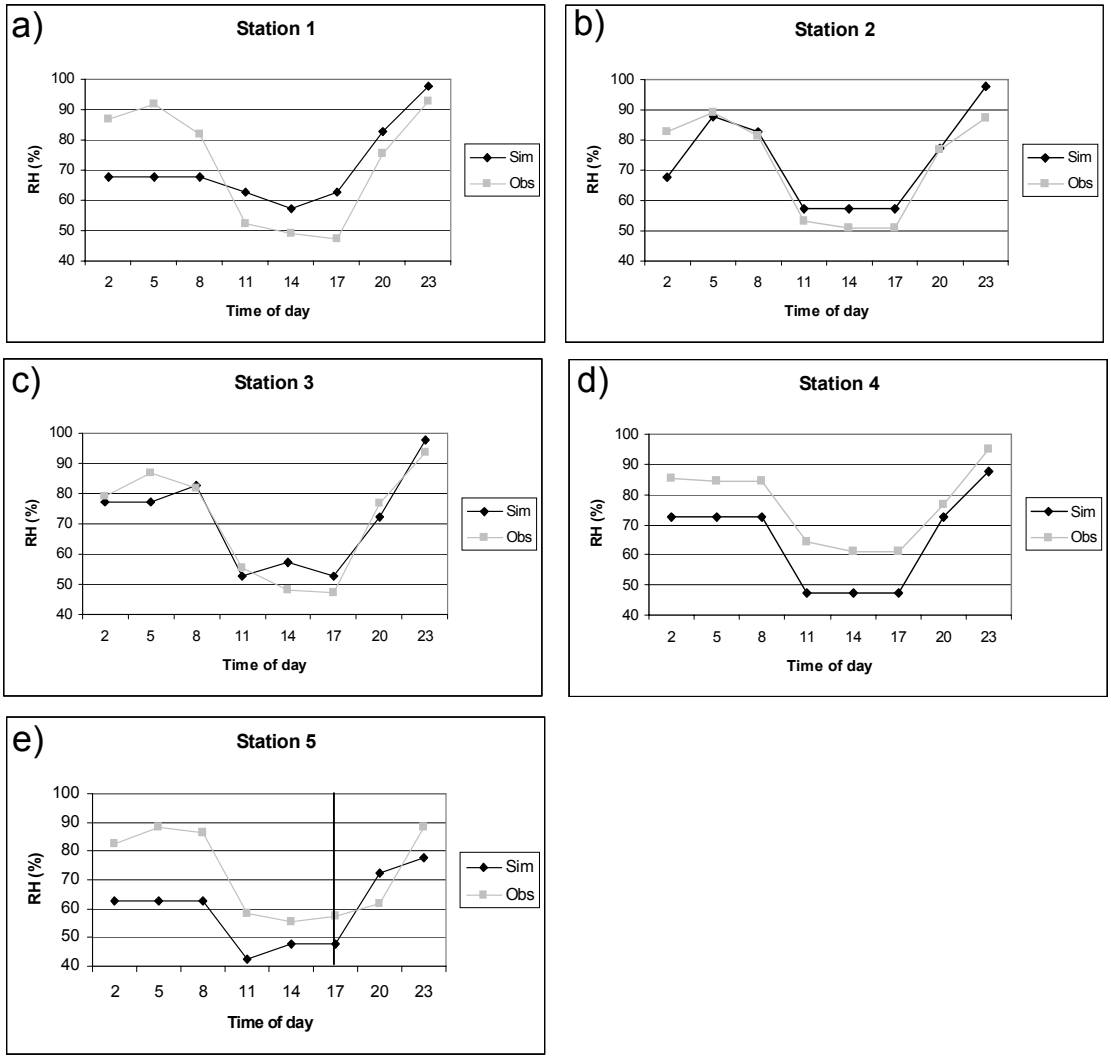

FIGURE 4.6: A comparison between observed RH (gray) and simulated RH (black) in % at the position of five automatic weather stations for 3 February, 2000.

The observed and simulated RH compares very well at Stations 2 and 3 (Fig. 4.5b and c), where the observed and simulated RH was within 15% of one another. The inland stations (Stations 4 and 5) observed RH much higher (as much as 24%) than was forecast by RAMS. The notable exception was at Station 5 at 20:00 (black line in Fig. 4.5e) where the AWS observed a lower RH than was simulated for this time. At the coastal station (Station 1) RAMS underestimated the RH in the early morning (before 08:00) by 20%. The model was also not capable of simulating the sharp drop in RH between 08:00 and 11:00. However, RAMS indicated the increase in RH from 17:00 very well at all five stations. This increase in RH is indicative of the passage of the sea breeze front. Note the sharp increase in RH from 17:00 at Stations 4 and 5 (black line in Fig. 4.6e). Being located further away from the coast, the sea breeze reached these stations later than it reached Stations 1, 2 and 3.

The observed data show the passage of the sea breeze between 17:00 and 20:00. This is clear from the decrease in temperature and increase in RH during this period. The inland progression of the sea breeze is also identified in the AWS data as cooling occurs first at the stations close to the coast (decrease of between 5°C and 6°C) and slightly later over the interior (decrease of 3°C). RAMS showed the passage of the sea breeze slightly earlier (14:00 to 17:00). Considering the time discrepancies, RAMS was found to simulate the general characteristics of the sea breeze adequately and a more detailed description of the RAMS output follows.

4.3.2 Rams simulations

The SAWS surface observations at 08:00 were analysed over the Cape Peninsula (not shown). This analysis showed a small low over False Bay with an off-shore flow over the southern parts of the Peninsula. The temperatures along the coast were higher than over the interior due to the adiabatic heating caused by an off-shore flow.

The RAMS model simulated cold to cool temperatures in the early morning (05:00 and 08:00, not shown), varying between a minimum of 10°C in the low lying areas and 21°C on the slopes of Helderberg. Relative humidity (not shown) was high over most of the area with low values over the high lying areas of Helderberg. RAMS simulated light to moderate south-easterly winds over most of the study area. However, RAMS modelled fresh winds off the Helderberg and east of Papegaaiberg (not shown) due to the funnel effect through the mountains.

The sea breeze becomes visible for the first time in the 11:00 simulations. The surface temperature map (Fig. 4.7) shows a tight temperature gradient along the coast and adjacent low lying coastal plain. The temperatures along the coast varied between 20-22°C. The temperatures over the

remainder of the area were as high as 27°C. Note the blocking of the sea breeze in the south western corner due to the coastal dunes (Fig. 4.1) in the area which rise to 75m ASL very close to the coast.

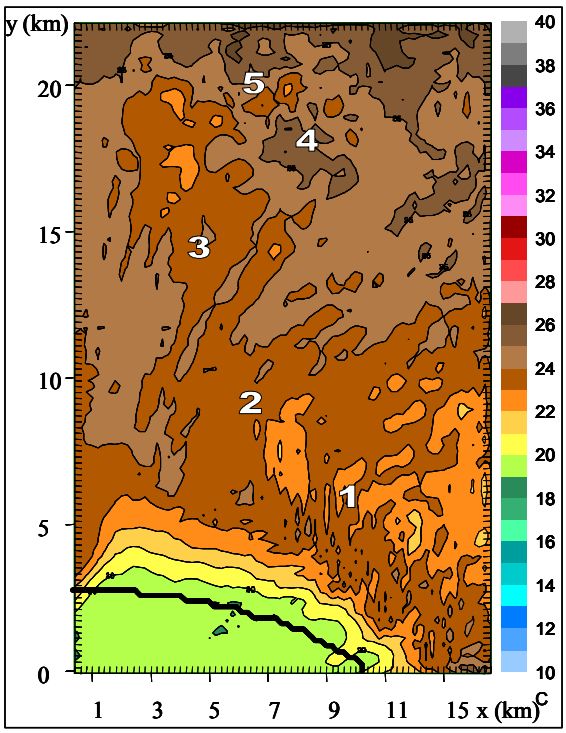

FIGURE 4.7: Simulated surface temperature (°C) at 11:00 SAST on 3 February, 2000. The numbers 1 – 5 indicate the geographical positions of the AWSs used in the verifications.

In the vertical cross sections (X1, X2 and X3) of temperature at this time (11:00) the layer of cool air with the raised head of the sea breeze front as described by Sha *et al.,* (1991) was visible over False Bay and the coast (cross section X2 shown in Fig. 4.8).

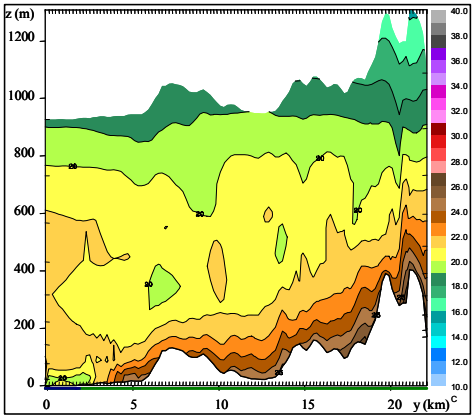

FIGURE 4.8: Simulated temperature (°C) at 11:00 SAST on 3 February, 2000, in the south-north cross section X2

This is indicative of the sea breeze in the immature to early mature stage of development as found by Clarke (1984). The area represented by the third cross section (X3) did not include any ocean and very

little of the coastal plain. In this cross section, the sea breeze was not visible at this time as it was situated over False Bay (Fig. 4.9).

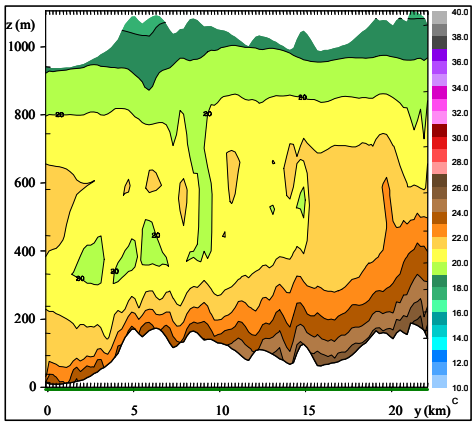

FIGURE 4.9: Simulated temperature (°C) at 11:00 SAST on 3 February, 2000, in the south-north cross section X3

However, in figure 4.10, which is a vertical cross section of RH at X3, the sea breeze is visible in the high to very high RH values (maximum of 82.5%) at the southern edge of the cross section up to a height of 100m ASL. The horizontal distribution of the RH in this cross section shows it reached the peak of the first foothill of Helderberg 5km into the study area at the surface.

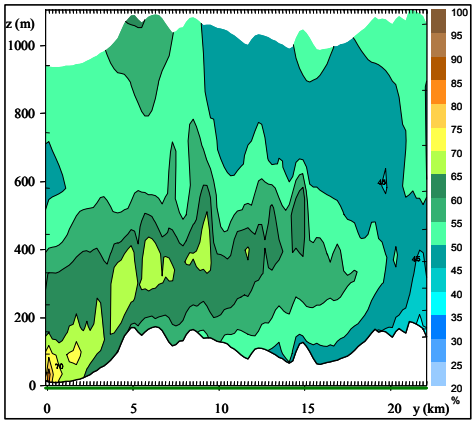

FIGURE 4.10: Simulated relative humidity (%) at 11:00 SAST on 3 February, 2000, in the south-north cross section X3.

Surface relative humidity showed a similar gradient over the bay and the coastal plains, however, the layer of moist air (high RH) reached further inland than the cool temperatures (Fig 4.11).

The simulated wind speeds are available at the first sigma level, 30m above the surface. The wind direction over False Bay and the coast were shown by RAMS to be south-westerly, agreeing with the inland penetration of the sea breeze over this area (not shown).

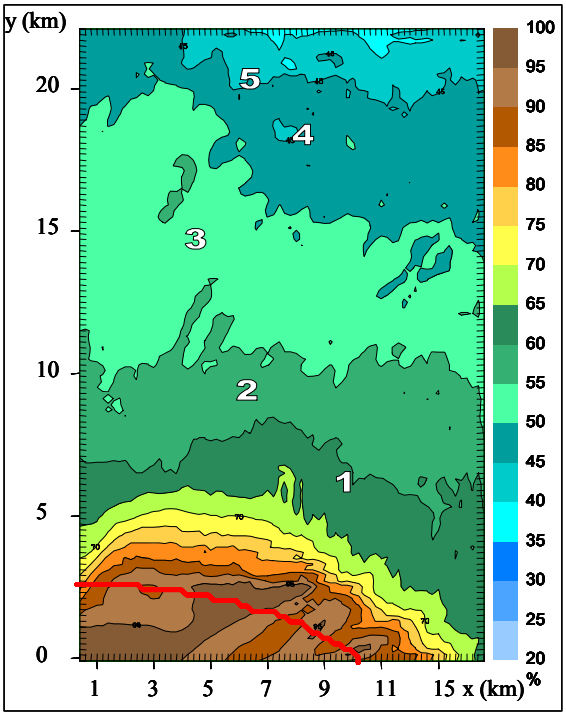

FIGURE 4.11: Simulated surface relative humidity (%) at 11:00 SAST on 3 February, 2000. The numbers 1 – 5 indicate the geographical positions of the AWSs used in the verifications.

The wind farther inland was southerly to south-westerly around Helderberg Mountain, Papegaaiberg and the Eerste River Valley. In cross section X1 (Fig. 4.12), fresh to strong wind speeds were simulated in a layer between 50 and 150m above sea level, reaching beyond the coastal dunes. This layer of higher wind speed is indicative of the passage of the sea breeze front as explained by Clarke (1984). In X2, the fresh winds only reach the coastline with light to moderate wind speeds at the surface over the coastal plain (not shown). The winds at X3 (not shown) were southerly in the bottom layers, but the high winds of the sea breeze were not as clearly visible as in the other two cross sections.

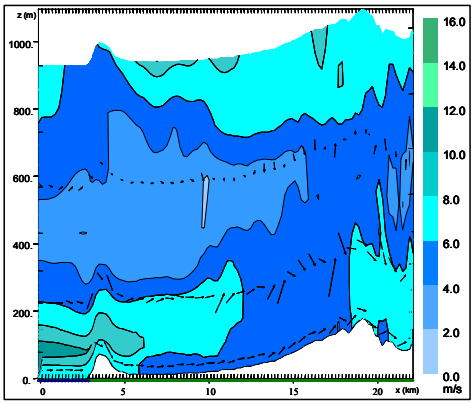

FIGURE 4.12: Simulated wind speed (ms^{-1}) and direction (black arrows) at 11:00 SAST on 3 February, 2000, in the south-north cross section X1.

Further analysis of the SAWS data at 14:00 found that the coastal low which was over False Bay at 08:00 moved southward and had deepened (not shown). The pressure gradient at this stage was relatively weak over the northern parts of the Peninsula, but there were found to be stronger pressure gradients west of the Table Bay low. A tight temperature gradient existed between the interior and the coast.

At this time, the RAMS simulations showed temperatures higher than 28°C (not shown) on the northern slopes of the Eerste River Valley. At the coast, the temperatures were simulated to have increased since 11:00, but there was still an 8°C difference between the temperatures at the coast and adjacent interior due to the influence of the sea breeze. The cooling effect of the sea breeze had not moved much further inland since 11:00 and still reached only 3km inland. The influence of topography on the temperature distribution was visible through the cooler temperatures over the high lying areas over Bottelaryberg Mountain, Bottelary Hills and Helderberg when compared to the hot temperatures over the low lying areas in the interior (e.g. in the Eerste River Valley and the low lying areas west of Bottelaryberg).

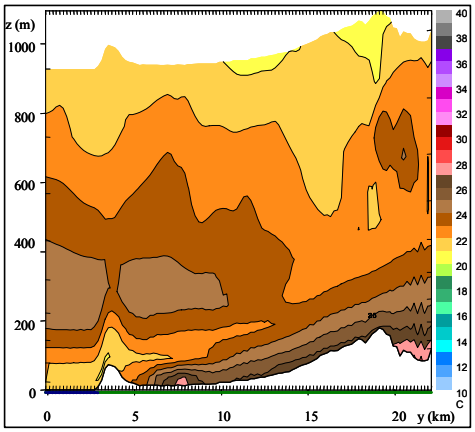

FIGURE 4.13: Simulated temperature (°C) at 14:00 SAST on 3 February, 2000, in the south-north cross section X2

The vertical profile of temperature (Fig. 4.13) showed the head of the sea breeze front still sharp, but flatter than it was at 11:00, which is indicative of the late mature stage of the sea breeze development as described by Clarke (1984). The cool temperatures reached further inland 50m above the ground, but these cooler temperatures did not reach the surface. In X3, the cooling effect of the sea breeze was visible for the first time over the southern slopes of Helderberg (not shown). High temperatures were visible in the Eerste River Valley in all three cross sections.

The moist air (high RH) reached 5km inland at the surface (Fig. 4.14), but at 50m above the ground it reached as far as 10km inland (X1, Fig. 4.15a and X3, not shown). In X2, it reached 7km inland to just north of Faure Hill (Fig. 4.15b). Interestingly, note the influence of the coastal dunes on the inland

advection of the moist air in the south-western corner of Fig. 4.14 where the dunes prevent the moist air (high RH) to reach as far inland as where there are no dunes, e.g. further to the east along the coast.

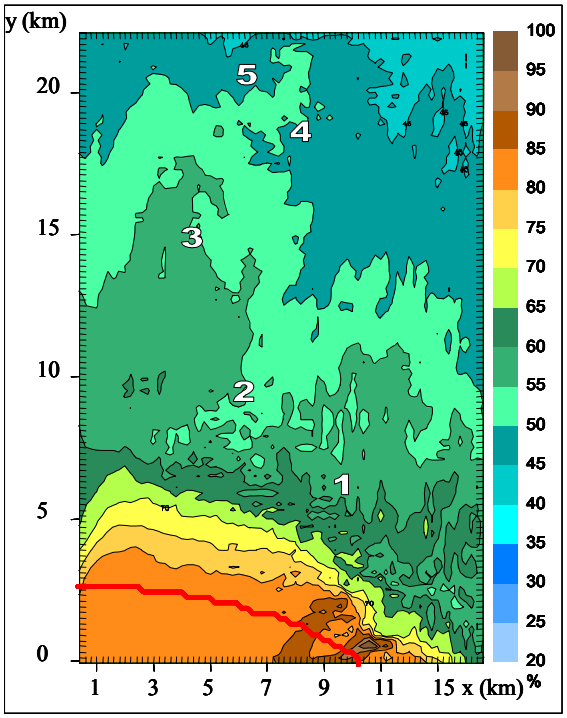

FIGURE 4.14: Simulated surface relative humidity (%) at 14:00 SAST on 3 February, 2000. The numbers 1 – 5 indicate the geographical positions of the AWSs used in the verifications.

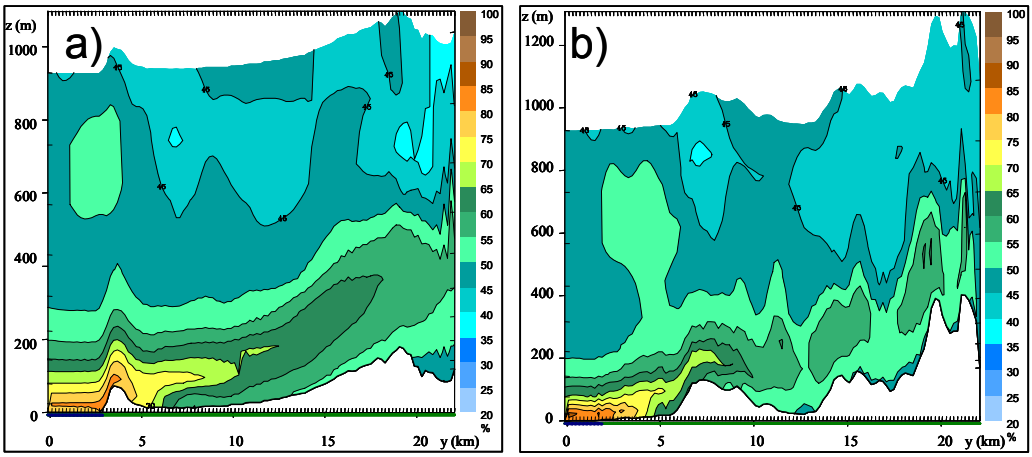

FIGURE 4.15: Simulated relative humidity (%) at 14:00 SAST on 3 February, 2000 in the south-north cross sections X1 (a) and X2 (b).

By this time the simulated wind speed had increased to a maximum of 11.5ms^{-1} over False Bay and Bottelaryberg (not shown). The vertical simulation of the wind showed high speeds in a layer between 50 and 200m above the surface, reaching inland for 10 km in X1, 7km in X2 and 6km in X3 (not shown). These observations agree with observations made by Cangialosi, (2003), in Florida, Hadi *et al.*,

(2002) in Indonesia and Batt (2005) in New South Wales, Australia, which show that the wind speed is higher approximately 50m above the ground than those speeds observed at ground level.

In the early degenerate stage, the sea breeze flattens and spreads inland. The height of the head is reduced from the early mature stage (Clarke, 1984). This stage was well simulated at 17:00 on 3 February, 2000. The RAMS temperature at this time was still high (26-34°C) over the interior and much lower over the coast and coastal plains, where cool temperatures were simulated (not shown). The vertical cross sections of the temperature distribution showed a much flatter profile of the sea breeze front (Fig. 4.16a and b), where the layer of cool temperatures were much narrower than at 14:00 and reached only 100m (X1, not shown) and 50m (X2) above the ground. Over the interior, the simulated temperatures were high in the Eerste River Valley as well as over Helderberg and Papegaaiberg in X2 and X3 (Fig. 4.16a for X2 and Fig. 4.16b for X3). In X3, the cooling effect of the sea breeze was less pronounced than in the cross sections that include ocean.

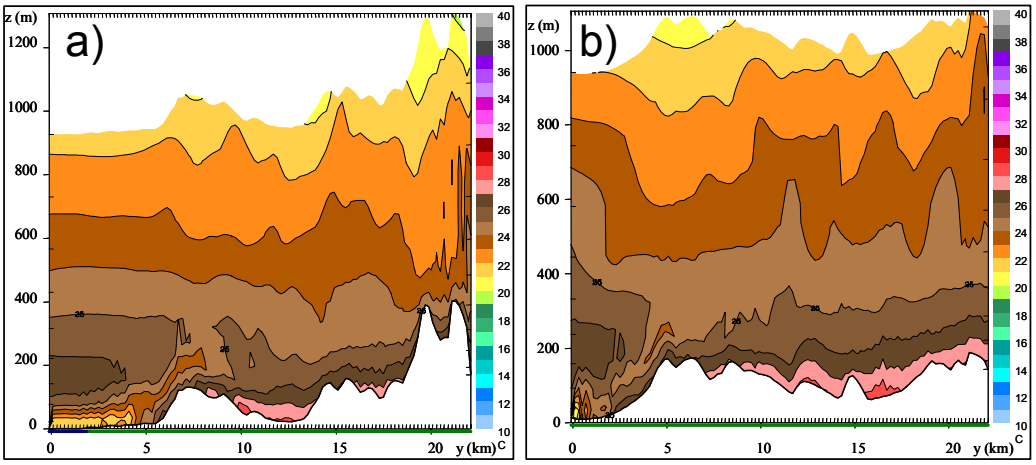

FIGURE 4.16: Simulated temperatures (°C) at 17:00 on 3 February, 2000 in south-north cross sections X2 (a) and X3 (b).

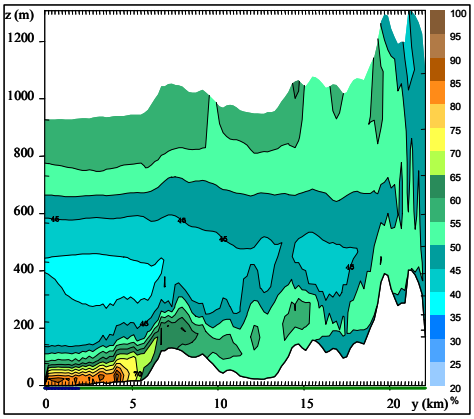

FIGURE 4.17: Simulated relative humidity (%) at 17:00 on 3 February, 2000 in south-north cross section X2.

It was in the vertical cross sections of RH that the moist influence of the sea breeze was visible in all three cross sections. The slightly flatter profile of the sea breeze, compared to the 14:00 visualisation, was also visible in the RH cross sections at this time (Fig. 4.17).

The simulated wind over False Bay was strong at this time with similar wind speeds over all the mountains in the study area. Light to moderate wind speeds were simulated over the coastal and inland plains (Fig. 4.18). A slight divergence of the wind is visible over the coast line, as the wind moves over the coast at a right angle. There is also convergence over the mouth of the Eerste River Valley where it opens onto the inland plain (slightly north of Station 2 in Figure 4.18).

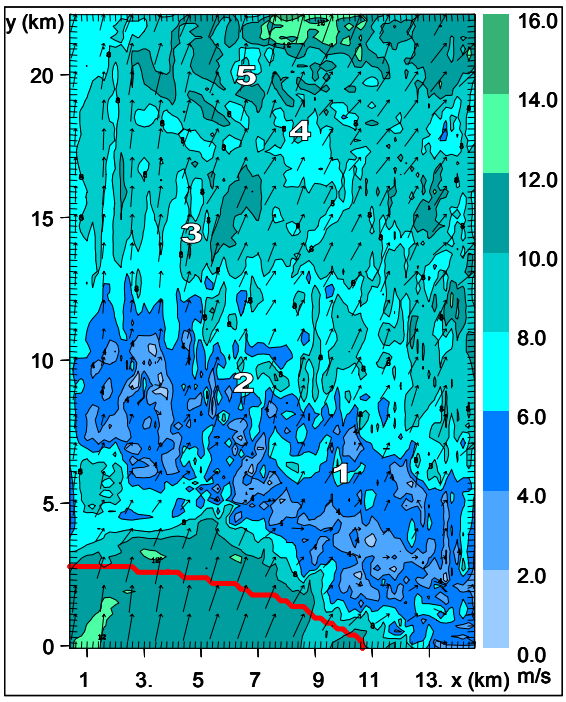

FIGURE 4.18: Simulated surface wind speed (ms^{-1}) and direction (black arrows) at 17:00 SAST on 3 February, 2000. The numbers 1 – 5 indicate the geographical positions of the AWSs used in the verifications.

The flatter profile of the sea breeze was in evidence in the layer of high wind speed in the cross sections and reached a height of only 150m (X1, not shown), 100m in X2 (Fig. 4.19) and 200m in X3 (not shown), although the layer of high wind speed did not reach very far inland at this time (compared to 14:00). Areas of higher wind speeds were simulated on the southern slopes of Bottelaryberg Mountain in X2 (Fig. 4.19). These areas of higher wind speed may be ascribed to the interaction of the sea breeze in the area with the valley breezes, which develop by day due to the temperature difference between the cooler valleys and warmer mountains (Preston-Whyte and Tyson, 1988).

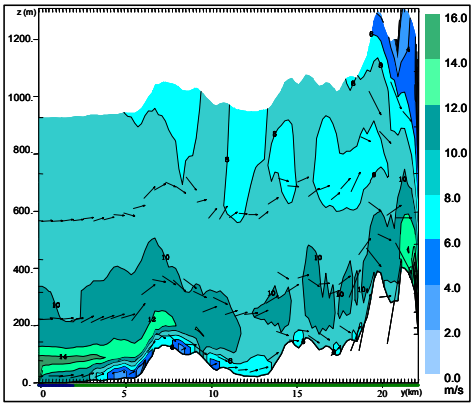

FIGURE 4.19: Simulated wind speed (ms^{-1}) and direction (black arrows) at 17:00 SAST on 3 February 2000 in the south-north cross section X1.

After sunset, at approximately 19:20, the sea breeze flattened more and spread further inland. This spread of the sea breeze was visible in the 20:00 maps (not shown). In the 20:00 cross sections, the cooling influence of the sea breeze was seen to spread as far inland as the Bottelary Hills, the Eerste River Valley and Papegaaiberg. A layer of high RH of 50m thick also reached to just south of the northern edge of the study area. The wind at this time (20:00) was mostly southerly over the study area with the passage of the False Bay sea breeze (not shown).

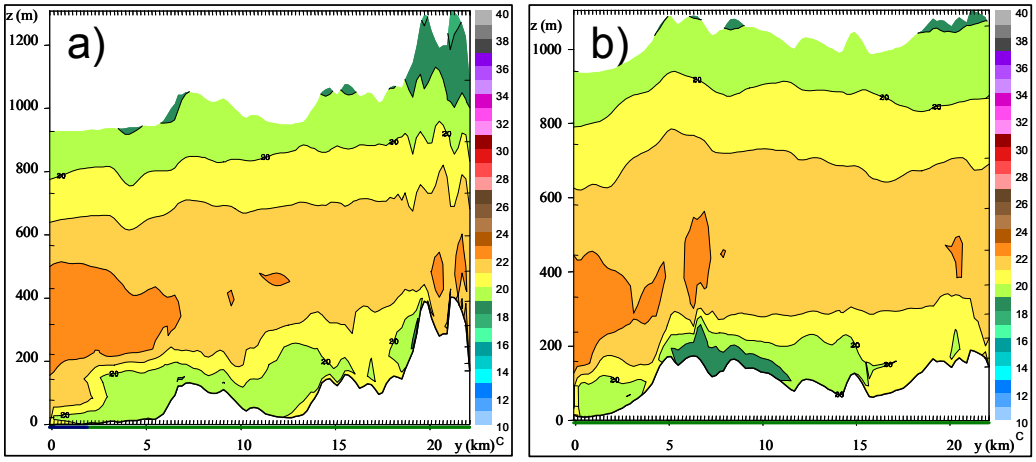

FIGURE 4.20: Simulated temperature (°C) at 23:00 SAST on 3 February, 2000 for south-north cross sections X2 (a) and X3 (b).

By 23:00 on 3 February, 2000, the sea breeze had weakened considerably and had spread past the northern edge of the study area. In the surface map (not shown), cool temperatures were simulated, although it showed higher values over Papegaaiberg and Bottelaryberg Mountain than over the low-lying areas of the study area. These higher temperatures could be ascribed to altitude as could be seen from the cross sections X2 and X3 (Figure 4.20a and b, respectively), where the peaks reach into the temperature inversion associated with the sea breeze which has already passed through northern edge of the study area (Bonnardot, 2002). The relative humidity at this time confirmed that the sea breeze has moved inland

past the edge of the study area. The entire area had very high relative humidity of more than 85% with the exception of the Bottelaryberg Mountain peaks (not shown). This was again due to the altitude of the peaks reaching through the layer of high relative humidity.

The wind had weakened considerably since 17:00, agreeing with the findings of Fosberg and Schroeder (1966), who found that the speed of the sea breeze slowed later in the day to 1- 2ms^{-1}. The wind over False Bay (Fig. 4.21) was still simulated as fresh southerly (6.8ms^{-1}), showing that the see breeze was still active at this time and had not reached the late degenerate stage where the density current decays as found by Buckley and Kurzeja (1997). Interestingly, weak mountain breeze circulations could be seen starting to develop over the slopes in the study area in the cross sections (X2 shown in Fig. 4.22). Mountain breezes develop between the cooler areas of the peaks and the warmer areas of the valleys and the plains at night (Preston-Whyte and Tyson, 1988). In all three of the cross sections at 23:00, areas of light down-hill wind could be seen on the slopes of the hills and mountains in the cross sections. These mountain breezes were at times found to be moving against the general southerly flow of the rest of the atmosphere (Fig. 4.22).

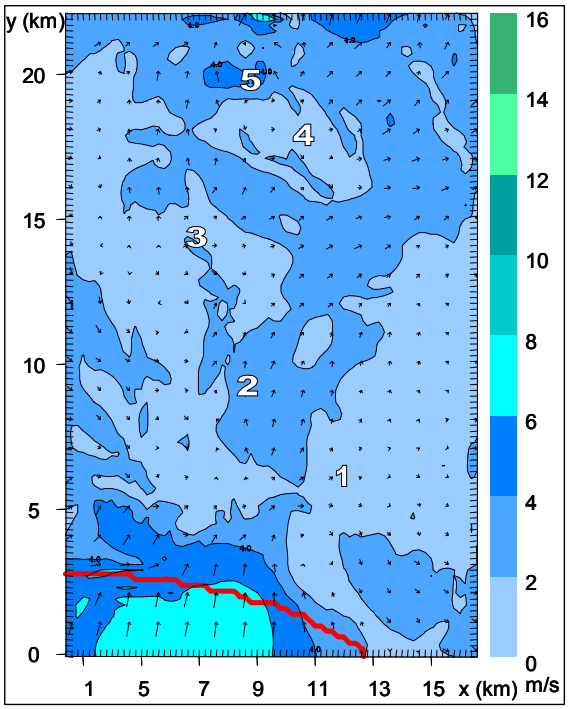

FIGURE 4.21: Simulated surface wind speed (ms^{-1}) and direction (black arrows) at 23:00 SAST on 3 February, 2000. The numbers 1 – 5 indicate the geographical positions of the AWSs used in the verifications.

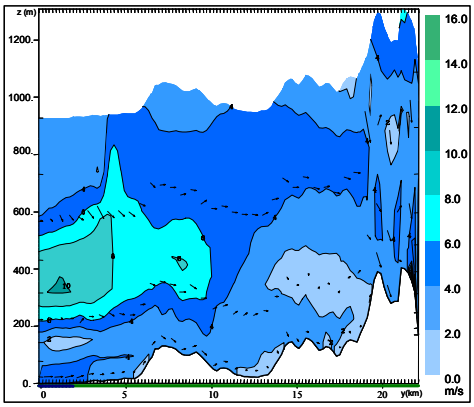

FIGURE 4.22: Simulated wind speed (ms^{-1}) and direction (black arrows) at 23:00 SAST on 3 February, 2000 for south-north cross section X2.

4.3.3 Conclusions

This case study was chosen to show the influence of a weak onshore synoptic flow on the False Bay sea breeze. The AWS data in the area show the penetration of the sea breeze between 17:00 and 20:00. This is clearly visible in the decrease in temperature and increase in RH and wind speed. The RAMS model also identified the sea breeze front, but simulated it to occur approximately 3 hours earlier than it actually did. However, RAMS output provided detailed information about the vertical structure of the sea breeze.

At 11:00, the raised head of the sea breeze front, indicative of the early mature stage, is clearly visible (Fig. 4.8) in the vertical cross sections of both temperature and relative humidity. By 14:00, the typical raised head flattened, which characterises the late mature stage of the sea breeze. Note also in figure 4.13, how the cool temperatures penetrate further inland above the ground than on the ground. This is also where stronger winds occurred, again depicting typical sea breeze characteristics. The degeneration of the sea breeze is also captured well at 20:00 and 23:00

This case study shows that the RAMS model handles the influence of the topography very well. Firstly, it shows the temperature and RH distribution in high lying and low lying areas (Fig. 4.20) and the strong wind simulated early in the morning due to funnel effect by the Helderberg and Papegaaiberg. After sunset, the mountain breeze circulation is captured at 23:00 in the wind speed and direction simulations over the mountains (Fig. 4.22), especially on the southern slopes when the mountain breeze opposes the southerly flow.

In summary, the RAMS model produced an excellent simulation of the sea breeze for this case study.

4.4. Case study 2: 18 February, 2000

The 18th of February was chosen in order to investigate the influence of off-shore synoptic flow on the sea breeze in the Cape Peninsula. Two sea breezes are discussed for this day. First, is the Table Bay sea breeze which occurred in the early morning hours and, second, is the False Bay sea breeze which developed in the late morning (similar to the development of the sea breeze in the first case study). The Table Bay sea breeze is defined in this study as the sea breeze that develops over Table Bay and moves into the study area from the west or north-west. The influence which these sea breezes had on temperature, RH and wind speed and direction in the study area are discussed.

4.4.1 Verification of simulations with observed data

The simulated RAMS temperature and relative humidity are compared to the observed temperature and relative humidity at the five AWSs in the study area. The comparison starts at 23:00 on the 17th and ends at 23:00 on the 18th. However, the observed values start at 20:00 on the 17th in order to capture the onset of the Table Bay sea breeze in the study area.

The AWS data (gray line in figure 4.23) show the passage of the Table Bay sea breeze at 20:00 on the 17th February. From 23:00 (Stations 3 and 5) and from 02:00 (Stations 1, 2 and 4), the observed temperatures increased as the Table Bay sea breeze decayed at the end of the late degenerate stage of sea breeze development as described by Physick and Smith (1985). On the slope of Bottelaryberg Mountain (Fig. 4.23c), there is a sharp increase in temperature at 02:00 which is followed by a decrease in temperature between 05:00 and 08:00. This increase could have been caused by an increase in the berg wind intensity at that time. The passage of the Table Bay sea breeze is shown in the relative humidity observations from the AWSs in the area in Figure 4.24. The increase of the RH associated with the passage of the Table Bay sea breeze is visible between 20:00 and 02:00 at the stations, with the western stations (Stations 3 and 5) showing the passage of the sea breeze front earlier (23:00) than the eastern stations (02:00).

For the passage of the Table Bay sea breeze, RAMS showed the passage only at Station 3, six hours after the AWSs observed the sea breeze. Because of this failure to simulate the Table Bay sea breeze, the temperatures simulated by RAMS were higher than the temperatures observed by the AWSs from 23:00 on the 17th until 05:00 on the 18th at the positions of Stations 1 to 4. At Station 5, RAMS did not simulate the increase in temperature caused by the strengthening of the berg winds at 02:00 over Bottelaryberg Mountain and, thus, simulated temperatures lower than were observed by the station. The relative humidity (Fig. 4.24) simulated by RAMS was much lower than was observed by the AWSs at all the stations with the exception of Station 3, where the passage of the Table Bay sea breeze was observed by RAMS.

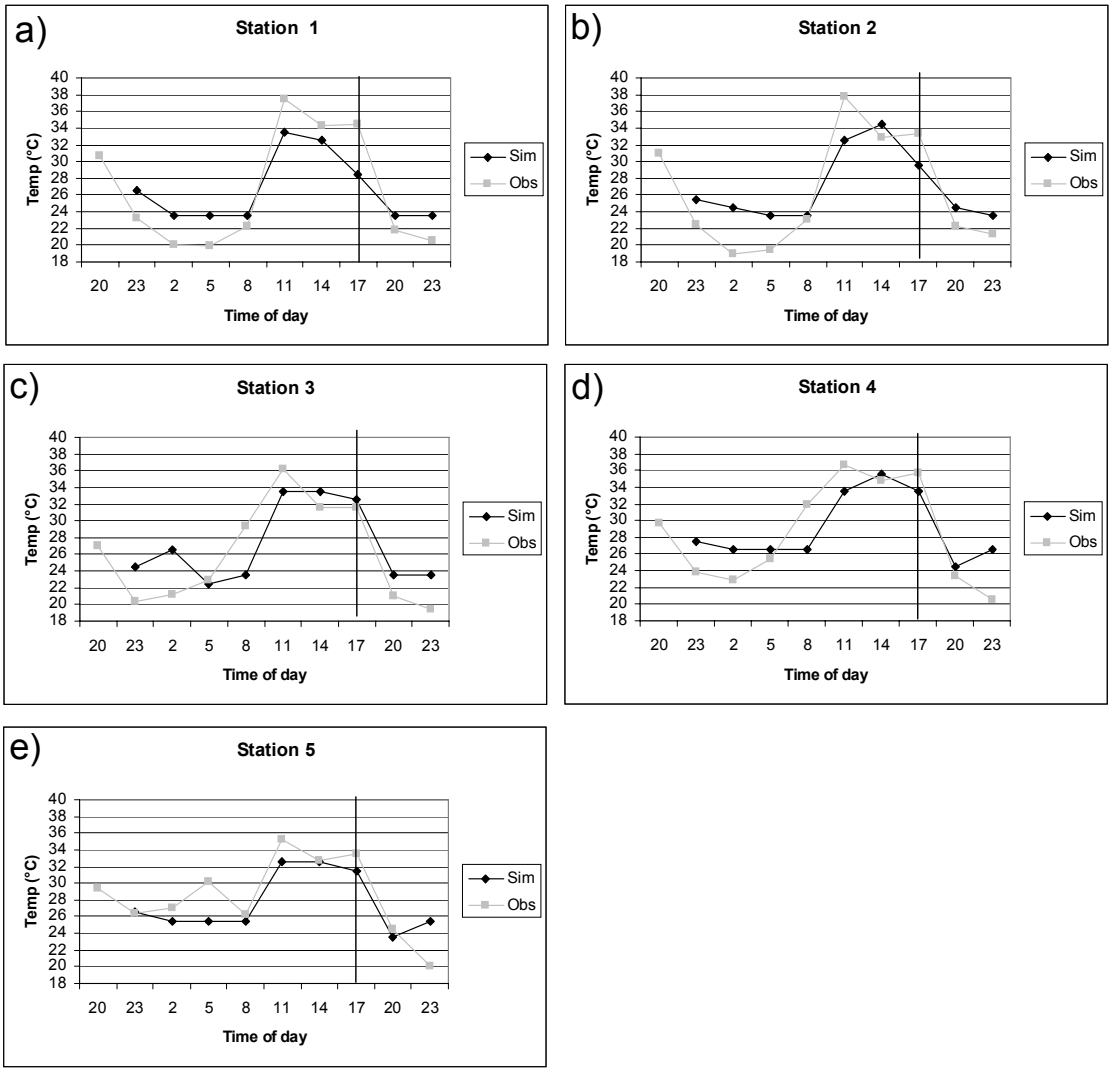

FIGURE 4.23: A comparison between observed temperature (gray) and simulated temperature (black) in °C at the positions of the five automatic weather stations for 18 February, 2000

Between 08:00 and 11:00, the temperature showed a sharp increase under the effect of the berg wind conditions. The largest increase of 15.2°C was observed at Station 1. The relative humidity decreased sharply at this time by as much as 40% at Station 1.

Between 11:00 and 14:00, the False Bay sea breeze became visible in the AWS data (Figures 4.23 and 4.24) as the temperatures cooled with its movement over the stations. The coastal stations showed the sharp decrease in temperature at 11:00, while the stations further inland observed a smaller decrease in temperature at the same time. The RH increased slightly at these times, but not by more than 10%, as the sea breeze front advected moist air from False Bay over the stations. Interestingly, some of the AWSs observed a slight increase in temperature at 17:00 (Fig. 4.23b-e) as hot air was most probably mixed down behind the head of the sea breeze front after it passed over the stations, as described by Simpson

(1994). Shortly after sunset, the temperatures decreased significantly under the cooling effect of the sea breeze.

The RAMS simulations observed the passage of the False Bay sea breeze between 11:00 and 14:00, but RAMS did not simulate the mixing of warm air behind the head of the sea breeze as was observed by the AWSs. The RAMS temperatures decreased similarly to the observed temperatures between 14:00 and 20:00. After 20:00, RAMS showed a sharp increase in temperature over interior stations as RAMS simulated the return of the berg wind conditions after the passage of the False Bay sea breeze, while the observed temperatures continued to decrease.

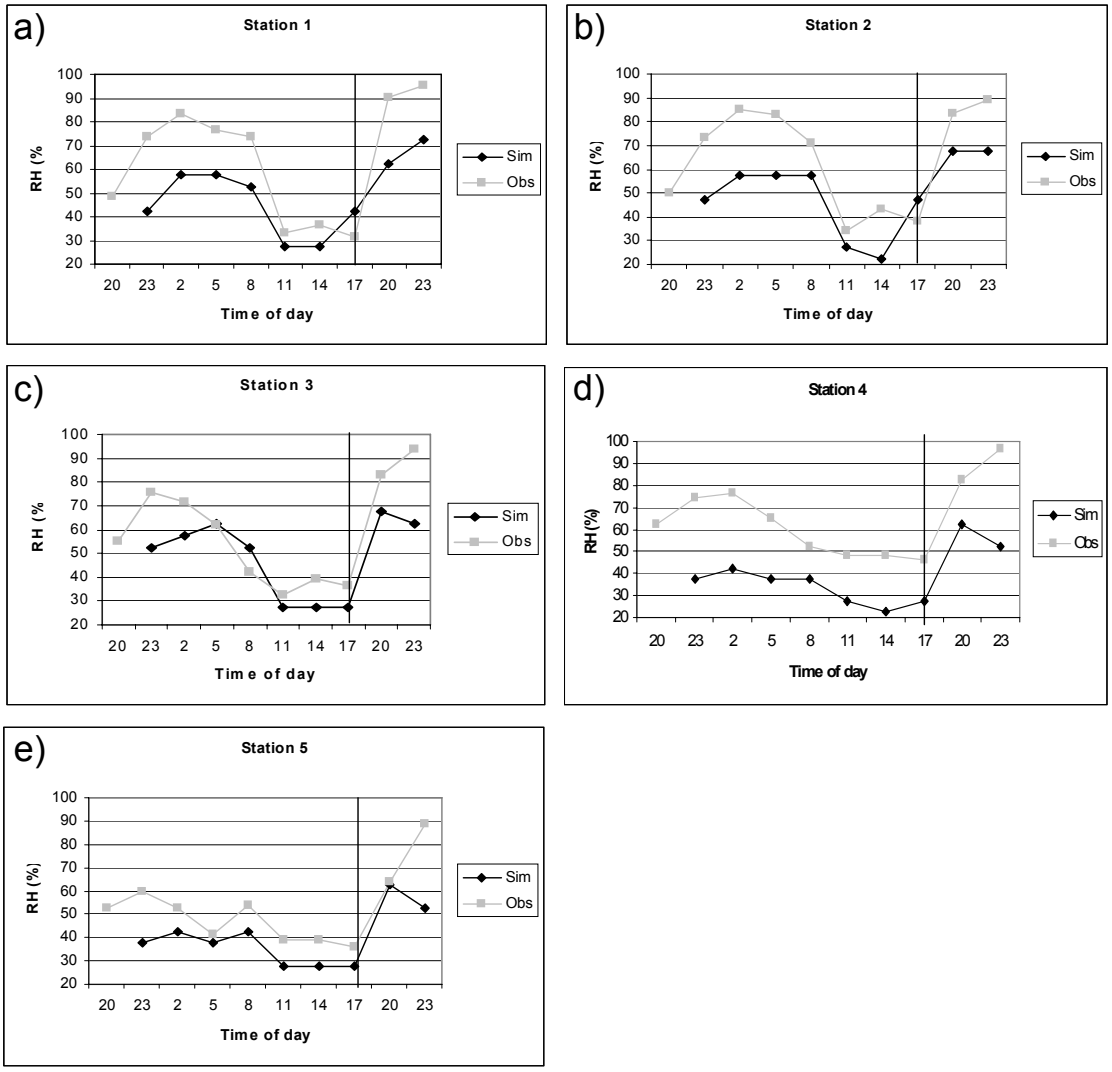

FIGURE 4.24: Comparison between observed RH (gray) and simulated RH (black) in % at the positions of the five automatic weather stations for 18 February, 2000.

The relative humidity simulated by RAMS stayed constant between 11:00 and 14:00 at Stations 1, 3 and 5, while it continued to decrease slightly at Stations 2 and 4. The passage of the sea breeze can be seen in the increase of RH after 14:00 in Stations 1 and 2 and after 17:00 in stations 3, 4, and 5. RAMS failed to simulate the drying of the air through the mixing of hot dry air behind the head of the sea breeze as was observed by the AWSs. After 20:00, the simulated RH decreased sharply at Stations 3, 4 and 5 as RAMS simulated the return of the berg wind conditions.

The observed data showed the passage of the Table Bay sea breeze between 20:00 and 23:00 on the 17th from the west in both temperature and relative humidity values. RAMS simulated this sea breeze six hours later, but showed the sea breeze characteristics clearly. The Table Bay sea breeze arrived at 11:00 at the two coastal stations as shown in the observed values and at 17:00 at the stations in the interior according to the simulated values. Observed values showed the slight increase in temperature and decrease in RH behind the sea breeze front as warm dry air was probably mixed in behind the head of the sea breeze front. RAMS showed the passage of the sea breeze at the same time as the observed values did, although it failed to simulate the downward mixing of the warm air behind the sea breeze front. Despite this, RAMS clearly showed the structure and movement of the False Bay sea breeze under opposing synoptic flow.

4.4.2 RAMS simulations

The sea-level pressure field at 14:00 (South African Weather Bureau, 2000) showed a deep surface trough situated over the western interior, while the Indian Ocean High extended in a ridge over the eastern part of the country (Fig. 4.25). A low pressure system over the western parts of the country was partially responsible for the occurrence of berg wind conditions over the Cape Peninsula. A berg wind is defined as a hot dry wind that blows from the interior plateau of South Africa roughly at right angles to the coast. These winds can bring a temperature rise of 15°-20°C and cause relative humidity to fall from nearly 100% to 30% or less. Berg winds may last two to three days (Schulze, 1996). The sea surface temperatures measured along the Cape Peninsula for this day was 9°C (Ocean Research Africa, 2002).

a) The Table Bay sea breeze

For this case, RAMS simulations were done from 23:00 on 17 February, 2000, in order to capture the Table Bay sea breeze in the study area. Figure 4.26 shows the cooler air moving into the study area from the west. The western most cross section (X1) showed a shallow layer of cool air over the Eerste River Valley and the inland plain at 23:00 on 17th February (Fig. 4.27).

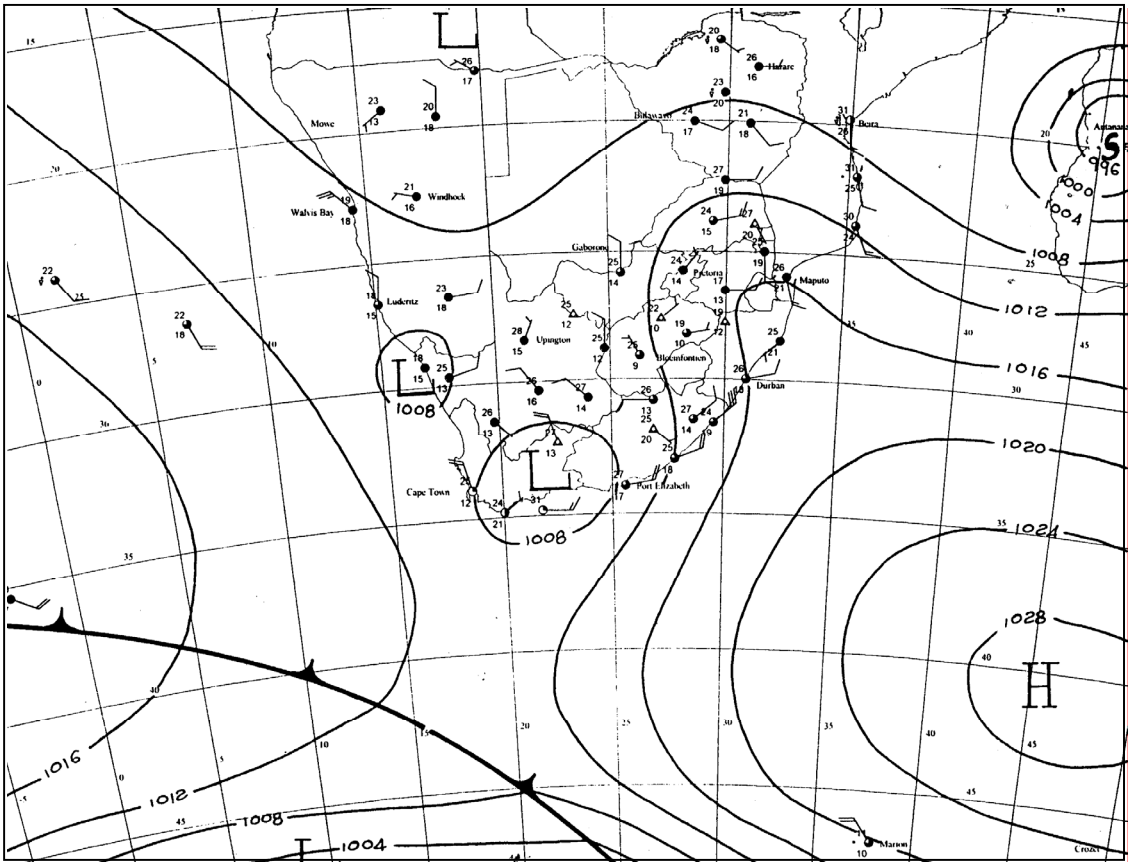

FIGURE 4.25: Synoptic map of southern Africa for 18 February, 2000 at 14:00 SAST (Adapted from: South African Weather Bureau, 2000)

Even though the raised head of the sea breeze was not easy to discern from the front, the restriction of the layer of cool air to the lower 200 meters of the atmosphere is a clear indication of the presence of a sea breeze. It also agrees with the findings of Cangialosi (2003) and Hadi *et al.* (2002) concerning the height of the sea breeze in Florida and Indonesia. The other two cross sections (not shown) do not show this shallow layer of cooler air, but they are situated further east and, therefore, not under the influence of the Table Bay sea breeze.

Relative humidity at 23:00 (not shown) showed a similar layer of high RH moving into the study area from the west with simulated values as high as 80% at places. The cross sections X1 and X2 showed that the layer of high RH did not reach higher than 200m into the atmosphere. The third cross section showed only slightly higher RH over the Eerste River Valley.

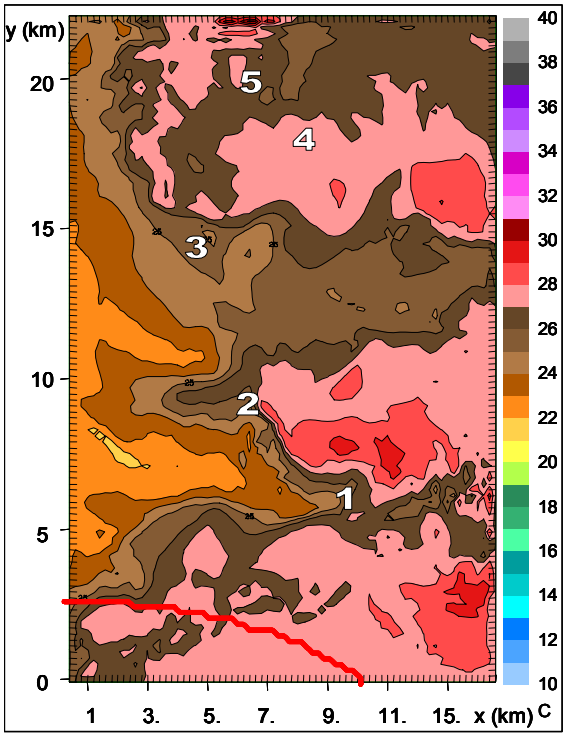

FIGURE 4.26: Simulated surface temperature (°C) at 23:00 SAST on 17 February, 2000.

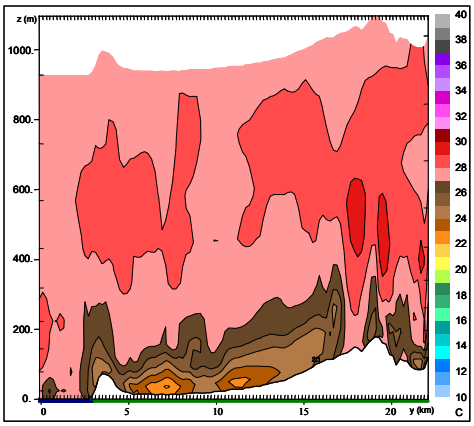

FIGURE 4.27: Simulated temperature (°C) at 23:00 SAST on 17 February, 2000 in the south-north cross section X1.

The analysis of SAWS surface observations at 02:00 over the Cape Peninsula showed an elongated low over the west coast and Peninsula with a strong high over the interior. The wind at Cape Point was fresh south-easterly and light north-easterly at Cape Town International Airport. Temperatures were warm, varying between 23°C and 18°C over the Cape Peninsula. At this time, the RAMS simulations showed high temperatures over the whole study area. The layer of cooler air from the Table Bay sea breeze reached the south-eastern edge of the study area over the coastal plain as it moved eastward (Fig. 4.2.8). Over the north-eastern parts, the temperatures were still high, reaching 27°C in the Eerste River Valley.

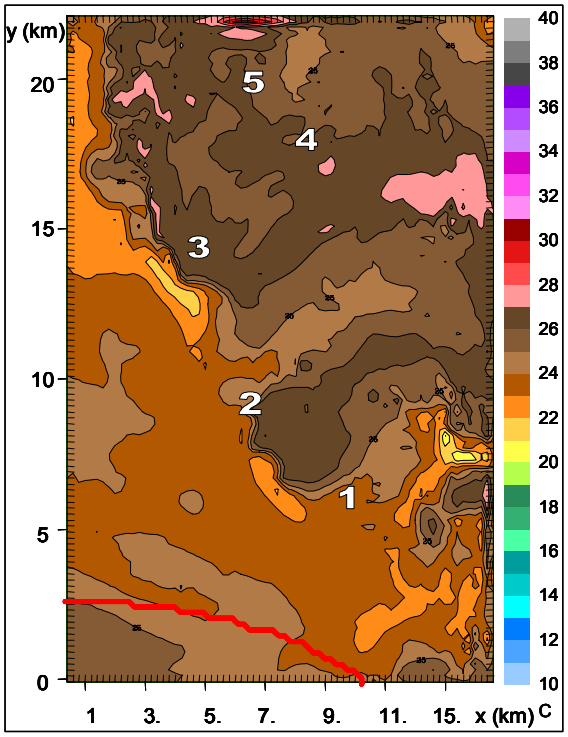

FIGURE 4.28: Simulated surface temperature (°C) at 02:00 SAST on 18 February, 2000.

All three of the cross sections at this time showed that the shallow layer of cool air did not reach higher than 250m ASL (Fig. 4.29a for X1 and Fig. 4.29b for X2). Above this layer, temperatures were considerably higher, providing further evidence of the presence of a sea breeze.

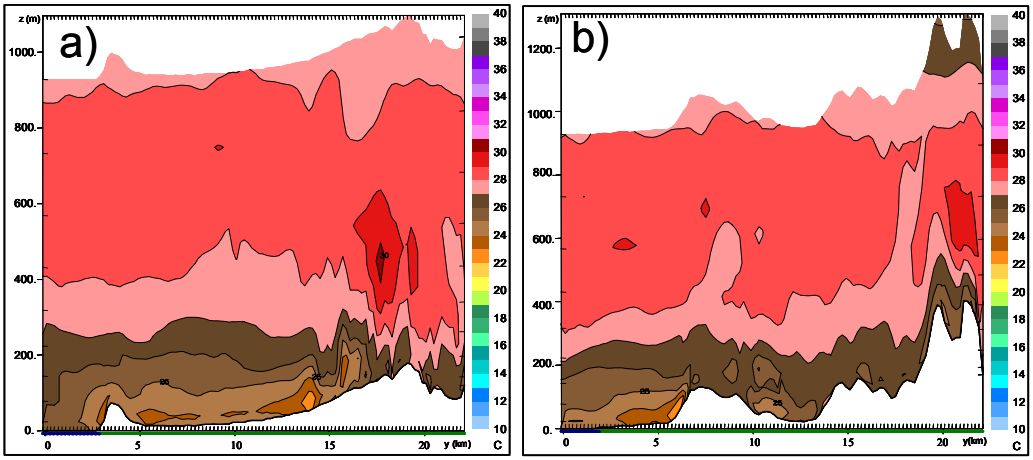

FIGURE 4.29: Simulated temperatures (°C) at 02:00 SAST on 18 February, 2000 in south-north cross sections X1 (a) and X2 (b).

The RH simulations at this time also showed the higher moisture carried inland by the Table Bay sea breeze with the layer of higher RH not reaching more than 200m ASL (Figures not shown). This is a clear example illustrating that the sea breeze is a temperature driven phenomenon which does not

necessarily occur during the daytime hours as explained by Simpson (1994). Over the north-eastern parts the RH was very low (35-50%).

The strong continental high moved westward according to the synoptic analysis of the SAWS data at 05:00 (not shown), pushing the low over the west coast and Cape Peninsula westward. The wind at Cape Point was fresh (10ms^{-1}) northerly and the temperature 30°C. RAMS simulated surface temperatures of between 21 and 28°C in a layer of between 300 and 400m ASL at this time (not shown). The relative humidity varied between 30% along the eastern slopes of Bottelaryberg Mountain and 65% west of Bottelaryberg Mountain where the influence of the night time Table Bay sea breeze was still visible (not shown). The simulated wind (not shown) strength was light over most of the study area, but moderate to fresh north-easterly over Bottelaryberg Mountain.

b) The False Bay sea breeze

By 08:00, a strong continental flow prevailed over the area (not shown). The strong high pressure system over the interior pushed the weak low even further westward in the early morning hours. By this time, the high was extending a ridge out over the west coast north of Saldanha Bay. A small low pressure system was situated over the interior north of the Cape Peninsula, contributing to the berg wind conditions in the area. The temperature at Cape Point at this time was still 30°C.

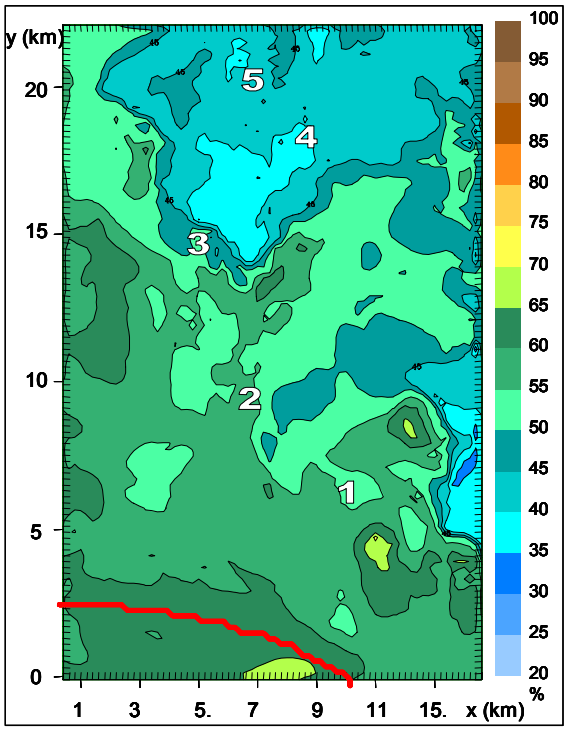

FIGURE 4.30: Simulated surface relative humidity (%) at 08:00 SAST on 18 February, 2000. The numbers 1 – 5 indicate the geographical positions of the AWSs used in the verifications.

The RAMS simulations forecast similarly high temperatures, (not shown) especially over the eastern slopes of Bottelaryberg Mountain and the Helderberg Foothills. The last vestiges of the Table Bay sea breeze were still visible in the cooler temperatures in the lowest 200m of the atmosphere (not shown). Figure 4.30 shows the moist air in the Eerste River Valley. At this time (08:00), the simulated wind was very light over most of the study area (Fig. 4.31) with the notable exception of the Helderberg Mountain area where the wind speed was in excess of 16ms^{-1} at places.

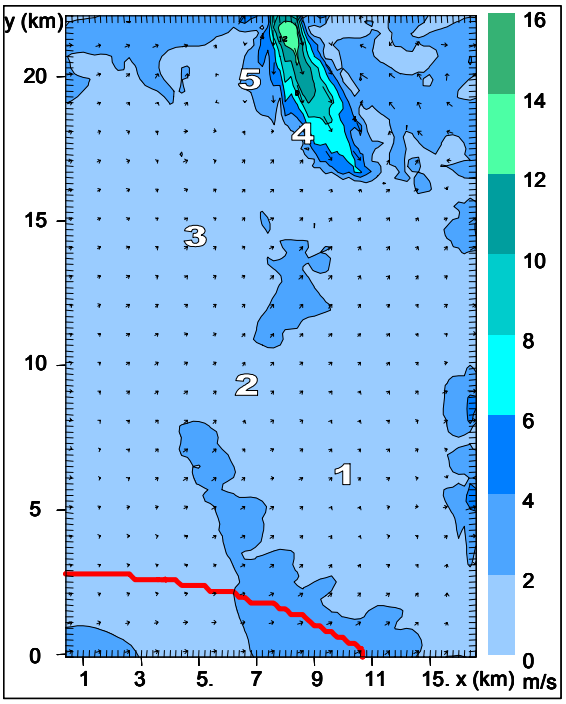

FIGURE 4.31: Simulated surface wind speed (ms^{-1}) and direction (black arrows) at 08:00 SAST on 18 February, 2000. The numbers 1 – 5 indicate the geographical positions of the AWSs used in the verifications.

By 11:00, there was no sign of the Table Bay sea breeze in the RAMS simulations. The temperatures were very high over the interior of the study area, being in excess of 34°C in places along the Eerste River Valley (Fig 4.32). However, similar to the case of 3 February, 2000, the influence of the False Bay sea breeze was visible in the cooler temperatures over the coast and coastal plain. The sea breeze was strong enough not to be influenced by the coastal dunes as much as it was in the first case study (e.g. Fig. 4.7). This concurs with the findings of Arritt (1993), who stated that weak opposing synoptic flow causes a stronger sea breeze.

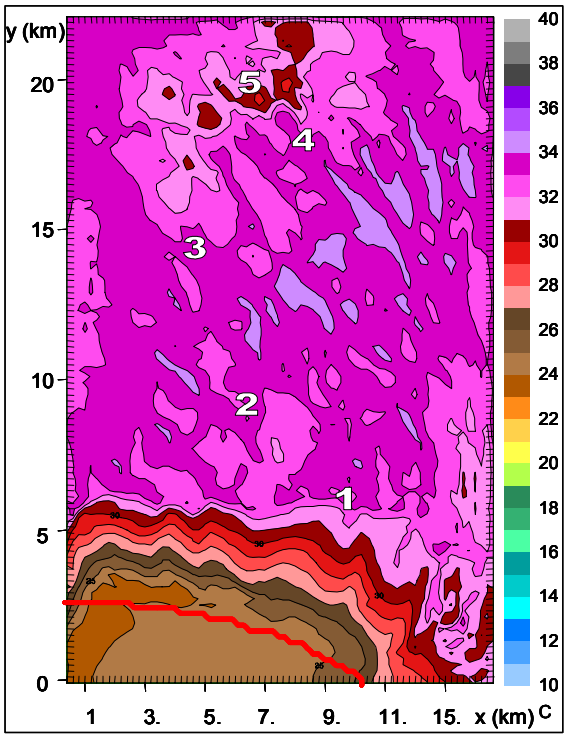

FIGURE 4.32: Simulated surface temperature (°C) at 11:00 SAST on 18 February, 2000. The numbers 1 – 5 indicate the geographical positions of the AWSs used in the verifications.

In the cross sections, (Fig. 4.33a and b) the sea breeze influence was visible as the layer of cooler air with the raised head as defined by (Sha *et al.,* 1991) over the ocean and the coast. This sea breeze reached further inland and caused a more significant decrease of temperature than the sea breeze of 3rd February, 2000, did at the same time.

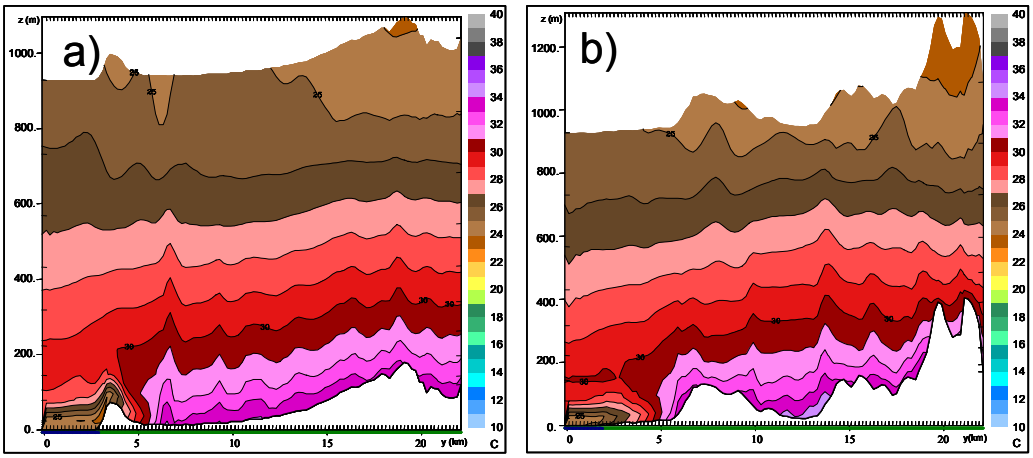

FIGURE 4.33: Simulated temperature (°C) at 11:00 SAST on 18 February, 2000 in the south-north cross sections X1 (a) and X2 (b).

The relative humidity at 11:00 on the 18th February, 2000, was extremely low (<25%). The area influenced by the sea breeze showed values of only 50% occurring over the coast (not shown). The very dry conditions on the 18th could be ascribed to the berg wind conditions (Schulze, 1996). The influence of the sea breeze was very noticeable in cross sections X1 and X2 (not shown), where the sea breeze head was visible reaching over the coastal dunes in X1 and up to the foot of Faure Hill in X2. The sea breeze head was flatter in this case than the 3rd February sea breeze, because the sea breeze wedged under the opposing synoptic flow similar to findings by Arritt (1990).

The biggest difference between 3rd February and 18th February, 2000, at 11:00 can be observed in the wind simulations. On the 3rd, the wind was simulated as southerly to south-westerly over the whole study area. On the 18th, (Fig. 4.34) the wind was north-westerly over the study area, with the exception of the area where the sea breeze moved in over the coast and south-westerly winds occurred with speeds varying between 2 and 6 ms^{-1}. This divergence due to the curvature of the coastline is not as clearly visible in this case as it was in the first case study. However there is a clear convergence line where the sea breeze and the berg winds meet over Station 1 in Fig. 4.34.

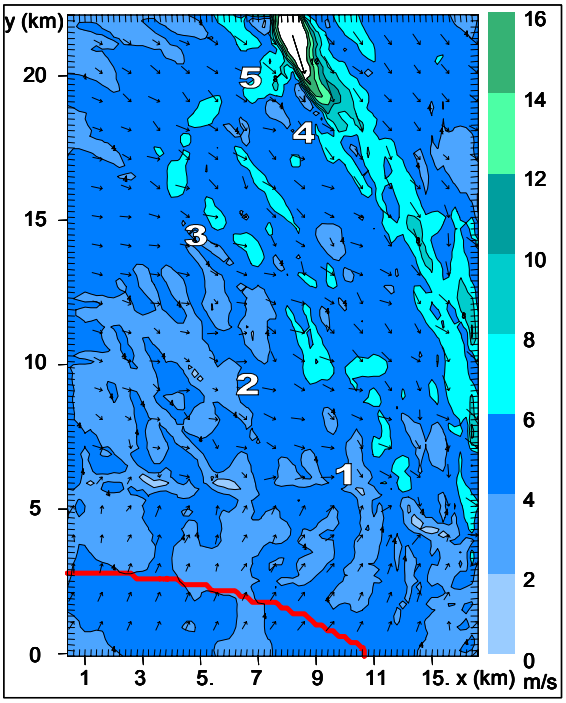

FIGURE 4.34: Simulated surface wind speed (ms^{-1}) and direction (black arrows) at 11:00 SAST on 18 February, 2000. The numbers 1 – 5 indicate the geographical positions of the AWSs used in the verifications.

The direction of the sea breeze was clearly visible (small black arrows) as southerly in the bottom most layer of all three cross sections (Fig. 4.35 a (X2) and b (X3); X1 not shown) and as northerly in the layer above it. On the 18th, the sea breeze was shallower than the sea breeze simulated on the 3rd.

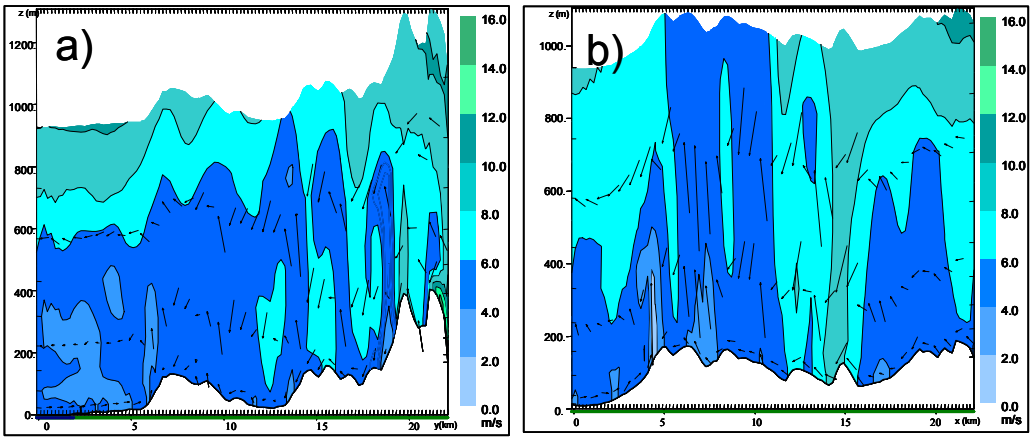

FIGURE 4.35: Simulated wind speed (ms^{-1}) and direction (black arrows) at 11:00 SAST on 18 February, 2000 in the south-north cross sections X2 (a) and X3 (b).

Analysis of the SAWS data (not shown) for 14:00 on 18th February, 2000, showed that the high had strengthened over the west-coast and Peninsula, while the small low over the interior of the province deepened. Temperatures were very high over the interior with 39°C at Worcester. Cape Town International Airport and Cape Point reported cumulonimbus clouds. The cool, moist air that was carried inland by the sea breeze and the lift at the front of the SBF caused convective cloud to develop, as explained by Ackerman (2005) for his study. The winds over the Cape Peninsula stations varied between north westerly and northerly with speeds of 5-10ms^{-1}.

The RAMS simulations for 14:00 showed extremely high temperatures over the study area with the cooling influence of the sea breeze visible over the coastline, but reaching only 3km inland (Fig. 4.36). The cross sections (Fig. 4.37 shows X1, X2 and X3 not shown) showed a much shallower layer of the cool sea breeze than was observed on the 3rd (Figure 4.13). However, the structure of the sea breeze is similar in both case studies.

The RAMS simulations for RH at 14:00 showed even drier conditions over the study area (not shown) than was simulated at 11:00. The sea breeze was visible in the simulated cross sections X1 and X2, reaching only a few kilometres inland, detailed only in the very slight elevation of the RH on the southern most edge of X3, the more mountainous of the three cross sections where the adiabatic heating of the winds would have been most severe (not shown).

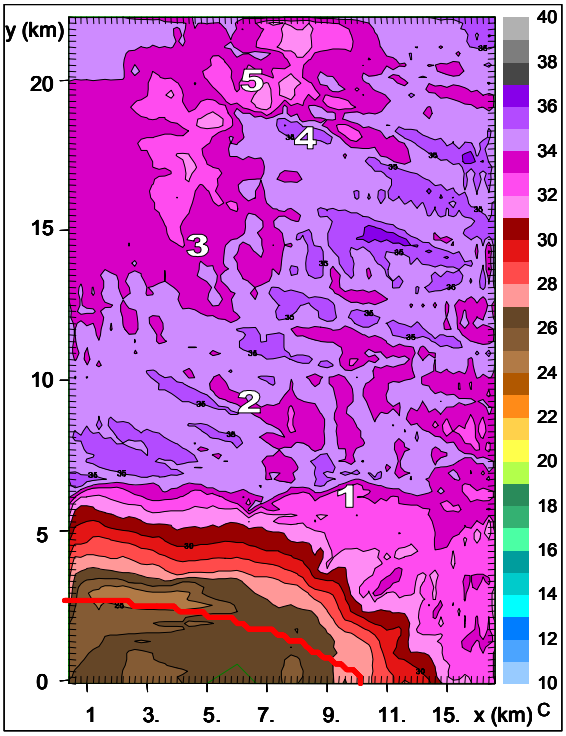

FIGURE 4.36: Simulated surface temperature (°C) at 14:00 SAST on 18 February, 2000. The numbers 1 – 5 indicate the geographical positions of the AWSs used in the verifications.

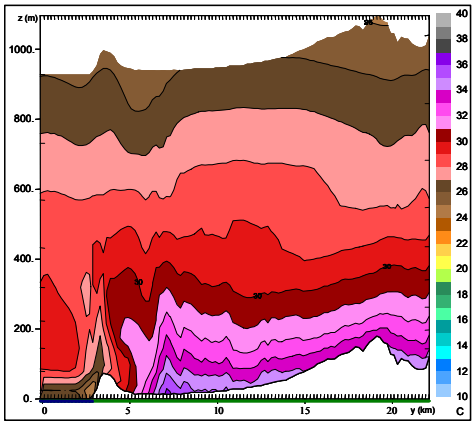

FIGURE 4.37: Simulated temperature (°C) at 14:00 SAST on 18 February, 2000 in the south-north cross section X1.

By 14:00 on the 18th, the wind speed had increased significantly from 11:00. The berg winds were simulated with speeds in excess of 16ms^{-1} over Bottelaryberg (Fig. 4.38). The sea breeze had also increased in speed and RAMS simulated it to have speeds higher than 6ms^{-1} over False Bay and the coast. According to Fosberg and Schroeder (1966), the speed of the see breeze varies between 5 and 7 ms^{-1} during the early mature stage of the sea breeze. In the cross sections, the sea breeze was now visible in the wind speed and direction of the simulations in X1, X2 and X3. The sea breeze reached as high as 400m ASL in X1 (not shown), and up to 7km inland at the surface. In X2 (Fig. 4.39a), the sea breeze

reached 200m ASL and only so far inland as the southern slopes of Faure Hill, 5km inland from the coast. In the third cross section the wind reached as far as 6km inland in the in the bottom most layer of the simulation (Fig. 4.39b).

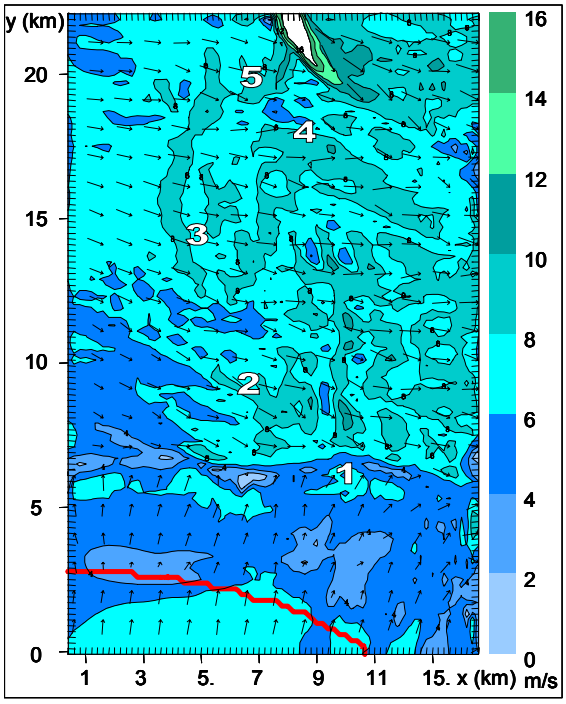

FIGURE 4.38: Simulated surface wind speed (ms^{-1}) and direction (black arrows) at 14:00 SAST on 18 February, 2000. The numbers 1 – 5 indicate the geographical positions of the AWSs used in the verifications.

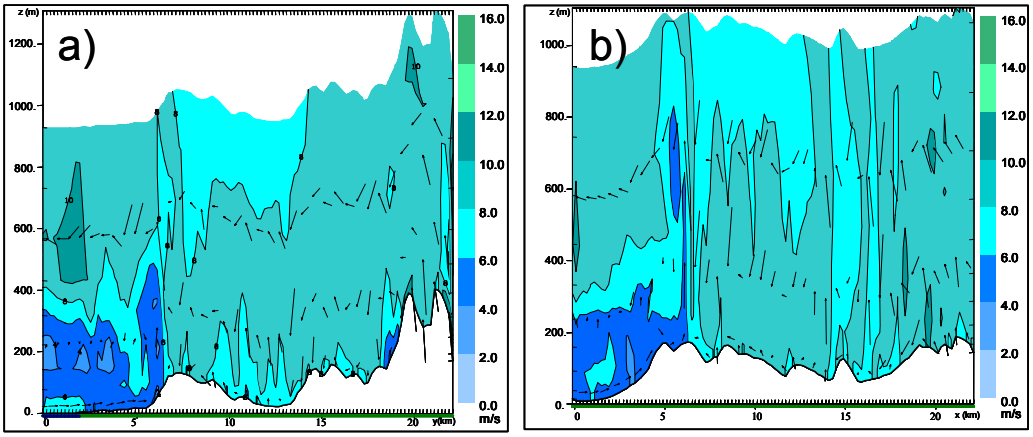

FIGURE 4.39: Simulated wind speed (ms^{-1}) and direction (black arrows) at 14:00 SAST on 18 February, 2000 in south-north cross sections X2 (a) and X3 (b).

The 17:00 simulations on this day showed significant cooling (not shown) from the earlier 14:00 simulations. The temperatures have decreased, falling as much as 6°C in places in the Eerste River Valley. The temperatures at the coast have decreased only 2°C from the 14:00 (Fig. 4.38) simulations. Most interestingly, the observed temperatures stayed the same or showed a slight increase from 14:00

which concurs with the findings of, amongst others, Simpson (1994), that the downward mixing behind the head of the sea breeze front causes slightly higher temperatures right behind the SBF. The simulated cross sections showed the sea breeze head in the cool air over the coast and a retreat of hot temperatures over the Eerste River Valley (not shown). The sea breeze cooling was still not clearly visible in X3 (not shown).

The relative humidity simulations at this time (not shown) showed the moist conditions as high as 80% over the coast, reaching much further inland than it did at 14:00. The cross sections indicated that the sea breeze reached: up to 7km inland (X1), to the northern slopes of the Eerste River valley; 12km inland (X2); and to the northern slopes of Helderberg Mountain (X3), which was further inland than the 3rd February sea breeze reached at 17:00. This indicates that the sea breeze in this case study was much stronger and extended further inland than the sea breeze simulated in the first case study.

The 30m wind simulations at 17:00 (not shown) showed moderate to fresh southerly winds, reaching the northern slopes of the Eerste River Valley and also showed the westerly winds over Bottelaryberg Mountain. The first cross section was not available for this time, but X2 and X3 both showed southerly winds in the lower 400m of the atmosphere, reaching the northern edges of the Eerste River Valley and the fresh to strong wind speeds 200 to 300m ASL similar to the sea breeze simulated for 3rd February, 2000.

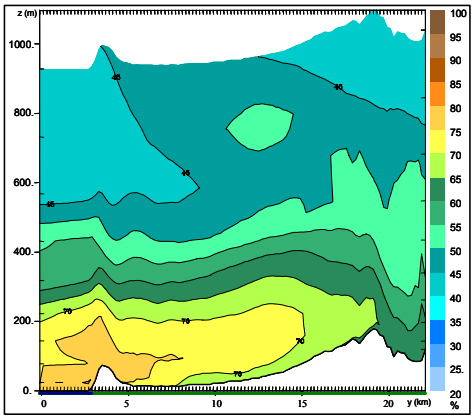

FIGURE 4.40: Simulated relative humidity (%) at 20:00 SAST on 18 February, 2000 in the south-north cross section X1.

At 20:00, the inland temperatures have cooled down further and the temperatures in the study area varied between 20°C and 25°C (not shown). The RH simulated for this time was more than 80% at the south-western edge of the study area with a low RH of just over 50% in the north-eastern corner (not shown). The RH observed by the AWSs also showed a significant increase from 17:00. The cross sections showed the sea breeze reached the Bottelaryberg Foothills in X1 (Fig. 4.40), the southern slopes

of Bottelaryberg Mountain in X2 and the northern slopes of Helderberg in X3. This is similar to what was observed in the 3 February simulations with the exception that the maximum RH simulated for the 18th is 20% lower than those simulated for the 3rd February.

The wind at 17:00 was southerly or south southwesterly over the whole study area as the sea breeze front has moved beyond the northern edge of the study area. These southerly winds were also visible in the cross sections of the wind speed and direction at 20:00.

By 23:00, the temperatures were still high over the study area. The temperature inversion left behind by the passing sea breeze was still visible in the three cross sections (not shown). The RH at this time still showed the shallow band of moist air in the lower 200m of the atmosphere (X2 shown in Fig. 4.41), the cross sections also indicating the sea breeze has passed beyond the northern edge of the study area.

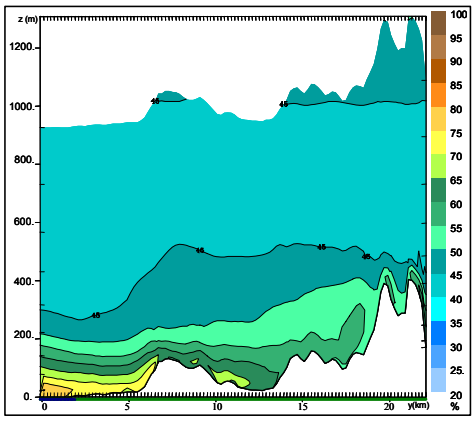

FIGURE 4.41: Simulated relative humidity (%) at 23:00 SAST on 18 February, 2000 in south-north cross section X2.

The wind at 23:00 was light southerly over most of the area agreeing with Fosberg and Schroeder (1966) who found that the wind speed decreased to 1-2ms^{-1} later in the day as the sea breeze reaches the late degenerate stage (Clarke, 1984). The notable exception to this is over Bottelaryberg Mountain. Here there were fresh to strong north-westerly winds simulated, indicating that RAMS simulated the return of the synoptic scale berg wind conditions after the passage of the sea breeze front through the area.

4.4.3 Conclusions

In this case study, the influence of off-shore synoptic flow (berg wind conditions in the Western Cape) on the development of the sea breeze was shown. Two sea breezes were observed on this day. The first sea breeze originating from Table Bay, reached the study area by 20:00 on the 17th according to the AWS data. The RAMS model simulated the Table Bay sea breeze in the study area from 23:00. The cooling effect of the Table Bay sea breeze was under-estimated by the RAMS model, but the penetration

pattern (Fig. 4.26) and vertical structure (Fig. 4.27) of the sea breeze was shown in great detail by the model.

By 14:00, the penetration of the sea breeze from False Bay was clearly shown by the AWS data. The RAMS model showed the penetration of the False Bay sea breeze slightly later than was observed. AWS data showed a decrease of temperature with the passage of the sea breeze front and a slight increase in temperature after the passage of the front, indicating the downward mixing of warm air behind the head of the sea breeze front. The character of the sea breeze under off-shore synoptic flow was clearly shown by the temperature, RH and wind cross sections. These cross sections show the flattened head and higher intensity of the sea breeze, indicative of the influence of an opposing synoptic flow (Fig. 4.33). When the simulations (temperature, RH and wind speed) for this case study were compared to the first case study, it was obvious that the sea breeze during off-shore conditions was stronger and reached further inland than during weak onshore conditions

This case study showed that RAMS handled berg wind conditions accurately, showing the high winds over Bottelaryberg Mountain and the high temperatures in the low lying areas of the Eerste River Valley (Fig. 4.32). The RAMS model also clearly simulated the sea breeze influence from both bays, where the temperature difference between land and sea was large enough to cause the development of the sea breeze in the area, regardless of the time. RAMS correctly simulated the speed of the False Bay sea breeze in theory in both the early mature and late degenerate stages.

In summary, the RAMS model simulated both sea breezes and their influences on temperature, RH and wind speed and direction appropriately for this case study.

4.5. Case study 3: 19 February, 2000

The third case study (19th February, 2000) was chosen to investigate the character of the sea breeze when a strong onshore synoptic flow occurs. Strong southerly winds are relatively common in the Western Cape Province. Sixty-five percent of wind directions, observed in February between the years 1956 and 1970, vary between southeast and southwest as measured at Cape Town International Airport (South African Weather Bureau, 1975). Of these winds 55% have wind speeds higher than 5.5ms^{-1}. The strong on-shore flow discussed in this case study is, therefore, a common event over the Western Cape.

4.5.1 Verification of simulations with observed data

The RAMS temperature and relative humidity were compared to the observations of the five AWSs for the 19th February, 2000. The comparisons are discussed below.

a) Temperature

The simulated temperatures did not compare as favourably to the observed temperatures in this case study (Fig. 4.42).

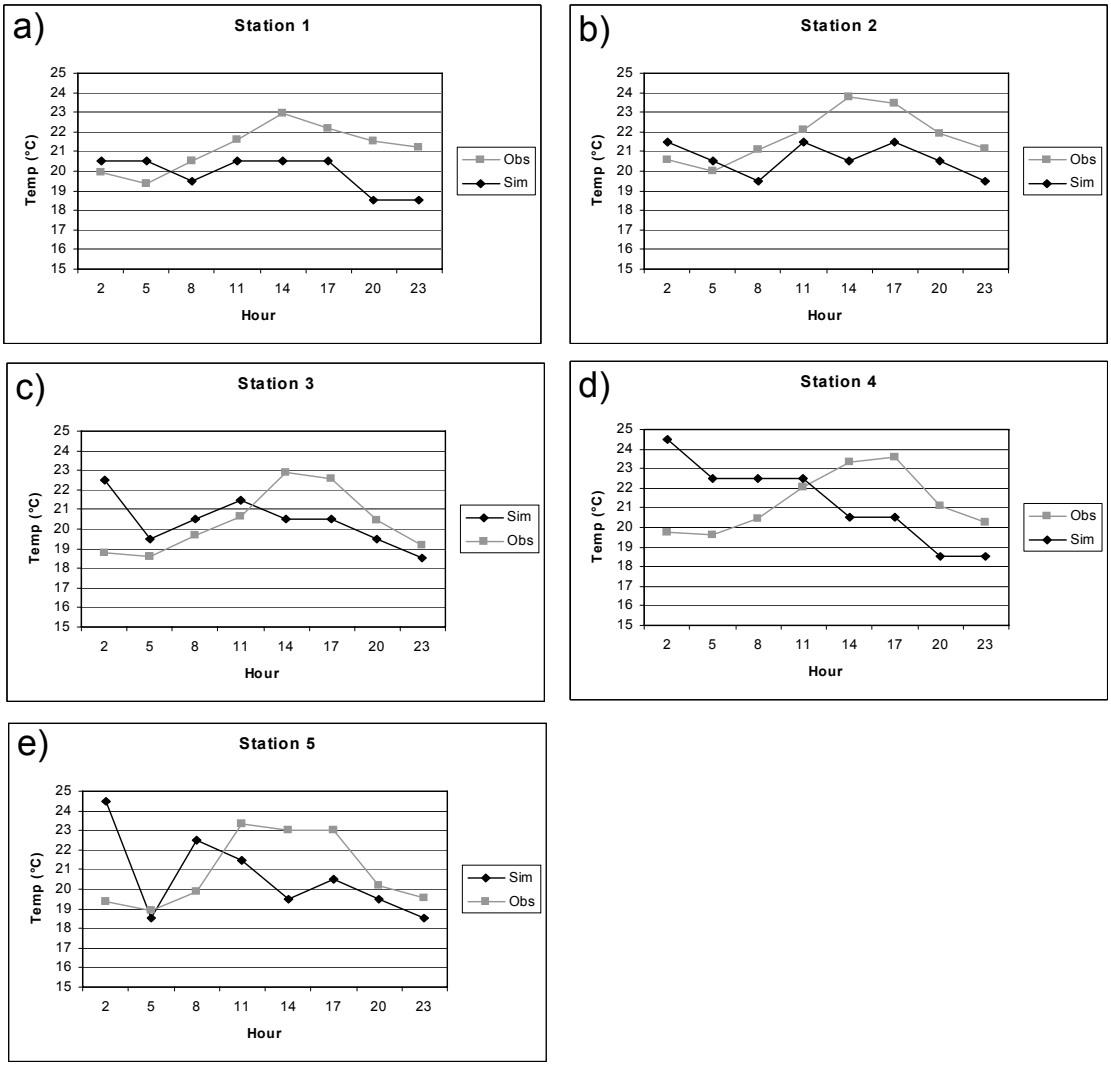

FIGURE 4.42: Comparison between observed temperature (gray) and simulated temperature (black) in °C at the positions of the five automatic weather stations for 19 February, 2000.

The largest differences between observed and simulated temperatures occurred in the early morning hours (02:00) at Stations 3, 4 and 5 (the stations over the interior, Fig. 4.42 d and e) where the model simulated the remnants of the berg wind conditions from the 18th of February, 2000. RAMS failed to observe the diurnal change in temperature at Stations 2, 4 and 5. At Station 4, the RAMS temperature decreased from early in the morning (02:00) until late at night (23:00). The observed temperature at these stations showed

a more common diurnal change with minimum temperatures in the early morning, followed by temperatures increasing later in the afternoon and decreasing again after sunset. At Stations 2 and 5, RAMS predicted a decrease in temperature at 14:00 while the observed temperatures were still increasing. By 14:00, the model had under-predicted the temperatures by 3°C. RAMS simulated temperatures at Stations 1 and 3 were closer to the observed values with the exceptions being: early morning at Station 3 (02:00); and late evening at Station 1. During this strong on-shore, flow RAMS under-predicted temperatures during the afternoon and evening.

b) Relative humidity

The observed RH values in the early morning were higher than those which RAMS simulated at all the stations.

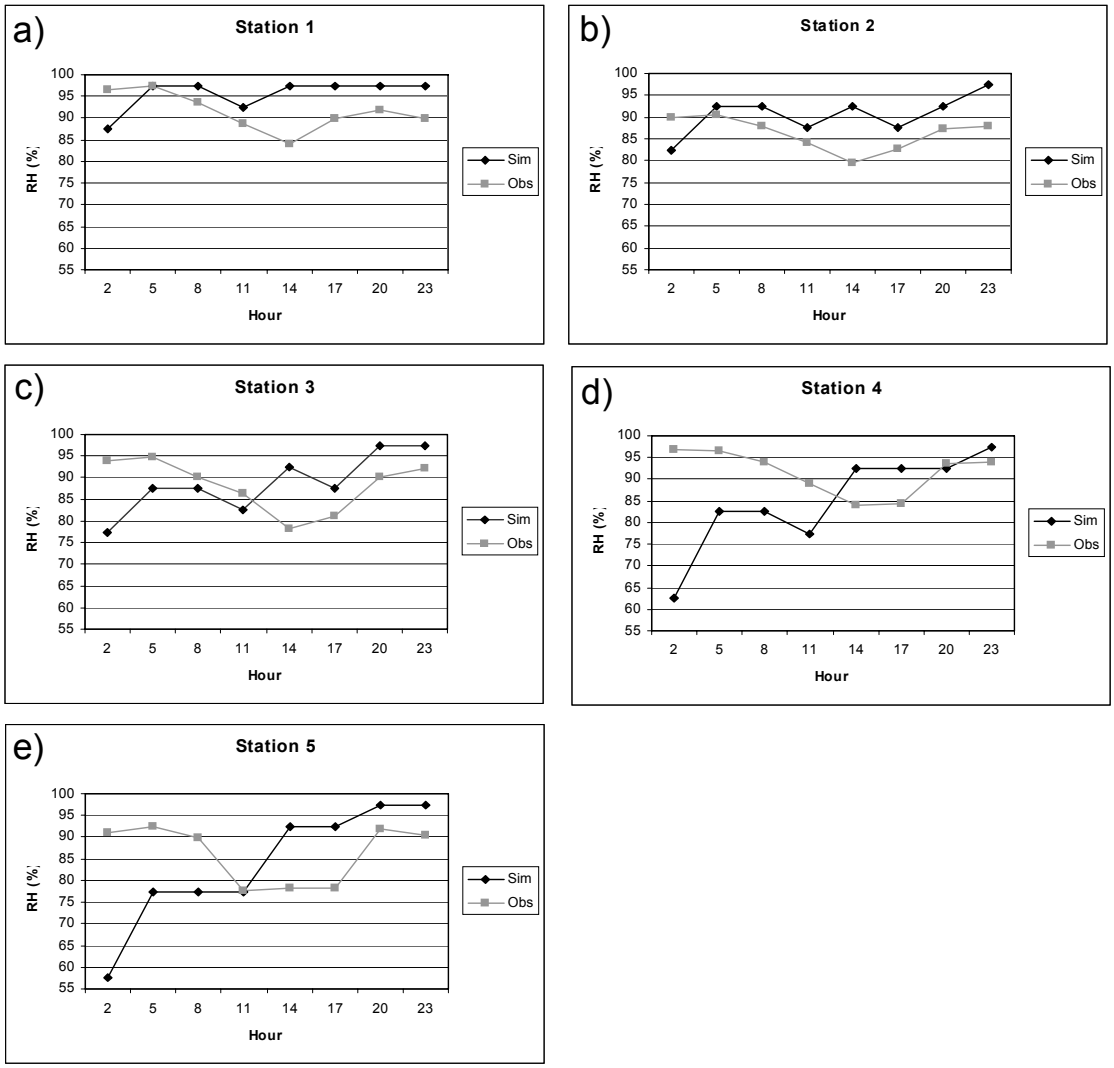

FIGURE 4.43: Comparison between observed relative humidity (gray) and simulated relative humidity (black) in % at the positions of the five automatic weather stations for 19 February, 2000.

The difference in values between the observed and simulated RH were not as large at the coastal stations (Station 1 and 2) as at the interior stations. RAMS failed to simulate the pattern of RH change at most stations. This was especially true at Stations 4 and 5 where the simulated RH continued to rise throughout the day, while the observed values showed a normal decrease toward the afternoon and an increase of RH later in the day in conjunction with the decrease in temperature (Fig. 4.43).

Both the observed and simulated data showed the temperature and relative humidity expected during strong onshore conditions. The domination of the strong onshore flow is shown in the failure of the sea breeze to develop on this day, as shown in both observed and simulated data. RAMS failed to simulate the change of temperature and RH at the interior stations. A more detailed description of the RAMS results follows.

4.5.2 RAMS simulations

On the 19th February, 2000, the 14:00 sea-level pressure field (SAWS, 2000) showed a surface trough situated over the central and western parts of the country, while the Indian Ocean High ridged in over the eastern parts of the country.

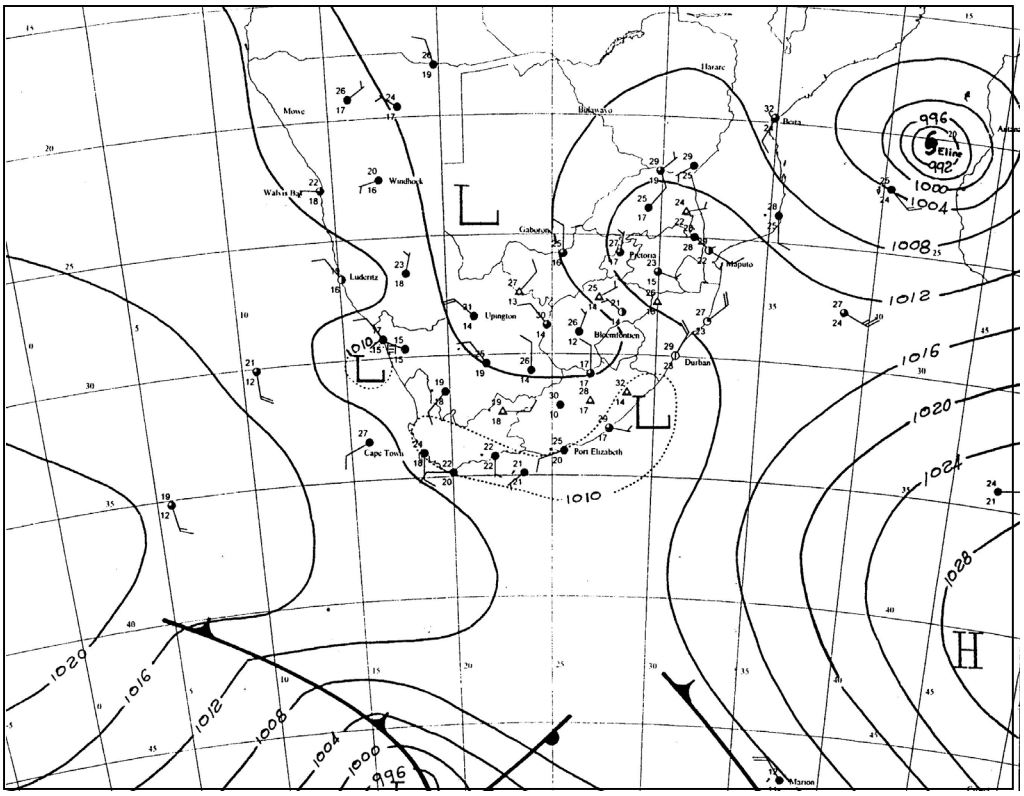

FIGURE 4.44: Synoptic map of southern Africa for 19 February, 2000 at 14:00 (Adapted from: South African Weather Bureau, 2000)

There was a coastal low present over the West Coast and an elongated low pressure cell over the South and East Coasts (Fig. 4.44)

The analysis of the SAWS surface observations for the Western Cape Province at 02:00 (not shown) showed a high pressure ridge over the Cape Peninsula with an elongated low reaching into the western interior from the west coast. The temperatures at Cape Town International Airport and Cape Point were 15°C and 18°C respectively, with winds of 2.5ms^{-1} and 5ms^{-1}, respectively.

The RAMS simulations at 02:00 (not shown) forecasted temperatures between 19°C (False Bay and the Coastal Plains) and 26°C (the western slopes of Bottelaryberg Mountain). The high temperatures over Bottelaryberg Mountain were remnants of berg wind conditions that were erroneously simulated late on the 18th. The cross sections showed the last vestiges of the temperature inversion of the sea breeze of the 18th in the lower 200m of the atmosphere, showing that the effects of a strong sea breeze as were observed on the 18th could last well into the night. The RAMS RH varied between 100% over False Bay and 45% over Bottelaryberg Mountain. In the cross sections, the high RH associated with the onshore flow was visible over the coastal dunes (X1), the southern slopes of Bottelaryberg Mountain (X2) and the southern foothills of Helderberg (X3). The simulated wind at this time concurred with the observations late on the 18th, with light winds over most of the study area and strong northerly winds over Bottelaryberg Mountain. These high wind speeds over Bottelaryberg Mountain were visible only in X2, in the simulated cross sections of wind speed at 02:00 (not shown).

By 05:00, RAMS simulated light to moderate southerly winds in the lower 700m of the atmosphere (Fig. 4.45 shows X1 (b) and X2 (a)) in the cross sections. Strong winds were visible in X2 (Fig. 4.45a) on the northern peak of Bottelaryberg Mountain, as RAMS continued to simulate berg wind conditions over this area from the 23:00 simulations on 18th February, 2000.

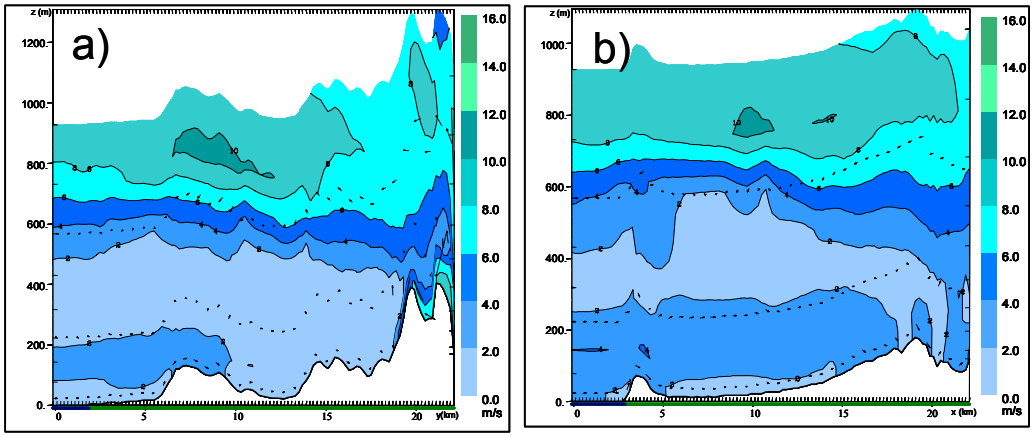

FIGURE 4.45: Simulated wind speed (ms^{-1}) and direction (black arrows) at 05:00 SAST on 19 February, 2000 in the south-north cross sections X1 (b) and X2 (a).

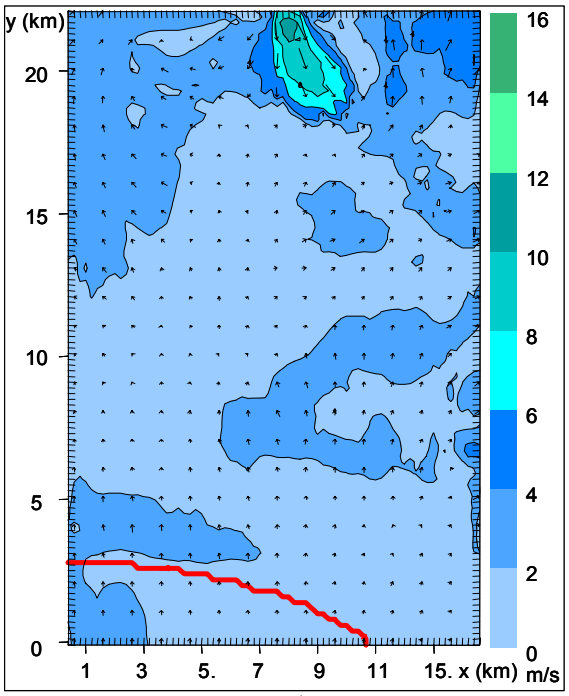

FIGURE 4.46: Simulated surface wind speed (ms^{-1}) and direction (black arrows) at 05:00 SAST on 19 February, 2000. The numbers 1 – 5 indicate the geographical positions of the AWSs used in the verifications.

The surface winds over the study area (Fig. 4.46) were light, the strong winds simulated over Bottelaryberg Mountain having weakened somewhat from 02:00 to approximately $12ms^{-1}$. The temperatures simulated at this time were cool over the whole study area which can be ascribed to the cool air carried inland from the south (not shown).

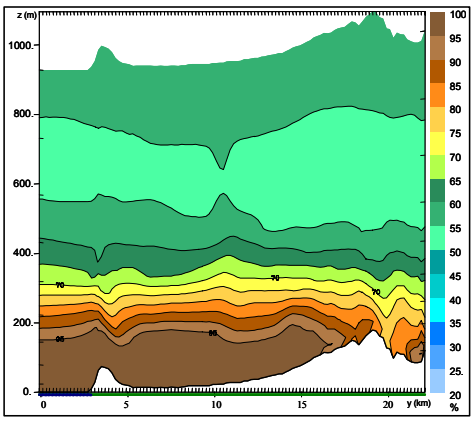

FIGURE 4.47: Simulated relative humidity (%) at 05:00 SAST on 19 February, 2000 in the south-north cross section X1.

The RAMS simulated RH at 05:00 showed very high values over most of the study area (not shown). The cross sections (X1, Fig. 4.47, X2) showed that the layer of high to very high RH was just over 400m deep in the atmosphere.

At 08:00, the RAMS simulated temperature increased over the interior and the cross sections (not shown) showed the cool air to be in the lower 300m of the atmosphere. The RH in the interior had decreased slightly at the surface, but in the cross sections of RH taken at 08:00, the layer of high RH reached to the upper boundary at 1km ASL. The wind was light to moderate southerly with the fresh northerly component over Bottelaryberg Mountain. This northerly component of the berg wind was much lighter now than earlier in the day. The cross sections showed that the wind was southerly through the depth of the simulated atmosphere with the exception of the berg wind over the Bottelaryberg Mountain's northern slopes and at heights above 700m ASL.

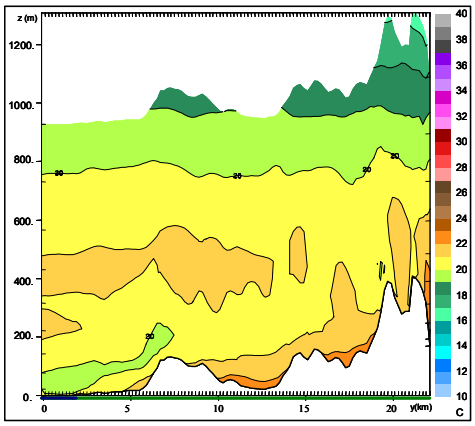

FIGURE 4.48: Simulated temperature (°C) at 11:00 SAST on 19 February, 2000 in south-north cross section X2.

In the previous case studies the False Bay sea breeze was clearly visible by 11:00 in the temperature, RH and wind fields. On 19th February, 2000, the 11:00 temperature simulations showed something that appeared to be the first sign of a sea breeze in the cross sections (Fig. 4.48) and in the surface temperatures (Fig. 4.49).

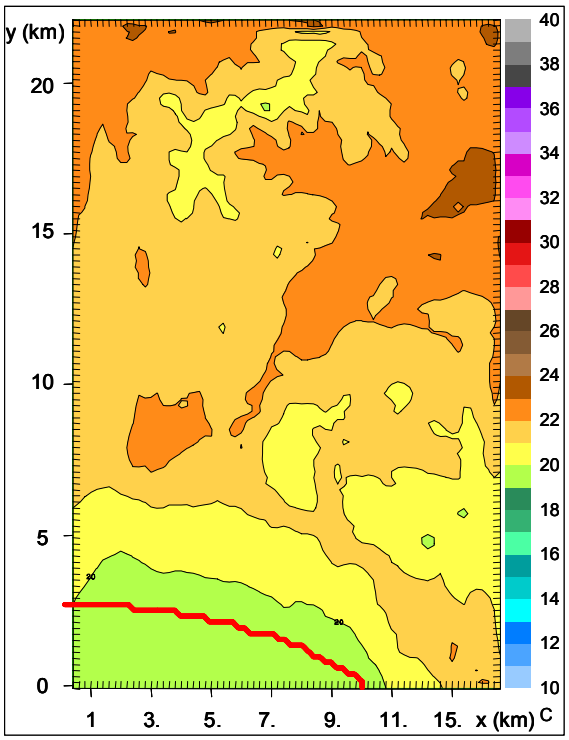

FIGURE 4.49: Simulated surface temperature (°C) at 11:00 SAST on 19 February, 2000. The numbers 1 – 5 indicate the geographical positions of the AWSs used in the verifications.

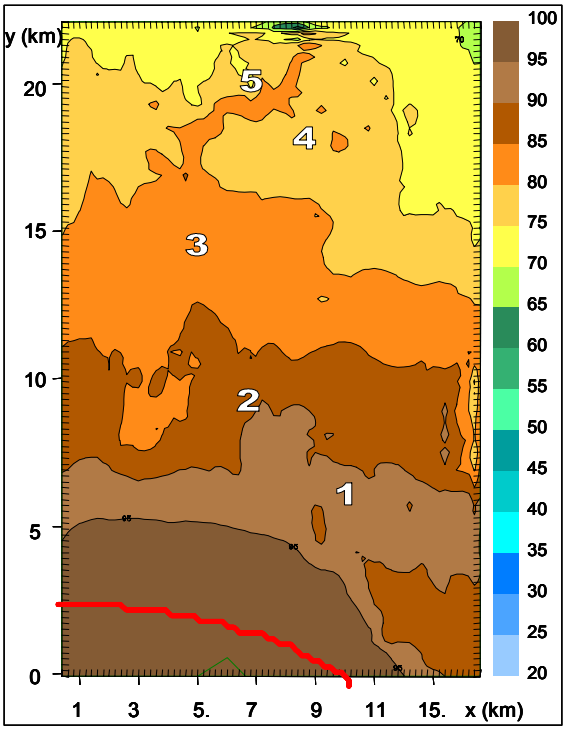

FIGURE 4.50: Simulated surface relative humidity (%) at 11:00 SAST on 19 February, 2000. The numbers 1 – 5 indicate the geographical positions of the AWSs used in the verifications.

This was not as clear in the surface simulations of RH (Fig. 4.50) and the RH cross sections (Fig. 4.51, X2), where the high RH values stretched through the length of the study area and beyond the top of the simulated atmosphere. This is not indicative of a sea breeze front and the cooler temperatures were most likely due to the onshore flow in the area. The surface maps (Fig. 4.49 and Fig. 4.50) show no indication of the steep temperature and RH gradients that suggest the development of the sea breeze as was indicated in the first two case studies.

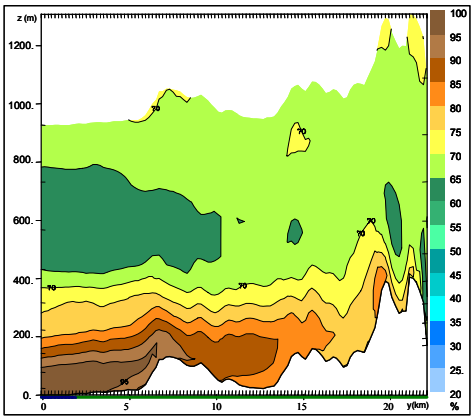

FIGURE 4.51: Simulated relative humidity (%) at 11:00 SAST on 19 February, 2000 in south-north cross section X2.

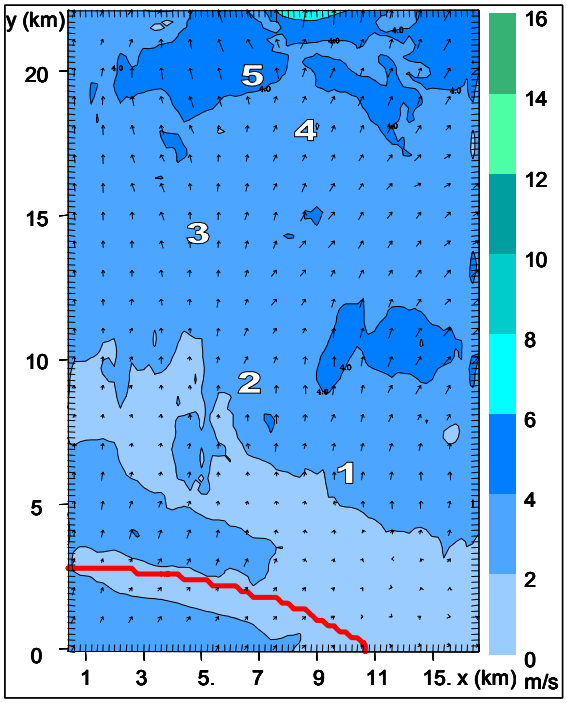

FIGURE 4.52: Simulated surface wind speed (ms^{-1}) and direction (black arrows) at 11:00 SAST on 19 February, 2000. The numbers 1 – 5 indicate the geographical positions of the AWSs used in the verifications.

The wind graphs at the surface (Fig. 4.52) and the cross sections (Fig. 4.53) showed no indications of a sea breeze front. Nor did they show even a slight opposing flow further inland or at the higher levels of the simulated atmosphere which would have indicated the passage or development of the sea breeze.

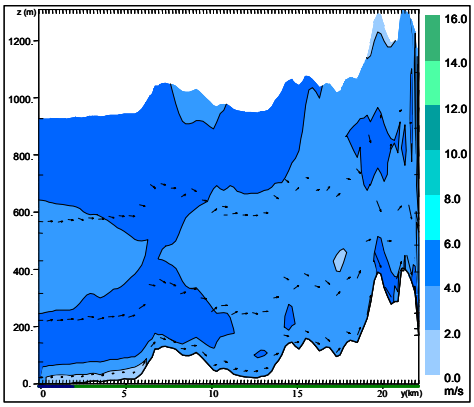

FIGURE 4.53: Simulated wind speed (ms^{-1}) and direction (black arrows) at 11:00 SAST on 19 February, 2000 in south-north cross section X2.

Analysis of the 14:00 observations over the Western Cape Province showed that the low pressure over the interior had strengthened since 02:00, pushing the ridging high slightly westward. The winds over the Peninsula were southerly to south-westerly at this time. The 14:00 RAMS simulations of temperature confirmed that there was no sea breeze visible at this time. The surface temperatures increased slightly from 11:00, but were still cool over the whole study area (not shown). The cross sections all showed the warmer layer of air at the surface, with cool to cold temperatures higher in the atmosphere (X1 in Fig. 4.54). In the cross sections, there were no signs of the shallow layer of cold air which would have indicated the sea breeze moving in from False Bay or Table Bay.

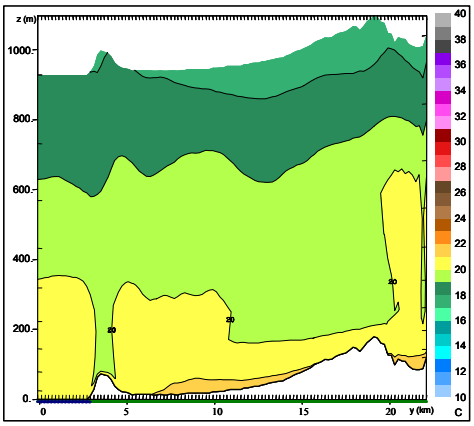

FIGURE 4.54: Simulated temperature (°C) at 14:00 SAST on 19 February, 2000 in south-north cross section X1.

The simulated RH was very high over the whole study area to a height of 400m ASL. The wind at this time was light at the surface over the coastal and inland plains, but moderate to fresh southerly over the rest of the study area to a height of 1km ASL (the top of the simulated atmosphere).

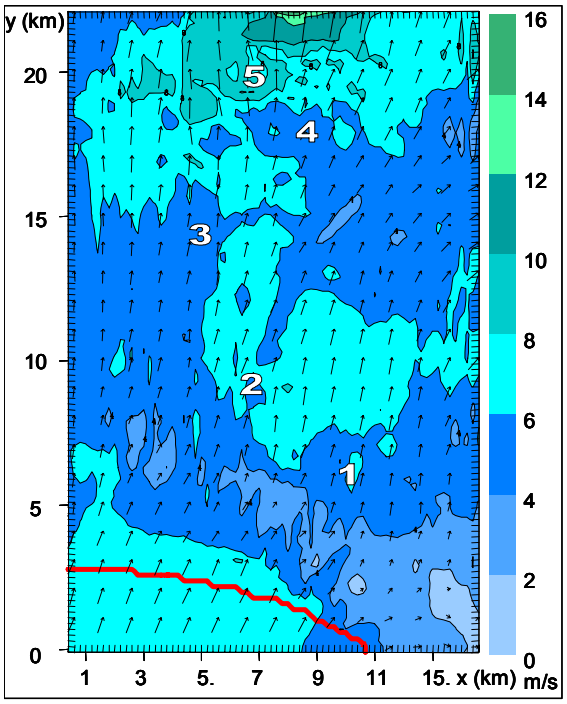

FIGURE 4.55: Simulated surface wind speed (ms^{-1}) and direction (black arrows) at 17:00 SAST on 19 February, 2000. The numbers 1 – 5 indicate the geographical positions of the AWSs used in the verifications.

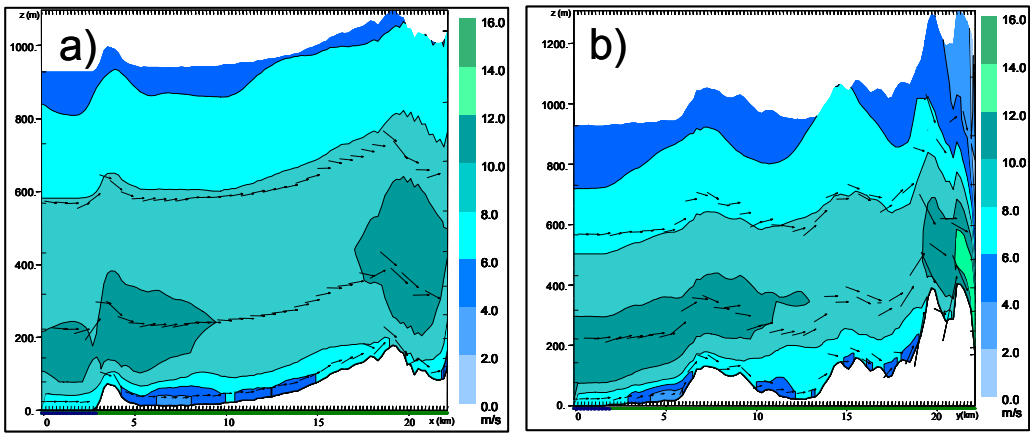

FIGURE 4.56: Simulated wind speed (ms^{-1}) and direction (black arrows) at 17:00 SAST on 19 February, 2000 in south-north cross sections X1 (a) and X2 (b).

By 17:00, there was a shallow layer of warmer air at the surface, while the cool air carried by the strong southerly flow was visible in the cross sections. This RH was still very high over all of the study

area and was now visible up to the top of the cross section in X1. The very high RH reached 700m ASL in X2 and X3. The wind speed at this time was moderate to fresh southerly to south-westerly at the surface (Fig. 4.55). The cross sections showed that the wind was simulated as moderate to strong southerly up to 900m in X1 (Fig. 4.56a), 800m in X2 (Fig. 4.56b).

At sunset, the temperatures had cooled further and decreased with height, whereas the presence of the sea breeze would have shown a temperature inversion in the lower layers of the atmosphere (X1 and X2, shown in Fig. 4.57).

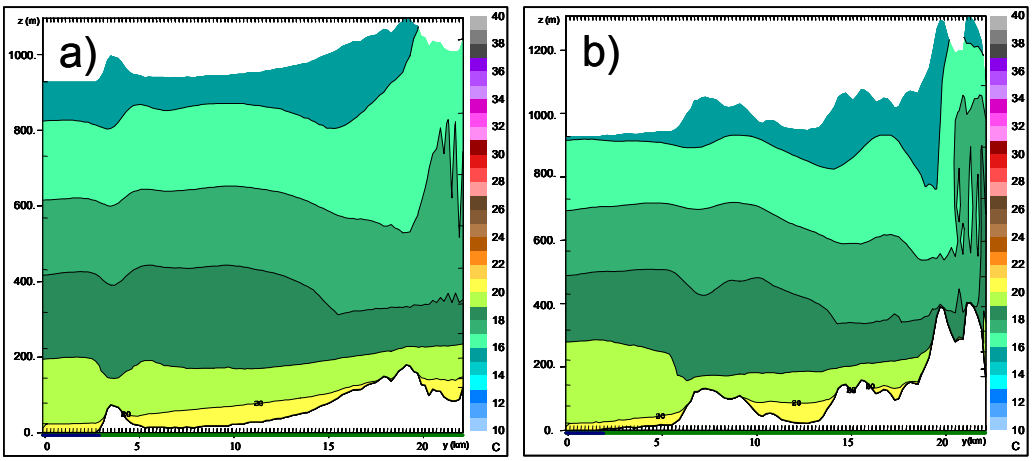

FIGURE 4.57: Simulated temperature (°C) at 20:00 SAST on 19 February, 2000 in south-north cross sections X1 (a) and X2 (b).

The RH was very high throughout the depth of the simulation over the whole of the study area. The wind speed had increased from the 17:00 simulations. Surface winds were now moderate to fresh with strong winds over Bottelaryberg Mountain (not shown). These conditions continued in the 23:00 simulations (not shown).

4.5.3 Conclusions

The influence of strong onshore synoptic flow on the sea breeze was shown in this case study. Both AWS data and RAMS simulations showed cool temperatures and high relative humidity on this day with strong southerly winds blowing over the entire study area. The RAMS simulations show a continuation of the berg wind conditions over Bottelaryberg Mountain in the early morning hours that are not observed by the AWS data at that time.

Throughout the day, there was no indication of the sea breeze penetrating the study area in the RAMS simulations. The cool temperatures and high relative humidity occurred up to the top of the vertical cross sections (1km ASL) by 14:00 (Fig. 4.54), whereas in the first two case studies, the shallow

layer of cool, moist air was clearly visible. The RAMS model showed clearly how the strong onshore flow prevented any meso-scale circulation to penetrate the study area on this day.

The model handled the strong onshore synoptic flow appropriately showing the cool temperatures and high relative humidity caused by the onshore flow in the area. With the exception of the berg winds in the early morning hours, the RAMS model was very close to the observed values in this case study.

To summarise, the RAMS model simulated the influence of the strong onshore synoptic conditions and indicated that the False Bay sea breeze did not develop during strong onshore synoptic flow.

Chapter 5 Summary and Conclusions

5.1 Summary

The aims of this study were to:

- Determine how well the RAMS model simulated the sea breeze influence in the Western Cape wine growing districts.
- Investigate the influence of the sea breeze in the Stellenbosch winegrowing district on temperature, relative humidity (RH), and wind speed and direction for different synoptic conditions. This was done by investigating information gathered through the use of RAMS at 200m resolution and the automatic weather stations (AWSs) in the area.

A study area for three case studies was chosen south-west of Stellenbosch in order to focus on the influence of the False Bay sea breeze. Three days were identified with different synoptic scale conditions: 3rd February, 2000, with weak onshore synoptic flow; 18th February, 2000, with off-shore synoptic flow and 19th February, 2000, with strong onshore synoptic flow.

Observed temperature and RH values from five automatic weather stations located in the study area were used to verify the RAMS simulations for the three case studies. The RAMS output consisted of surface maps and vertical cross sections from south to north, spaced 5km from each other throughout the study area.

The first case study (3rd February, 2000) considered the influence of weak onshore synoptic flow on the sea breeze and its consequent effect on temperature, relative humidity and wind speed and direction. On this day, the AWS data showed the penetration of the sea breeze as a decrease in temperature and an increase in RH between 17:00 and 20:00. RAMS simulated the sea breeze to occur approximately 3 hours earlier. The cross sections showed the vertical structure of the sea breeze in great detail. The raised head of the sea breeze (indicative of the early mature stage) was clearly visible in the temperature and relative humidity cross sections at 11:00. Later in the afternoon (14:00), RAMS depicted the flattening of the head of the sea breeze front, indicating the late mature stage in sea breeze development. The vertical profile of the winds also adequately described the sea breeze, as stronger winds occurred above the surface level. RAMS dealt adequately with the complex topography in the study area. High wind speeds were predicted due to the funnel effect through the mountains in the early morning hours. The mountain breeze circulations after sunset were also accurately simulated.

The second case study considered the effect of off-shore synoptic conditions on the sea breeze on 18th February, 2000. On this day, the temperatures were very high due to the influence of the berg wind conditions associated with off-shore synoptic conditions in the Western Cape. Two sea breezes were observed and simulated in the study area on this day. The first sea breeze originated from Table Bay, west of the study area, and reached the study area at 23:00 on the 17th February, 2000, lasting until after 05:00 in the morning on the 18th. This sea breeze caused a cooling in the lower 200m of the atmosphere over the western edge of the study area and an increase in relative humidity. The cooling and moisture increase in the west was shown by RAMS despite the strong berg wind conditions dominating the synoptic flow at this time. The second sea breeze originated over False Bay and developed at 11:00 over the southern boundary of the study area. The AWS data showed the cooling associated with the passage of the sea breeze front at 14:00 with RAMS showing the passage slightly later. AWS data showed a decrease in temperature with the passage of the sea breeze front, along with a slight increase in temperature after the passage of the front, indicative of the downward mixing of warm air behind the head of the sea breeze front. RAMS simulated the False Bay sea breeze approximately 3 hours after the AWSs observed it and failed to show the rise in temperature behind the head. However, RAMS simulated the vertical structure of the sea breeze well, showing the flatter profile indicative of the sea breeze under off-shore synoptic conditions. The RAMS model also showed that the sea breeze in this case study was stronger, caused a bigger decrease in temperature and reached further inland than the sea breeze under weak onshore synoptic conditions.

The third case study investigated the development and character of the sea breeze under strong onshore synoptic flow. On this day, the AWS data and RAMS simulations showed cool temperatures and high RH values associated with the strong onshore flow throughout the day. RAMS showed berg wind conditions in the early morning, a continuation of the berg wind the previous day (18 February, 2000), while the AWSs did not observe it. On this day, there was no indication of sea breeze development from False Bay. The cool temperatures and high RH were simulated throughout the depth of the cross sections and the temperatures did not show the typical shallow layer of cool air indicative of the passage of the sea breeze front. The strong synoptic flow dominated and no sea breeze developed.

In the three case studies, the influence of the sea breeze on temperature, relative humidity and wind speed and direction was simulated well by the RAMS model. The influence of the different synoptic conditions on the sea breeze systems (through the investigation of temperature, RH and wind speed and direction) were clearly illustrated by both the simulated and observed values in this study.

5.2 Conclusions

The results of the three case studies completed here form the basis of ongoing research into climate of the South-western Cape for the wine growing industry. It is clear that the sea breeze has a significant influence on temperature, relative humidity and wind speed and direction in the area discussed.

5.2.1 The sea breeze in the Stellenbosch wine growing district as observed by the Automatic Weather Stations.

a) The sea breeze caused a decrease in temperature of at least 5°C and an increase in RH of 17% with its passage through the area.

b) Temperature decreased more at the coast than in the interior. The increase in RH was also higher at the coast than over the interior. The cooling and increase in RH occurred later at the stations over the interior as the sea breeze penetrated northwards.

c) It was clear from the different synoptic conditions investigated that onset time and intensity of the sea breeze was influenced by the synoptic flow. With light onshore flow, the passage of the sea breeze caused a decrease in temperature of between 3°C and 7°C. The RH, in this case, increased by between 16% and 29% and the sea breeze reached the southern most AWS between 14:00 and 17:00. For the off-shore synoptic flow, the sea breeze developed earlier and reached the southern most AWS at 11:00. In this case, the decrease in temperature caused by the passage of the sea breeze was between 11°C at the northern most station and 16°C at the southern most station. The increased in RH varied between 25% and 57%. The third case study produced no sea breeze.

d) Although the change in temperature (cooling) and increase in RH was larger during offshore flow, the actual values of temperature and relative humidity caused by the sea breeze were not higher than in the case of onshore synoptic flow. While the cooling effect of the sea breeze front in case study 2 caused the temperature to drop by 17:00, the temperatures were still >32°C. The RH rose at the passage of the SBF, but was still very low afterwards (<50% at 17:00). This is important for farming practices in the area as different vines have different threshold values for optimum production and the temperatures, after the cooling caused by the sea breeze on days with off-shore flow, might not be low enough.

e) The horizontal extent of the sea breeze was more than 20 km (northern edge of the study area). The sea breeze front passed Station 5 at 17:00 for the onshore flow case, while it passed at 23:00 for the off-shore flow case study as the sea breeze front moved at a slower pace through the study area under the influence of the off-shore flow.

5.2.2. The sea breeze in the Stellenbosch wine growing district as simulated by RAMS

a) RAMS simulated the theoretical vertical profile of the sea breeze accurately. The model simulated the raised head of the sea breeze in the immature stage, the flattening of the head and spread of the sea breeze surge as the sea breeze moved inland during the early degenerate stage. The cool temperatures, strong wind and high RH values reached further inland above the ground than on the ground, depicting typical sea breeze characteristics.

b) The model also simulated the characteristics of the sea breeze under different synoptic conditions well. The weaker sea breeze of the onshore flow case study was influenced by the coastal dunes adjacent to the coast line and RAMS showed the sea breeze veering around the dunes. The influence of topography on the sea breeze was simulated well as RAMS simulated the funnel effect of the mountains in the early morning hours of 3rd February, 2000. The sea breeze was simulated to reach further inland in the Eerste River Valley which suggested further influence of the topography on the sea breeze. The interaction between mountain/valley breezes with the sea breeze was also simulated well by the model, showing stronger southern components on the northern slopes and weaker southern components on the southern slopes of mountains as the mountain breezes complimented or opposed the sea breeze flow in the area. In the second case study the offshore flow caused a flattening of the head of the False Bay sea breeze front as it was wedged under the synoptic scale flow. RAMS simulated this flattening of the head very well. The sea breeze was also stronger and caused stronger cooling and a rise in RH under this situation. The stronger sea breeze of this case was not influenced by the coastal dunes as was the case in the first case study. The model simulated the berg wind conditions in the area very well with the northerly winds and the high temperatures in the low lying areas. During the off-shore conditions RAMS, simulated the influence of both the False Bay and Table Bay sea breeze well.

c) At the surface, the sea breeze is visible but the time of onset is out by three hours. During onshore conditions the onset time is three hours early and during off-shore conditions the onset time is three hours late. This might be due to RAMS slightly over estimating the influence of synoptic flow on the onset of the sea breeze. During strong inland synoptic conditions, no sea breeze developed.

d) Details of the simulated sea breezes:

   i) The simulated sea breezes had vertical heights of up to 200m above sea level in the first case study and heights up to 100m ASL in the off-shore flow case study.

   ii) The sea breeze front reached as far as 10km inland for the onshore case and 7km inland for the off-shore case, during the early mature stage.

iii) The wind speed of the sea breeze at the surface was simulated to be up to 6ms^{-1} in the off-shore case and 8ms^{-1} in the onshore case.

iv) The decrease in temperature caused by the 3rd February, 2000 sea breeze was up to 4°C and on the 18 February, 2000, the simulated sea breeze caused a cooling of up to 10°C.

v) On the 3rd February, 2000, RH increased by up to 30% and on the 18th February, 2000, RH increased by up to 45%.

vi) Divergence was visible along the coastline as the sea breeze crossed the coastline at a 90° angle. Convergence was visible in the Eerste River Valley in the onshore flow case study and, during berg wind conditions in the second case study, a convergence line was visible where the sea breeze and the berg wind met.

e) It was clear that RAMS has potential to be used to identify climatological areas to identify terroir units in the area.

5.3 Recommendations

a) Further case studies are required to determine a possible bias toward time of onset of the sea breeze for different synoptic conditions and to investigate if RAMS has a bias towards temperature and RH.

b) There is a need for more AWSs in the wine growing areas of South Africa, in order to obtain more detailed climatological information for comparison with model outputs.

c) Additional case studies of the sea breeze are required in order to establish a clear understanding of the characteristics of the sea breeze for different synoptic conditions.

d) The location and placement of AWSs need to be optimised in order to capture the influence of the sea breeze. This is needed particularly in an area with complex terrain such as the Western Cape.

e) These results form the basis of ongoing research into the climate of the South-western cape. It is recommended that a thorough climatology of the area be completed and that the information is consequently made available to the viticultural sector. Because of the extensive cost of using RAMS, other numeric models need to be investigated to determine if the climate of the winegrowing district can be simulated with the same level of accuracy.

REFERENCES

Abbs, D.J., 1986: Sea-Breeze Interactions along a Concave Coastline in Southern Australia: Observations and Numerical Modeling Study. *Monthly Weather Review,* 114**,** 831 – 848.

Abbs, D.J. & Physick, W.L., 1992: Sea-breeze observations and modeling: a review. *Australian Meteorological Magazine,* 41**,** 7 – 19.

Ackerman, S., 2005: *Sea and land breezes.* University of Wisconsin-Madison Space Science and Engineering Center, Cooperative Institute for Meteorological Satellite Studies.
http://cimss.ssec.wisc.edu/wxwise/seabrz.html

ARC-ISCW, AgroMet Climate Monitoring Network. 2000: *Long term averages of five weather stations in the Stellenbosch area.* Pretoria, 0001.

Arrit, R.W., 1993: Effects of the large-scale flow on characteristic features of the sea breeze. *Journal of Applied Meteorology,* 32, 116 –125.

Asimakopoulos, D.N., Helmis, C.G., Papadopoulos, K.H., Kalogiros, J.A., Kassomenos, P. & Petrakis, M., 1999: Inland propagation of Sea Breeze under Opposing Off-shore Wind. *Meteorology and Atmospheric Physics,* 70**,** 97 – 110.

Atkinson, B.W., 1981: *Meso-scale Atmospheric Circulations.* Academic Press. 495 pp.

Bannon, P.R., 1995: Hydrostatic adjustment: Lamb's problem. *Journal of Atmospheric Science,* 52, 1743 – 1752.

Barnes, S.L., 1973: Mesoscale objective map analysis using weighted time-series observations. *NOAA Technical Memorandum ERL NSSL-62 [NTIS COM-73-10781], March, National Severe Storms Laboratory, Norman, Oklahoma, 60pp.*

Batt, K., 2005: *Sea breezes on the NSW coast.* Commonwealth of Australia 2005, Bureau of Meteorology.
http://www.bom.gov.au/weather/nsw/amfs/Sea%20Breeze.shtml

Bechtold, P., Pinty, J., & Mascart, P., 1991: A numerical investigation of the influence of large-scale winds on the sea breeze and inland breeze type circulations. *Journal of Applied Meteorology,* 30, 1268 – 1279.

Becker, N.J., 1977: The influence of geographical and topographical factors on the quality of the grape crop. *OIV Symposium proceedings 'Quality of the Vintage', Oenological and Viticultural Research Institute, Cape Town.*

Black, J.F., & Tarny, B.L., 1963: The use of asphalt coating to increase rainfall. *Journal of Applied Meteorology,* 2, 557 – 564.

Bleck, R. & Haagenson, P.L., 1968: Objective analysis on isentropic surfaces. *NCAR technical note, TN, TN-39, December, National Center for Atmospheric Research, Boulder, Colorado, 27pp.*

Bonnardot, V.M.F., 2004: Guidelines and procedures, Project GW50/031, ARC-ISCW, "Atmospheric modelling with application for the zoning of viticultural regions". *Unpublished report ARC-ISCW,* Pretoria.

Bonnardot, V.M.F., Carey, V.A., Planchon, O., & Cautenet, S., 2001: Sea breeze mechanism and observations of its effect in the Stellenbosch wine producing area. *Wynboer,* 10, 107 – 113.

Bonnardot, V.M.F., Cautenet, S., Du Preez, C.B., Planchon, O., & Carey, V.A., 2002 : Atmospheric modeling: A tool to assess the sea breeze effect in the south-western Cape winegrowing area. In: *Proc. 27th World congress of Vine and Wine, OIV. (June 2002) Bratislava, Slovakia.*

Bonnardot, V.M.F., Planchon, O. & Cautenet, S., 2005: Sea breeze development under and off-shore synoptic wind in the South-Western Cape and implications for the Stellenbosch wine-producing area, *Theoretical and Applied Climatology,* 81, 203-218.

Britter, R.E. & Simpson, J.E., 1978: Experiments on the dynamics of a gravity current head. *Journal of Fluid Mechanics,* 88, 223 – 240.

Buckley R.L. & Kurzeja, R.J., 1997: An Observational and Numerical Study of the Nocturnal Sea Breeze. Part I: Structure and Circulation. *Journal of Applied Meteorology,* 36, 1577-1598.

Burk, S.D. & Staley, D.O., 1978: Comments on "On the rotation rate of the direction of sea and land breezes". *Journal of Atmospheric Science,* 36, 369-371.

Campbell-Clause, J.M., 1988: Stomatal response of grapevines to wind. *Australian Journal of Experimental Agriculture,* 38, 77-82.

Cangialosi, J., 2003: *An analysis of the south Florida sea breeze circulation: An idealized study.* University of Miami/RSMAS, Miami.
http://orca.rsmas.miami.edu/~johnc/SFseabreeze/SFLA.pdf

Carey, V.A., Bonnardot, V.M.F., Schmidt, A. & Theron, J.C.D. 2003: The interaction between vintage, vineyard site (mesoclimate) and wine aroma of Vitis vinifera L. cvs. Sauvignon blanc, Chardonnay and Cabernet Sauvignon in the Stellenbosch-Klein Drakenstein wine producing area, South Africa (1996-2000). *Bulletin De L'OIV,* 2003, 863-864.

Chang, Y.S., Carmichael, G.R., Kurita, H., & Ueda, H., 1989 : The transport and formation of photochemical oxidants in central Japan. *Atmospheric Environment,* 23, 363 – 393.

Chiba, O., 1993: The turbulent characteristics in the lowest part of the sea breeze front in the atmospheric surface layer. *Boundary Layer Meteorology*, 65, 181-195.

Clancy, R.M., Thompson, J. D., Hurlburt, H.E., & Lee, J. D., 1979: A model of Mesoscale Air-Sea Interaction in a Sea breeze – coastal upwelling regime. *Monthly Weather Review,* 107, 1476-1505.

Clarke, R.H., 1955: Some observations and comments on the sea breeze. *Australian Meteorological Magazine,* 11, 47 – 68.

Clarke, R.H., 1983: Fair weather nocturnal inland wind surges and atmospheric bores: Part I Nocturnal wind surges. *Australian Meteorological Magazine,* 31, 133 – 145.

Clarke, R.H., 1984: Colliding sea-breezes and the creation of internal atmospheric bore waves: two dimensional numerical studies. *Australian Meteorological Magazine,* 32, 207 – 226.

Clarke, R.H., Smith, R.K., & Reid, D.G., 1981: The morning glory of the gulf of Carpentaria: an atmospheric undular bore. *Monthly Weather Review,* 109, 1726 – 1750.

Coombe, B.G., 1987: Influence of temperature on composition and quality of grapes. *Acta Horticulturae,* 206, 23-33.

Cotton, W.R., Pielke Sr., R.A., Walko, R.L., Liston, G.E., Tremback, C.J., Jiang, H., McAnelly, R.L., Harrington, J.Y., Nicholls, M.E., Carrio, G.G., & McFadden, J.P. 2003: RAMS 2001: Current status and future directions. *Meteorology and Atmospheric Physics,* 82**,** 5-29.

Davis, W.M., Schultz, L.G., & Ward, R. de C., 1980: An investigation of the sea breeze, *Annals of Harvard College. Observatory.,* Cambridge, Mass., 21, 215-263.

Defant, F., 1951: Local winds. *Compendium of meteorology.* American Meteorological Society.

De Wet. L.W., 1984: The dynamic forcing of coastal lows. *Paper presented at the Coastal Low Workshop, Simonstown, March 1984.*

Düring, H., 1976: Studies on the environmentally controlled stomatal transpiration in grape vines. I Effects of light intensity and air humidity. *Vitis,* 15, 2, 82-87.

Estie, K.E., 1984: Forecasting the formation and movement of coastal lows. *Paper presented at the Coastal Low Workshop, Simonstown, March 1984.*

Estoque, M.A., 1961: A theoretical investigation of the sea breeze. *Quarterly Journal of the Royal Meteorological Society* 87**,** 136 – 146.

Estoque, M.A., 1962: The sea breeze as a function of the prevailing synoptic situation. *Journal of Atmospheric Science,* 19, 244 – 250.

Estoque, M.A., J. Gross, and H.W. Lai, (1976). A Lake Breeze over Southern Lake Ontario. *Monthly Weather Review* 104, 386 – 396.

Falcetti, M., 1994 : Le Terroir. Qu'est-ce qu'un terroir ? Pourqoui l'étudier? Pourqoui l'enseigner? Bull. l'O.I.V. 67, 246-275.

Fosberg, M.A., & Schroeder, M.J., 1966: Marine air penetration in Central California. *Journal of Applied Meteorology,* 5, 573 – 589.

Franchito, S.H., Rao, V.B., Stech, J.L., & Lorenzzetti, J.A., 1998: The effect of coastal upwelling on the sea breeze circulation at Cabo Frio, Brazil: A numerical experiment. *Annales. Geophysicae,* 16, 866 – 881.

Freeman, B.M., Kliewer, W.M. & Stern, P., 1982: Research note: Influence of windbreaks and climatic region on diurnal fluctuation of leaf water potential, stomatal conductance and leaf temperature of grapevines, *American Journal of Enology and Viticulture,* 33 (4), 233-236.

Frizzola, J.A. & Fisher, E.L., 1963: A series of sea breeze observations in the New York City area. *Journal of Applied Meteorology,* 2**,** 722 – 739.

Glen, S., Dunk, R., Bowers, L., Oman, L., Frye, J., Dreyer, D., Cope, A., Szatkowski, G., & Bielory, L., 2003: *The role of coastal upwelling in sea breeze frontogenesis along the NJ shore.* Rutgers, The State University of New Jersey, Institute of Marine and coastal sciences, Coastal Ocean Observation Lab. http://marine.rutgers.edu/cool/seabreeze/tutorial.html

Glickman, T.S. (Ed.), 2000: American Meteorological Society Glossary of Meteorology, 2nd Edition.

Godske, C.L., Bergeron, T., Bjerknes, J., & Bundgaard, R.C., 1957: *Dynamic meteorology and weather forecasting.* Carnegie Institution and American Meteorological Society, Washington and Boston.

Goldreich, Y., Druyan, L.M., & Berger, H., 1986: The interaction of valley/mountain winds with a diurnally veering sea/land breeze, *Journal of Climatology,* 6, 551-561.

Hadi, Tri W., Horinouchi, T., Tsuda, T., Hashiguchi, H., Fukao, S., 2002: Sea-Breeze Circulation over Jakarta, Indonesia: A Climatology Based on Boundary Layer Radar Observations. *Monthly Weather Review,* 130, 2153-2166.

Hamilton, R.P., 1989: Wind and its effects on viticulture, *The Australian Grape growers and Winemaker,* March, 16-17.

Holton, J.R., 1992: *An introduction to dynamic meteorology.* Third edition, Academic press, San Diego.

Hughes, C., & Maze, K. 2006: Wine and conservation in the Cape, Percy FitzPatrick Institute, University of Cape Town, Cape Town.
http://www.botanicalsociety.org.za/ccu/downloads/articles/Veld&Flora_Wine&Conservation_March2002.PDF.

Huschke, R.E. (Ed.) 1959: *Glossary of Meteorology,* American Meteorological Society, 638pp.

Kimble, G.H.L., 1946: Tropical land and sea breeze (with special reference to the East Indies). *Buletin of the American Meteorological Society,* 27, 99 – 113.

Kingsmill, D.E. 1995: Convection initiation associated with a sea breeze front, a gust front and their collision. *Monthly Weather Review,* 123**,** 2913-2933.

Kliewer, W.M. & Torres, R.E., 1972: Effect of controlled day and night temperatures on grape coloration. *American Journal of Enology and Viticulture,* 23(2), 71-77.

Kondo, H., 1990: A numerical experiment on the interaction between sea breeze and valley wind to generate the so-called "extended sea breeze". *Journal of the Meteorological Society of Japan.* 68**,** 435 – 446.

Koschmieder, H., 1933: *Dynamische Meteorologie.* Akademische Verlagsgesellshaft, Leipzig.

Koschmieder, H., 1936: Danziger Seewindstudien, I. *Danziger Meteorologie. Forschungsarbeiten,* 8.

Koschmieder, H., & Hornickel, K. 1942: Danziger seewind studies I – III. *Danziger Meteorologie. Forschungsarbeiten,* 8, 10, 11.

Kurita, H., Sasaki, K., Muroga, H., Ueda, H., & Wakamatsu, S., 1985: Long-range transport of air pollution under light gradient wind conditions. *Journal of Climate and Applied Meteorology,* 24, 425 – 434.

Kusuda, M, & Alpert, P., 1983: Anticlockwise rotation of the wind hodograph. Part I: Theoretical study. *Journal of Atmospheric Science,* 40, 487-499.

Linacre, E., 2002: *Ocean currents off southern Africa*, University of Wyoming, 1000E University Ave. Laramie, WY 82071.
http://www-das.uwyo.edu/~geerts/cwx/notes/chap11/safrica.html

Lindesay, J.A., & Tyson, P.D. 1990: Thermo-Topographically Induced Boundary Layer Oscillations over the Central Namib, Southern Africa. *International Journal of Climatology,* 10, 63- 77.

Lyons, W.A., & Olsson, L.E., 1973: Detailed meso-meteorological studies of air pollution dispersion in the Chicago lake breeze. *Monthly Weather Review,* 101, 387 – 403.

Mahrer, Y., & Pielke, R.A., 1977a: The effects of topography on sea and land breezes in a two-dimensional numerical model. *Monthly Weather Review,* 105, 1151 – 1162.

Mahrer, Y., & Pielke, R.A., 1977b: A numerical study of the airflow over irregular terrain. *Beiträge zur Physik derAtmosphäre,* 50, 98-113.

McPherson, R.D. 1970: A numerical study of the effect of coastal irregularity on the sea breeze. *Journal of Applied Meteorology,* 9**,** 767 – 777.

Mellor , G.L. & Yamada, T., 1974: A hierarchy of turbulence closure models for planetary boundary layers. *Journal of Atmospheric Sciences,* 31, 1791-1806.

Miao, J.-F., Kroon, L.J.M., Vilà-Guerau de Arellano, J., & Holtslag, A.A.M., 2003: Impacts of topography and land degradation on the sea breeze over eastern Spain. *Meteorology and Atmospheric Physics.* 84, 157-170.

Neumann, J., 1951: Land breezes and nocturnal thunderstorms. *Journal of Meteorology,* 8, 60 – 67.

Neumann, J., 1977: On the rotation rate of the dirction of sea and land breezes. *Journal of Atmospheric Science,* 34, 1913 – 1917.

O'Brien, J.J. & Pillsbury, R.D., 1974: Rotary wind spectra in the sea breeze regime. *Journal of Applied Meteorology,* 13, 820-825.

Ocean Research Africa, 2002: *Sea Surface Temperature Data: Hout Bay*. Ocean Research Africa, Cape Town, South Africa. http://www.oceanafrica.com/sst/houtbay_sst.html

Oliphant, A.J., Sturman, A.P., & Tapper, N.J., 2001: The evolution and structure of a tropical island sea/land-breeze system, northern Australia. *Meteorology and Atmospheric Physics,* 78, 45 – 59.

Phillips, N.A., 1957: A coordinate system having some special advantages of numerical forecasting. *Journal of Meteorology,* 14, 184-185.

Physick, W.L., 1980: Numerical experiments on the inland penetration of the sea breeze. *Quarterly Journal of the Royal Meteorological Society,* 106, 735 – 746.

Physick, W.L., 1982: Sea Breezes in the Latrobe valley. *Australian Meteorological Magazine,* 30, 255 – 263.

Physick, W.L. & Smith, R.K., 1985: Observations and dynamics of sea breezes in northern Australia. *Australian Meteorological Magazine,* 33, 51-63.

Pielke, R.A., 1974: A three dimensional model of the sea breezes over south Florida. *Monthly Weather Review,* 102, 115 – 139.

Pielke, R.A., 1984: *Mesoscale meteorological modeling.* Academic Press, Orlando.

Pielke, R.A., Cotton, W.R., Walko, R.L., Tremback, C.J., Lyons, W.A., Grasso, L.D., Nicholls, M.E., Moran, M.D., Wesley, D.A., Lee, T.J., & Copeland, J.H., 1992: A comprehensive meteorological modeling system – RAMS. *Meteorology and Atmospheric Physics,* 49, 69-91.

Preston-Whyte, R.A. & Tyson, P.D., 1988: *The Atmosphere and Weather of Southern Africa,* Oxford University Press, Cape Town, 374 pp.

Prezerakos, N.G., 1986: Characteristics of the sea breeze in Attika, Greece. *Boundary Layer Meteorology,* 36, 245 – 266.

Schulze, B.R., 1965: Climate of South Africa: Part 8. General survey, *Weather Bureau, Department of Transport,* WB28.

Schulze, G.C., 1996: The weather and climate of the extreme south-western Cape. *South African Weather Bureau, Department of Environmental affairs and Tourism.*

Segal, M., Purdom, J.F.W., Song, J.L., Pielke, R.A., & Mahrer, Y., 1986: Evaluation of cloud shading effects on the generation and modification of mesoscale circulations. *Monthly Weather Review,* 114, 201 – 1212.

Sha, W., Kawamura, T., & Ueda, H., 1991: A numerical study on sea/land breezes as a gravity current: Kelvin-Helmoltz billows and inland penetration of the sea breeze front. *Journal of Atmospheric Science,* 48, 1649 – 1665.

Simpson, J.E., 1994: *Sea breeze and local winds.* Cambridge University Press, New York, 243 pp.

Simpson, J.E. & Britter, R.E., 1980: A laboratory model of an atmospheric mesofront. *Quarterly Journal of the Royal Meteorological Society,* 106, 485 – 500.

Simpson, J.E., Mansfield, D.A., & Milford, J.R. 1977: Inland penetration of sea-breeze fronts. *Quarterly Journal of the Royal Meteorological Society,* 103, 47 – 76.

Simpson, J.E., Westcott, N.E., Clerman, R.J., & Pielke, R.A., 1980: On cumulus mergers. *Archiv Für Meteorologie, Geophysik und Bioklimatologie,* 29, 1-40.

South African Weather Bureau, 1975: Climate of South Africa. Part 12: Surface Winds. WB38, Government Printer by Weather Bureau. Pretoria

South African Weather Bureau, 1986: Climate of South Africa. Climate Statistics up to 1984. WB40, Government Printer by Weather Bureau, Pretoria.

South African Weather Bureau, 2000: Daily Weather Bulletin, February 2000, Government Printer by Weather Bureau, Pretoria.

Sturman, A.P. & Tyson, P.D., 1981: Sea breezes along the Canterbury coast in the vicinity of Christchurch, New Zealand, *Journal of Climatology,* 1, 203 –219.

Taljaard, J.J., 1994: *Atmospheric circulation systems, synoptic climatology and weather phenomena of South Africa. Part 1: Controls of the weather and climate of South Africa,* Technical paper, 27, Government printer, Pretoria.

Tijm, A.B.C., & Van Delden, A.J., 1999: The role of sound waves in sea-breeze initiation. *Quarterly Journal of the Royal Meteorological Society,* 125, 1997 – 2018.

Tijm, A.B.C., Holtslag, A.A.M., & Van Delden, A.J., 1999a: Observations and Modeling of the Sea Breeze with the Return Current. *Monthly Weather Review* 127, 625 – 640.

Tijm, A.B.C., Van Delden, A.J., & Holtslag, A.A.M., 1999b: The inland penetration of Sea Breezes. *Contributions to Atmospheric Physics.* 72**,** 317 – 328.

Tremback, C.J. & Walko, R.L., 2004: Implementing Very-High Resolution Capabilities into a Mesoscale Atmospheric Model: New Capabilities for the Regional Atmospheric Modeling System (RAMS), *In: Proc. AHPCRC Workshop for Mesoscale and CFD Modeling for Military Applications, May 25-26 2004, Jackson State University, Jackson, Mississippi, USA.*

Trini-Castelli, S., Ferrero, E., & Anfossi, D., 2003: Atmospheric dispersion in non-homogeneous conditions – simulations of a wind tunnel tracer experiment. *In: Proc. Del. International workshop on Physical modeling of flow and dispersion phenomena, Prato FI, Itally, 3-5 September 2003*.

Trini-Castelli, S., Ferrero, E., Anfossi, D., & Ohba R., 2004: Turbulence closure models and their application in RAMS. *Enviromental Fluid Mechanics,* Special issue RAMS 5th Workshop.

Walker, N.D., 1984: Passage of coastal lows on the west coast as shown in coastal weather station data. *Paper presented at the Coastal Low Workshop, Simonstown, March 1984.*

Walko, R.L. and Tremback, C.J., 2000: RAMS, Regional Atmospheric Modeling System, Version 4.3/4.4. Model input namelist parameters. *ASTeR Division, Mission Research Corporation, Fort Collins, USA.*

Wesgro, 2002: *Sector fact sheet: Wine,* Wesgro's Sector Research Section, Cape Town. www.wesgro.co.za/assetlibrary/assets/221925024.pdf

Willett, H.C. & Sanders, F., 1959: *Descriptive meteorology.* Academic Press, New York.

Wilson, J.W. & Megenhardt, D. L., 1997: Thunderstorm initiation organization, and lifetime associated with Florida boundary layer convergence lines. *Monthly Weather Review,* 125, 1507-1525.

Xian, Z. & Pielke, R.A. 1991: The effects of width of landmasses on the development of sea breezes. *Journal of Applied Meteorology,* 30, 1280 – 1301.

Yan, H. & Anthes, R.A., 1988: The effect of variations in surface moisture on mesoscale circulations. *Monthly Weather Review,* 116, 192-208.

Zhong, S. & Takle, E.S., 1993: The effects of large-scale winds on sea-land-breeze circulations in an area of complex coastal heating. *Journal of Applied Meteorology,* 32, 1181 – 1195.